2-P

FLUID PHYSICS BRANCH

RESEARCH DIVISION

OFFICE OF ADVANCED RESEARCH AND TECHNOLOGY

FIFTH INTERCENTER AND CONTRACTORS CONFERENCE ON PLASMA PHYSICS

Part IV NASA Ames Research Center and Jet Propulsion Laboratory

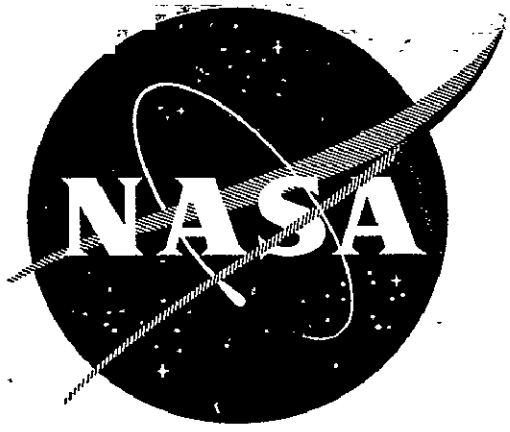

WASHINGTON, D. C.

MAY 24 – 26, 1966

FIFTH NASA INTERCENTER AND CONTRACTORS CONFERENCE ON PLASMA PHYSICS

Part IV: Plasma Physics Research
at NASA Ames Research Center
and at Jet Propulsion Laboratory

Washington, D. C.
May 24-26, 1966

Table of Contents

B. Plasma Physics Research at Jet Propulsion Lab.

Abstract of paper to be presented at the Fifth NASA Intercenter and Contractor Conference on Plasma Physics at NASA Headquarters on May 24-26, 1966

MAGNETIC-COMPRESSION WAVES IN COLLISIONLESS PLASMAS

OBLIQUE AMBIENT MAGNETIC FIELD

By Vernon J. Rossow*

National Aeronautics and Space Administration
Ames Research Center
Moffett Field, Calif.

Numerical analysis is made of the structure of one-dimensional unsteady magnetic compression waves propagating into collisionless plasmas when the ambient magnetic field is oblique to the wave direction. It is found that both the sub- and supercritical solutions change continuously from one limiting situation to the other. A similarity rule is found for correlating the subcritical cases so that the two parameter family of solutions in mass ratio and field angle are reduced to a single set. A comparable rule was not found for supercritical wave strengths.

---

*Assistant Chief, Theoretical Branch

National Aeronautics and Space Administration
Ames Research Center
Moffett Field, Calif.

Abstract of paper to be presented at the Fifth NASA Intercenter and Contractor Conference on Plasma Physics at NASA Headquarters on May 24-26, 1966

COIL SYSTEMS FOR MEASURING CONDUCTIVITY AND VELOCITY OF PLASMA STREAMS

By Vernon J. Rossow*

National Aeronautics and Space Administration
Ames Research Center
Moffett Field, Calif.

A theoretical and experimental study is made of a device that measures the conductivity and velocity of plasma streams. The instrument consists of a primary coil and several secondary coils. Alternating current through the primary coil produces an oscillating magnetic field in the shape of a dipole. Positions of the secondary coils relative to the primary are such that they respond to distortions of the applied magnetic field of the primary that are brought about by the presence and motion of an electrically conducting fluid. These signals on the secondaries vary linearly with the conductivity and with the product of conductivity times velocity. Various possible coil arrangements and tests conducted with a simple three-coil configuration in an electric arc jet are presented. Details of the probe tested, its calibration, and its theoretical basis are described. Results obtained with the three-coil system are in good agreement with theory.

---

*Assistant Chief, Theoretical Branch

National Aeronautics and Space Administration
Ames Research Center
Moffett Field, Calif.

Abstract to be presented at

Fifth NASA Intercenter and Contractor

Conference on Plasma Physics

to be held at Washington, D. C.

May 24-26, 1966

ABLATION PRODUCTS RADIATION

By Warren Winovich*

National Aeronautics and Space Administration
Ames Research Center
Moffett Field, Calif.

The trajectory of a probe designed for steep entry into the atmosphere of Mars at 6.7 km/sec is shown in figure 1. For this illustrated entry, the maximum radiative heat transfer occurs almost simultaneously with maximum convective heat transfer. Thus, spectroscopic examination of the Mars atmosphere by viewing the gas-cap radiation from within the probe may be hindered by the radiation from ablation vapors. A study of the effect of radiation from ablation vapors upon the detection of gas-cap radiation in a plasma tunnel forms the subject matter of the present paper.

Experimental Arrangement

The experimental arrangement is shown in figure 2. The source optics within the flat-faced test body directs radiation from the gas cap out the rear flange of the body via a first-surface mirror. After passing through the wind tunnel port, the radiation is reflected to a cylindrical first-surface mirror where the circular beam is focused as a line on the entrance slit of a spectrograph. The spectrograph had a focal ratio of 6.8 and

---

*Research Scientist

was equipped with a 1200 groove/mm grating blazed at 3500Å. The gas-cap spectra in the range 2700 to 6500Å were recorded by means of photographs. The plates were calibrated with the body in place by directing a collimated beam from a tungsten-ribbon filament lamp into the source optics. The radiative intensity of the tungsten filament was determined by measuring brightness temperature with an optical pyrometer and by recourse to the emissivity data of Larrabee to obtain the spectral energy distribution.

The film was Kodak Spectrographic plate film type 103 F. Exposure times for both tests and calibrations were such that the reciprocity law, i.e., $I \times \tau = \text{const.}$, pertains for the photographic emulsion. Photographic densities were read with a Joyce Loebel microdensitometer.

Results and Discussion

Gas-cap radiation was measured for non-ablating and ablating surfaces. Experimental results for a non-ablating copper surface are shown in figure 3. Total radiation per unit volume is plotted against velocity. The effect of density is accounted for by using the correlating parameter suggested by theoretical calculations. The gas mixture consisted of 46 percent CO_2, 23 percent N_2, and 31 percent Argon (percents by volume). The present results are compared with the molecular theory prediction for CO_2-N_2 mixtures of Arnold, Reis and Woodward, reference 1. The theory has been adjusted to correspond to the same percentages (by volume) as the test gas (i.e., 46 percent CO_2, 23 percent N_2, 31 percent A). This adjustment was made by applying (1) the experimental correlation obtained by James (ref. 2) for concentration effects and (2) the theoretical dilution correlation for Argon (ref. 2). The ballistic range and shock-tube data of references 1, 2 and 3 with no argon dilution are also shown. The theory of reference 2 agrees well with these results. The present data also show the predicted trend with velocity and agree with the dilution effect of argon predicted by the theory of reference 2. The adjusted theoretical curve which applies to the present gas mixture differs by factors of 2.5 at 5 km/sec to 1.2 at 7 km/sec.

In contrast to the non-ablating surface considered up until now, when an ablative surface is exposed to a hot plasma stream, the region close to the body contains a high concentration of ablation vapors at a relatively cool temperature. This is illustrated in figure 4. This figure shows a polyethylene surface ablating in a stream at an equivalent velocity of 5.5 km/sec and a density ratio of 10^{-4}. The heating rate is about 100 watts/cm^2. The stagnation zone is divided into two distinct regions: (1)

the high temperature stagnation zone and (2) the low temperature ablation vapor zone. Even at very low densities, the two zones remain quite distinct.

The effect of the radiation from the ablation vapor zone on the observed gas-cap spectra is shown in figure 5. This slide presents spectra of the gas cap for the non-ablating copper nose and for several plastic ablative materials. The gas mixture consisted of 7 percent CO_2, 91 percent N_2, and 2 percent A (by volume). The tests were made at an equivalent velocity of 8 km/sec. The wavelength range of the spectrograms is from 3500 to 6700Å. For the non-ablating copper surface the radiative flux is due almost solely to the CN violet band system (which is the same result found above for the other non-ablating case with more CO_2 present). The three lower spectra are for exactly the same flow conditions but with surfaces of polyethylene, $(C_2H_4)_x$, polytetrafluoroethylene, $(C_2F_4)_x$, and polyformaldehyde, $(CH_2O)_x$. The gas-cap spectra are quite similar in structure for each of the three plastics.

In addition to enhanced CN violet radiation, the ablation-vapor radiation consists of C_2 Swan band radiation and the C_2 High-Pressure band system. The hydrocarbon plastics also display a prominent CH 4300Å band series and appreciable hydrogen line radiation. A trace amount of hydrogen appears in the stream for the copper surface.

Because the CN violet band system appears to be well understood and amenable to analysis both in terms of species concentration and velocity derived from trajectory data, it represents a prime candidate for monitoring radiation during entry into an atmosphere with CO_2 and N_2 constituents. However, the plasma tunnel tests indicate sizable enhancement of the CN violet system by the presence of ablation ejecta in the boundary layer. The enhancement of the CN violet system by the ablators is shown in figure 6. Radiation only from the CN violet system is listed relative to the non-ablating copper surface. All of the plastic ablators increased the CN violet band system radiation by approximately the same amount (values range from 2 to 4). These data are apparently contrary to ballistic range and shock tube data which show little or no increase in total radiation with polytetrafluoroethylene and polyformaldehyde models. In the following discussion ablation measurements from an air study are used to show that there is in fact no inconsistency and that one can estimate the ablation vapor radiation relative to the gas-cap radiation using suitable scaling laws.

For an ablating surface, the scaling law for radiation is shown in figure 7. Integrated total radiative intensity over

the wavelength range 3600 to 6700Å is shown as a function of body radius for a polyethylene surface exposed to constant flow conditions in a plasma tunnel. The data are shown normalized to the intensity for the smallest body. These tests were performed in air using polyethylene models of the same blunt shape but with radii smaller than the 5 cm value of the test body described above. The effects of testing in air rather than in CO_2-N_2-A mixtures is considered to be unimportant since only relative changes in the ablation vapor zone radiation were considered. Moreover, the measurements indicate (fig. 6) that the gas-cap radiation represents a relatively small part of the total radiation. Therefore, the scaling law for ablation vapor radiation will depend only weakly on the main flow constituents. Since the flow conditions were constant for the test series, the decrease in radius for this test series is equivalent to an increase in the convective heating rate. The reason for this is that the velocity gradient must increase for the smaller radii with a resultant increase in the laminar heat transfer rate to the surface. Intuitively, then, as the body radius decreases, the increased shear at the surface will cause the ablation vapor zone to become thinner; and the radiation intensity would decrease. Based on these general considerations, a scaling law for radiation from the ablation vapor zone has been derived by Winovich and Croce (ref. 4), which yields the result that the intensity varies as the square root of the body radius for laminar flow. The solid line shown on figure 7 represents the predicted slope, and the experimental results agree well with this prediction.

Using the scaling law for ablation vapor radiation, (fig. 7), and the scaling law for the gas-cap radiation (fig. 3), and the measured enhancement of radiation found for polyethylene (fig. 6), the relative intensities of gas-cap radiation as compared to the total radiation can be predicted for various situations. The scaling laws have been applied to typical ballistic range measurements and to the contemplated Mars entry. These results are shown in figure 8. All comparisons are made for a velocity of 5.6 km/sec corresponding to the velocity at the peak heating condition. The test body shape and density range are selected as typical for each case. For the plasma tunnel tests with an ablating surface, the gas-cap radiation is only 25 percent of the total emitted radiation. On the other hand, the prediction for the ballistic range case is that over 90 percent of the total radiation emanates from the gas cap. Plastic models, therefore, can be used in ballistic ranges with negligible uncertainty regarding the radiation source. Finally, for the Mars entry case at the time of peak heating, the gas cap contributes 80 percent of the observed radiation. However, at an earlier time during the entry (4 seconds prior) the gas-cap radiation represents only 29 percent of the total radiation. The use of an ablative heat shield would result

in a measurement that contains a variable contribution from the ablation vapor zone radiation. This would introduce uncertainties into the interpretation of the gas-cap radiation during a critical period when spectral measurements are recorded. For this reason, atmospheric probes instrumented for spectral measurements should probably incorporate heat-sink-type thermal protection to avoid contamination of the shock layer with ablation vapors.

References

1. Arnold, J. O., Reis, V. H., and Woodward, H. T.: Studies of Shock-Layer Radiation of Bodies Entering Planetary Atmospheres; AIAA Journal, Vol. 3, No. 11, November 1965.

2. James, C. W.: Experimental Study of Radiative Transport From Hot Gases Simulating in Composition the Atmospheres of Mars and Venus; AIAA Journal, Vol. 2, No. 3, March 1964.

3. Thomas, G. M., and Menard, W. A.: Total Radiation Heat Transfer Gage for Hypervelocity Shock Tube Experiments; JPL TR No. 32-636, August 1964.

4. Winovich, W., and Croce, P. A.: Spectroscopic Study of the Gas-Cap Radiation Intensity for Simulated Martian Atmospheric Probes. Paper presented at Symposium on Interdisciplinary Aspects of Radiative Energy Transfer, Philadelphia, Pa., Feb. 24-26, 1966.

AAA029-1

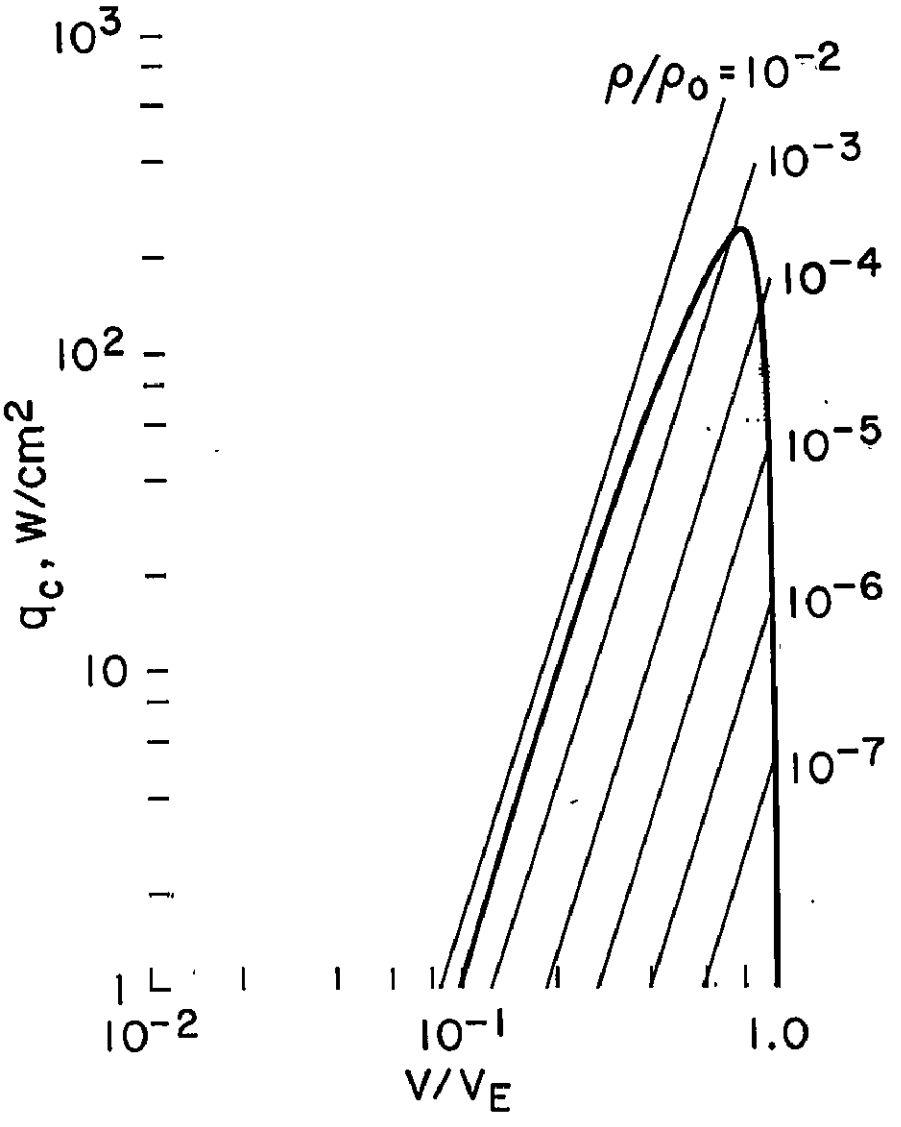

46% CO_2 – 23% N_2 – 31% A

ENTRY VELOCITY: 6.7 km/sec

SCALE HEIGHT: 8 km

RADIUS: 30 cm

NATIONAL AERONAUTICS AND SPACE ADMINISTRATION
AMES RESEARCH CENTER, MOFFETT FIELD, CALIFORNIA

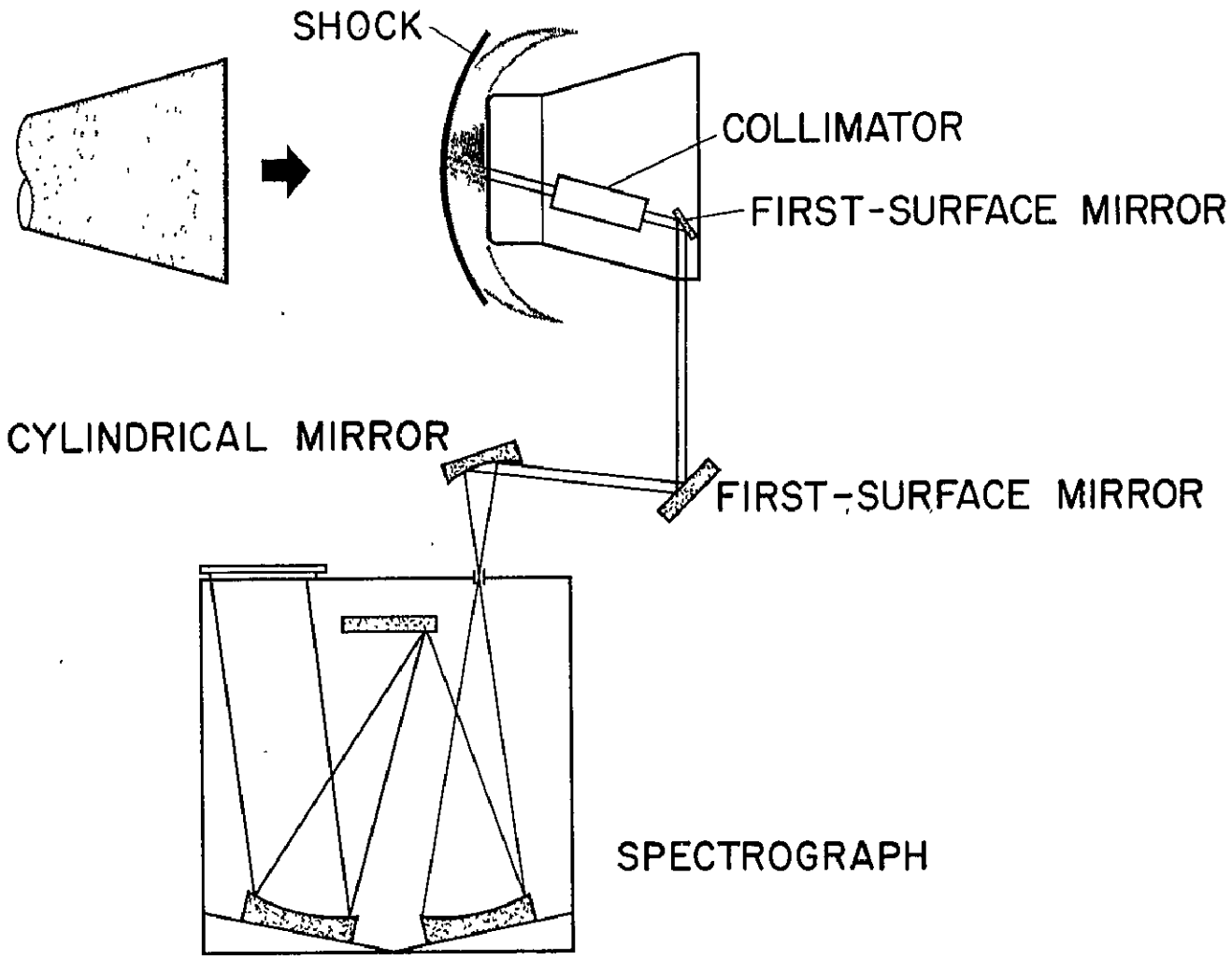

NATIONAL AERONAUTICS AND SPACE ADMINISTRATION
AMES RESEARCH CENTER, MOFFETT FIELD, CALIFORNIA

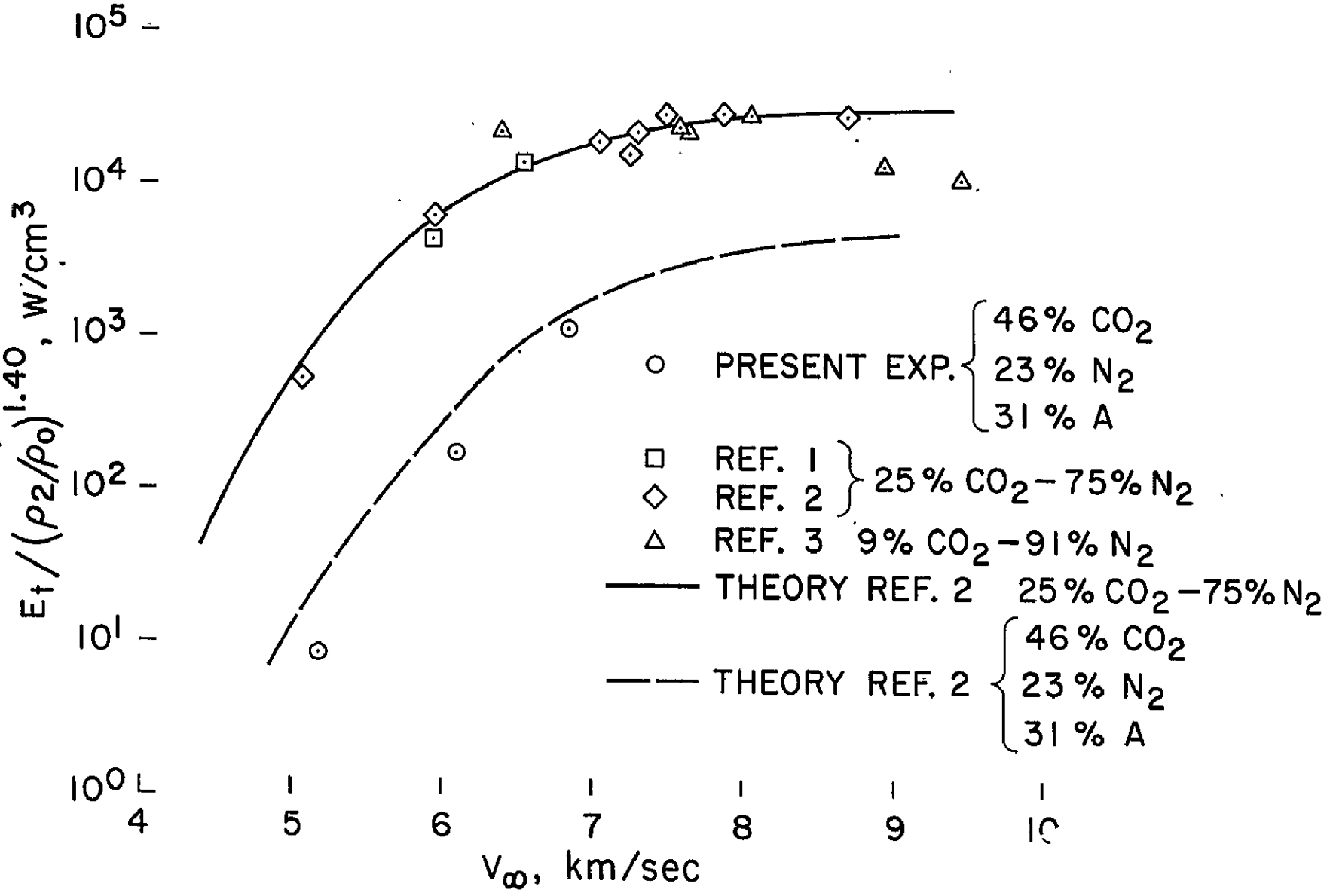

NATIONAL AERONAUTICS AND SPACE ADMINISTRATION
AMES RESEARCH CENTER, MOFFETT FIELD, CALIFORNIA

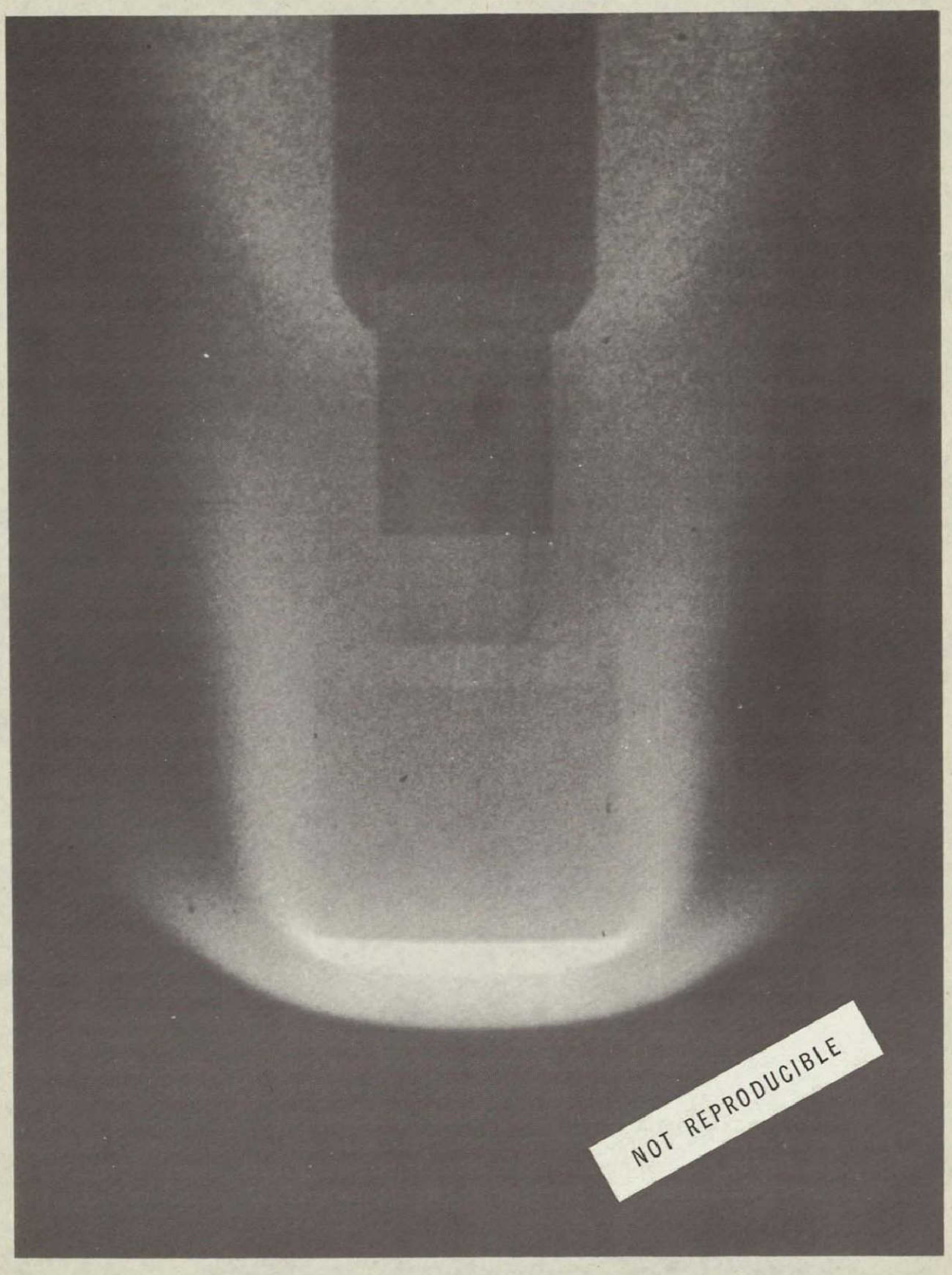

GAS: 7 % CO_2 – 91% N_2 – 2 % A; V_∞ = 8.37 km/sec; ρ_∞/ρ_0 = 1.60×10^{-5}

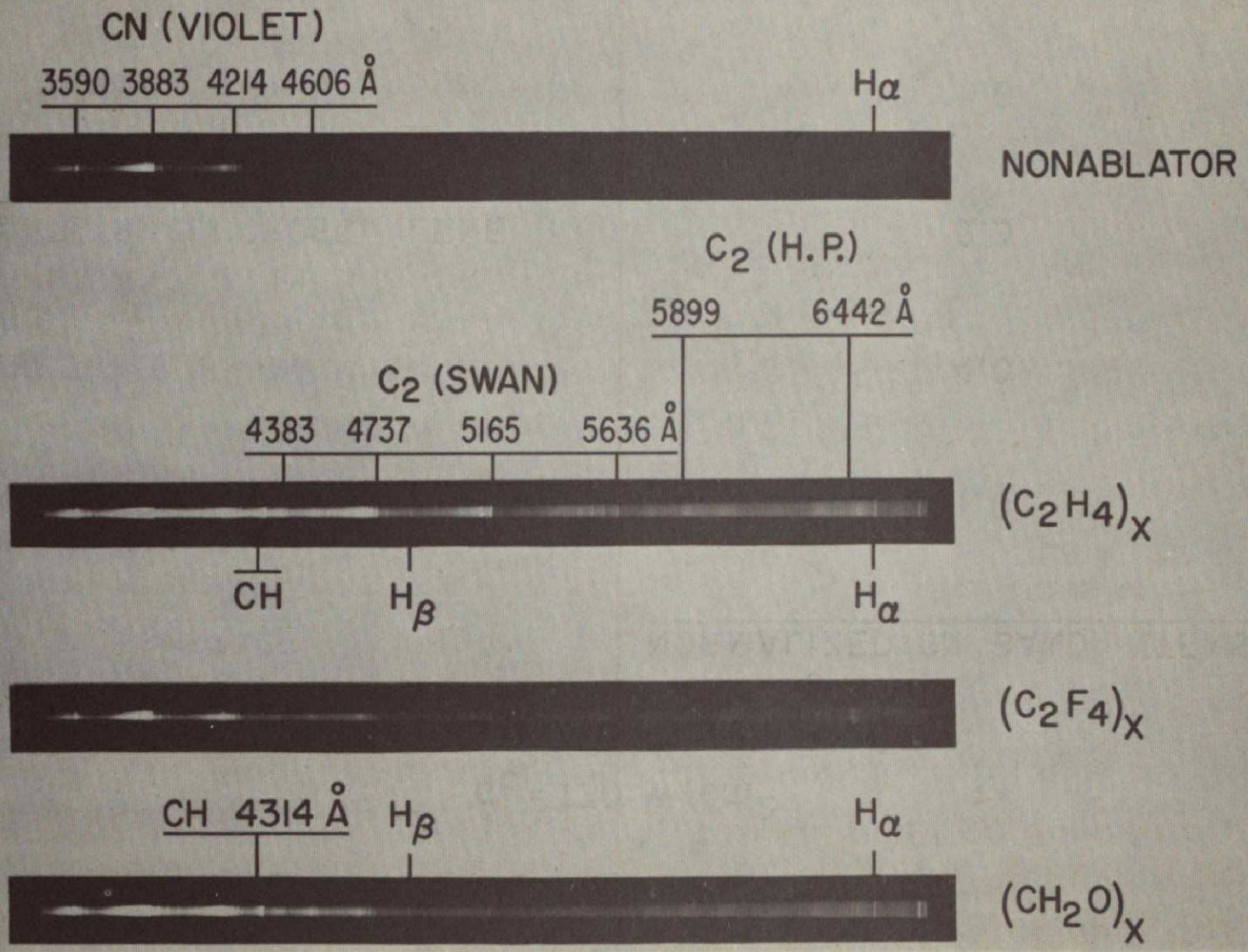

NATIONAL AERONAUTICS AND SPACE ADMINISTRATION
AMES RESEARCH CENTER, MOFFETT FIELD, CALIFORNIA

$q_c = 170\ W/cm^2$

$h_t = 36\ MJ/kg\ (8.5\ km/sec)$

SURFACE	NORMALIZED CN BAND INTENSITY
NONABLATOR	1.0
POLYETHYLENE	4.0
POLYTETRAFLUOROETHYLENE	2.3
POLYFORMALDEHYDE	3.0

NATIONAL AERONAUTICS AND SPACE ADMINISTRATION
AMES RESEARCH CENTER, MOFFETT FIELD, CALIFORNIA

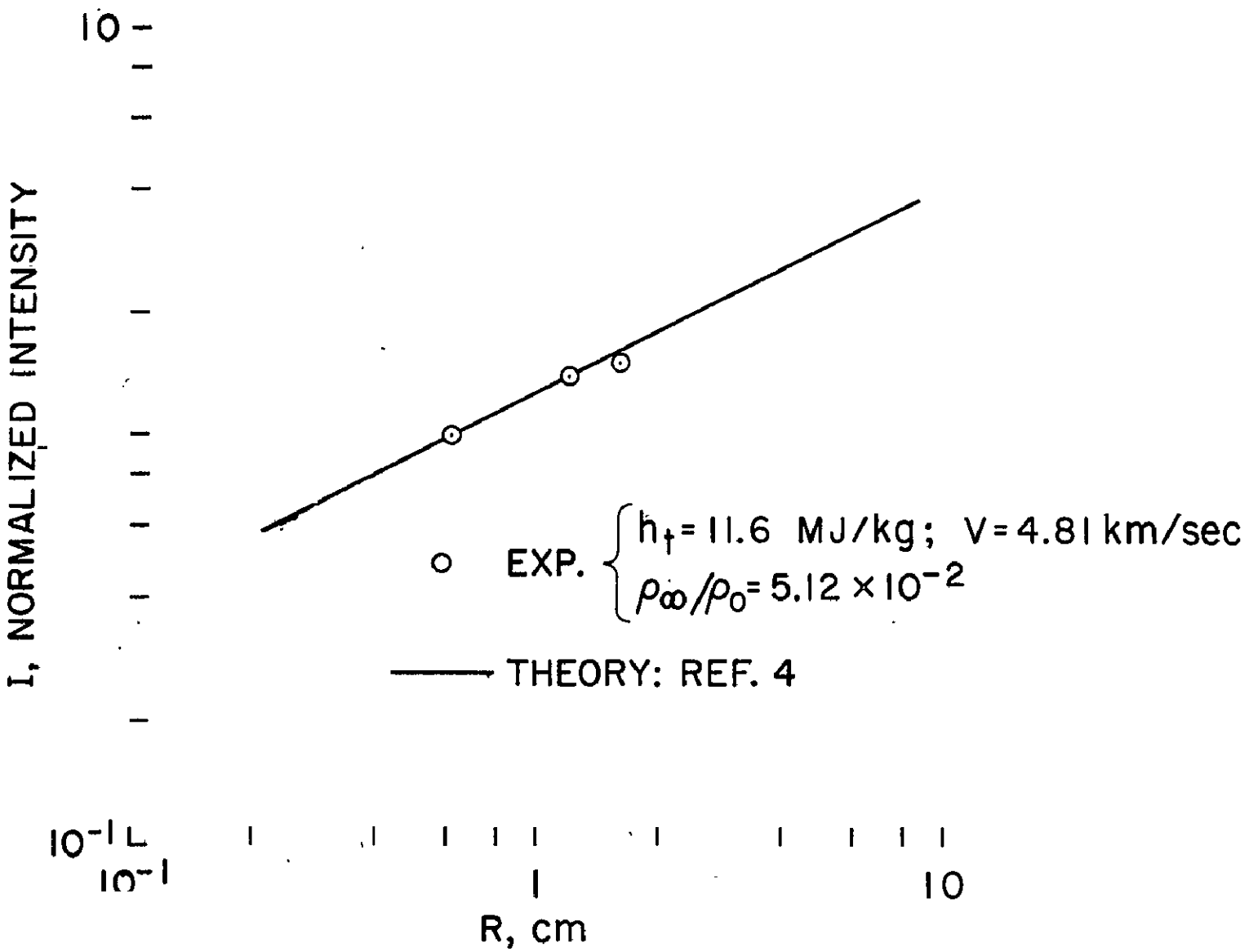

NATIONAL AERONAUTICS AND SPACE ADMINISTRATION
AMES RESEARCH CENTER, MOFFETT FIELD, CALIFORNIA

$V_\infty = 5.6$ km/sec

CASE	R_C, cm	ρ_∞/ρ_0	$\frac{E_{GAS\ CAP}}{E_{GAS\ CAP} + E_{ABL.\ VAPOR}}$
ARC JET	20	10^{-5}	.25
BALLISTIC RANGE	2	10^{-2}	.91
FULL SCALE			
a. PEAK HTG.	30	10^{-3}	.80
b. PEAK HTG.- 4sec	30	10^{-5}	.29

Abstract to be presented at

Fifth NASA Intercenter and Contractor

Conference on Plasma Physics

to be held at Washington, D. C.

May 24-26, 1966

EFFECTS OF TURBULENCE IN CONSTRICTED-ARC PLASMA GENERATORS

By Velvin R. Watson*

National Aeronautics and Space Administration
Ames Research Center
Moffett Field, Calif.

The first constricted-arc plasma generators that were constructed at Ames were operated at sufficiently low Reynolds Numbers that arc-column theories based on laminar flow yielded fair predictions of their performance (refs. 1 - 4). However, these theories do not predict properly the performance of the larger plasma generators at larger flow rates. For example, the experimental performance of a 1-inch diameter constricted-arc plasma generator operated at a mass flow of 65 grams per second of nitrogen is not predicted accurately by numerical calculations for a theoretical model that assumes laminar flow, as illustrated in figure 1. One possible cause of this discrepancy is the effect of turbulent mixing on energy transfer processes within the arc column.

To illustrate qualitatively the effects that turbulence may have, turbulent mixing was included in the theoretical model using Prandtl's Mixing Length Theory wherein momentum and energy transfer are proportional to the density and the velocity gradients. This turbulent mixing throughout the arc column appreciably changes the calculated enthalpy and mass flow distributions with length and radius, as shown in figure 2. The calculated variation of average enthalpy with length is compared with experiment in figure 3.

---

*Research Scientist

The addition of turbulent mixing to the theoretical analysis produces good, though perhaps fortuitous, agreement with the data.

The additional energy transfer due to turbulence shortens the characteristic constrictor length required for the enthalpy to approach an asymptotic limit, and it also reduces the value of this asymptotic enthalpy for a given current and mass flow. Thus the maximum enthalpy that could be contained in a constrictor having turbulent flow throughout the arc column should be less than would be possible were the flow entirely laminar.

An estimate of the reduction in the achievable enthalpy, and of other arc-column parameters, for the turbulent regime can be obtained from a one-dimensional analysis wherein the constrictor heating rate is assumed to vary in proportion to the bulk enthalpy and the specific mass flux. For a given maximum heat transfer rate to the constrictor wall, the solution for this one-dimensional model yields a maximum achievable enthalpy that is inversely proportional to the specific mass flux. Because, in a constricted-arc plasma generator the flow is aerodynamically choked, the constrictor inlet pressure can also be related to the specific mass flux and enthalpy, and a plot can be made of the maximum enthalpy that can be contained as a function of pressure, as shown in figure 4. In figure 4, the location of the turbulent containment limit was obtained by scaling from experimental data, and the laminar limit was obtained from reference 5. The Reynolds Number per cm is also shown on the abscissa of this figure. This figure illustrates that the limit formerly predicted from laminar theory is reduced appreciably by turbulence.

The one-dimensional solution also yields a characteristic constrictor length that is independent of flow rate and proportional only to the constrictor diameter. In contrast, for the laminar regime the constrictor length was proportional to the flow rate and independent of the diameter. The predicted characteristic length as a function of flow rate and diameter for both regimes is shown on figure 5.

These results suggest that if turbulent transfer processes occur in the arc column, the test Reynolds Numbers can be increased while maintaining a high enthalpy by using larger diameter constrictors and by reducing the ratio of the nozzle exit diameter to the constrictor diameter.

References

1. Stine, H. A., and Watson, V. R.: The Theoretical Enthalpy Distribution of Air in Steady Flow Along the Axis of a Direct-Current Electric Arc, NASA TN D-1331, August 1962.

2. Stine, H. A., Watson, V. R., and Shepard, C. E.: Effect of Axial Flow on the Behavior of the Wall-Constricted Arc, Paper presented at AGARD Specialists' Meeting on Arc Heaters and MHD Accelerators for Aerodynamic Purposes, Rhode-Saint-Genese, Belgium, September 21-23, 1964.

3. Shepard, C. E., Watson, V. R., and Stine, H. A.: Evaluation of a Constricted-Arc Supersonic Jet, NASA TN D-2066, January 1964.

4. Watson, V. R.: Comparison of Detailed Numerical Solutions with Simplified Theories for the Characteristics of the Constricted-Arc Plasma Generator, 1965 Heat Transfer and Fluid Mechanics Institute Meeting, June 21-23, 1965, Los Angeles, California.

5. Cann, G. L., and Buhler, R. D.: A Survey and Prediction of the Performance Capability of Coaxial Arc Heaters, AGARDograph 84, September 1964.

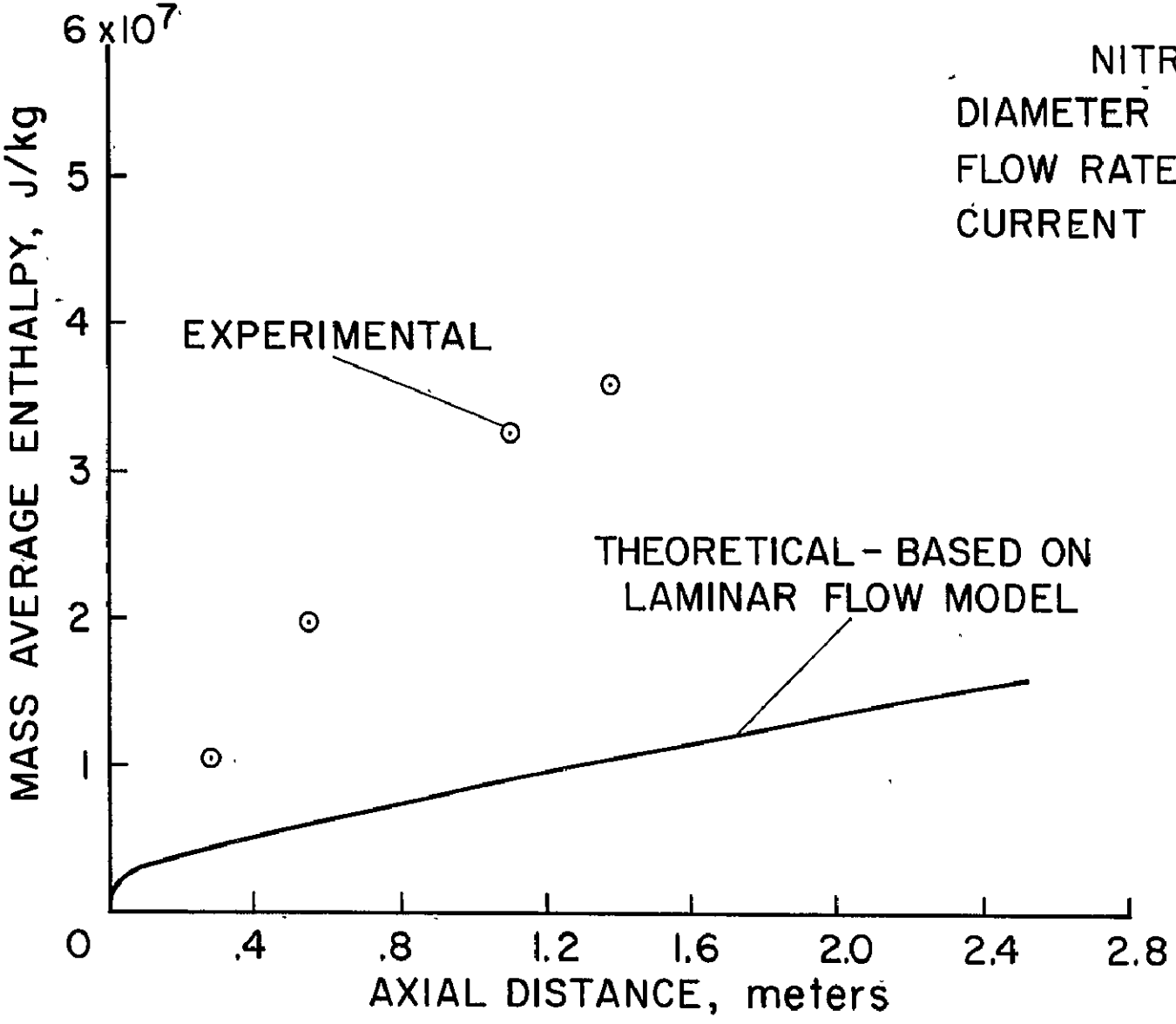

NATIONAL AERONAUTICS AND SPACE ADMINISTRATION
AMES RESEARCH CENTER, MOFFETT FIELD, CALIFORNIA

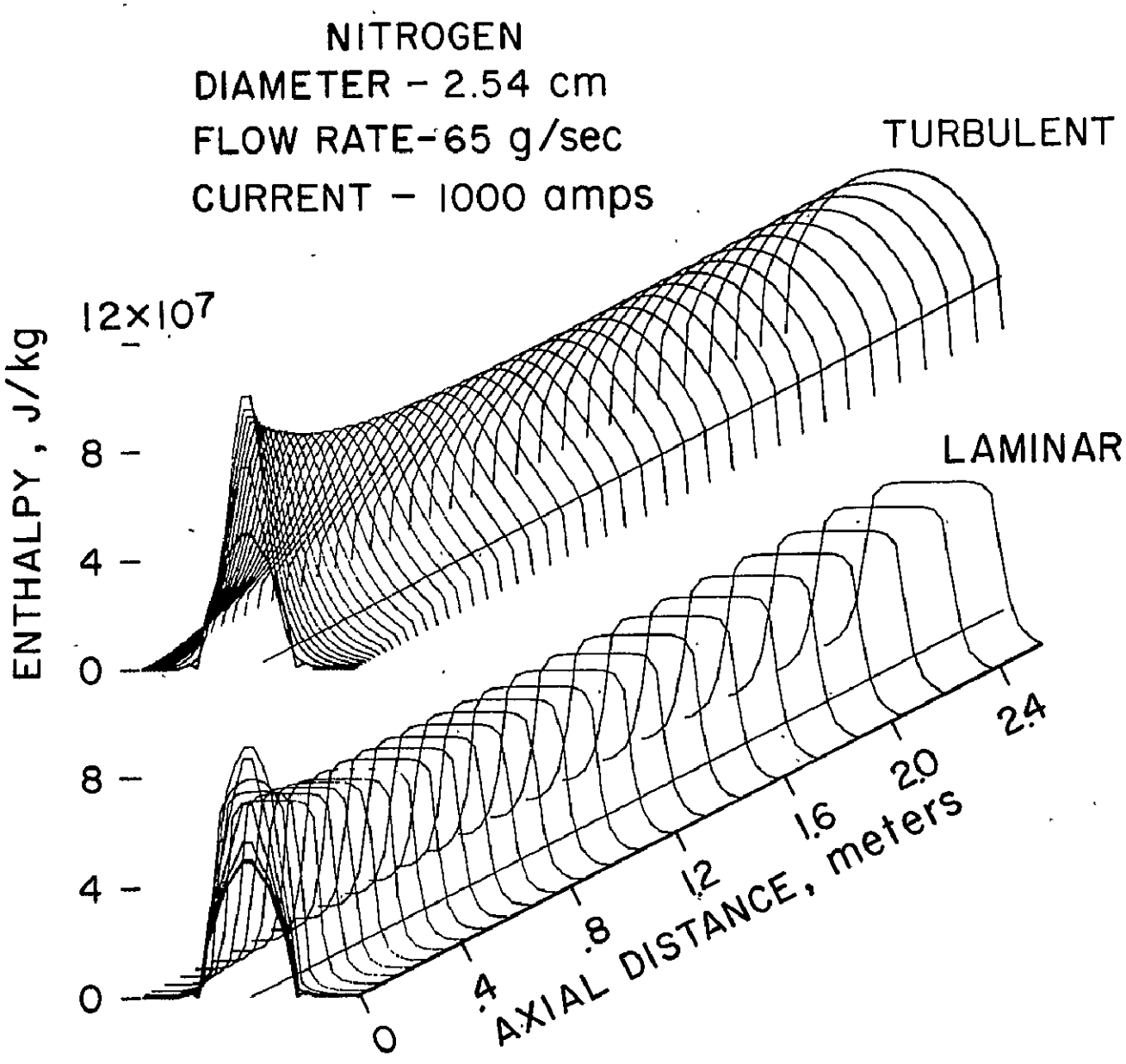

NATIONAL AERONAUTICS AND SPACE ADMINISTRATION
AMES RESEARCH-CENTER, MOFFETT FIELD, CALIFORNIA

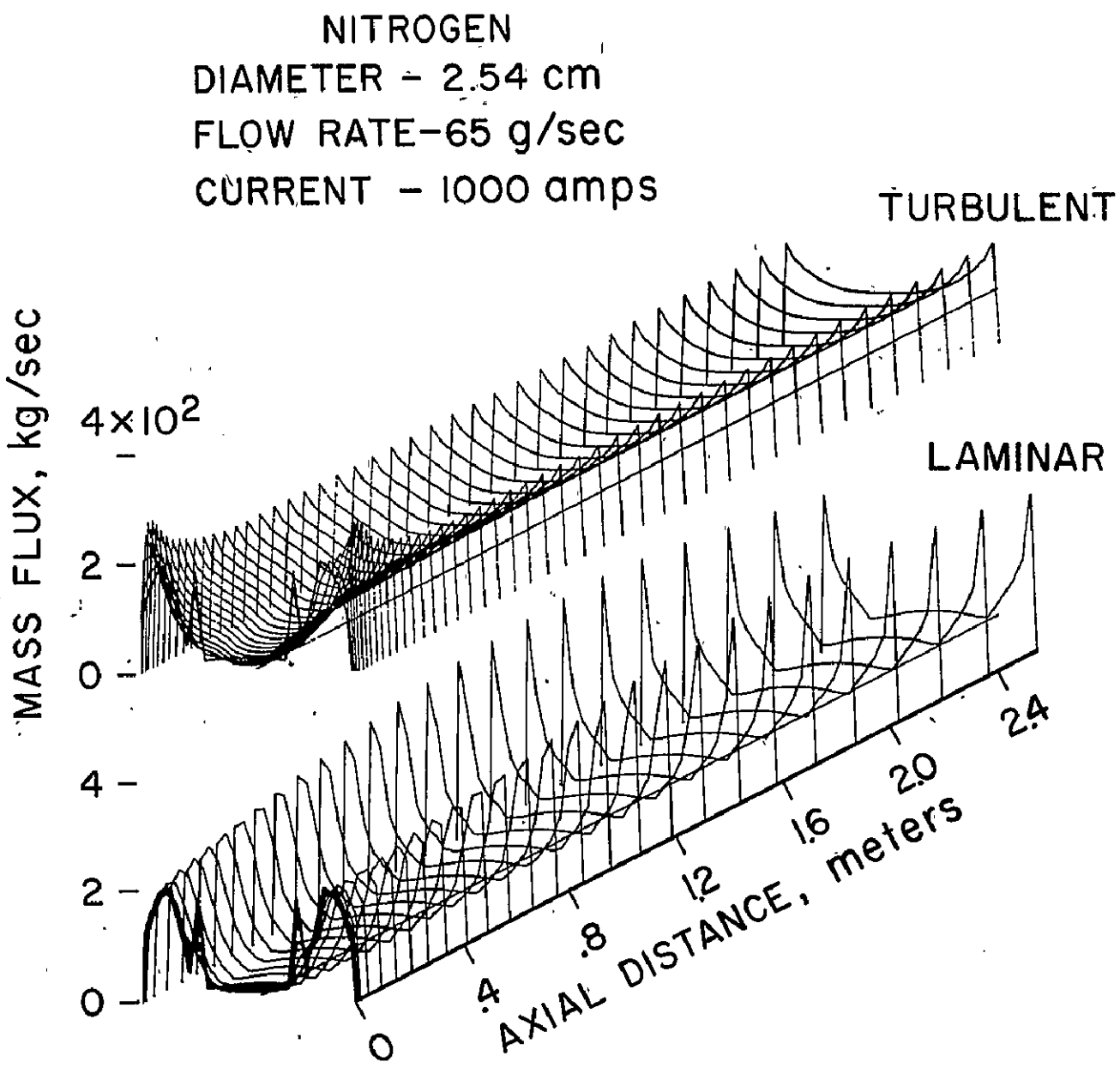

NATIONAL AERONAUTICS AND SPACE ADMINISTRATION
AMES RESEARCH CENTER, MOFFETT FIELD, CALIFORNIA

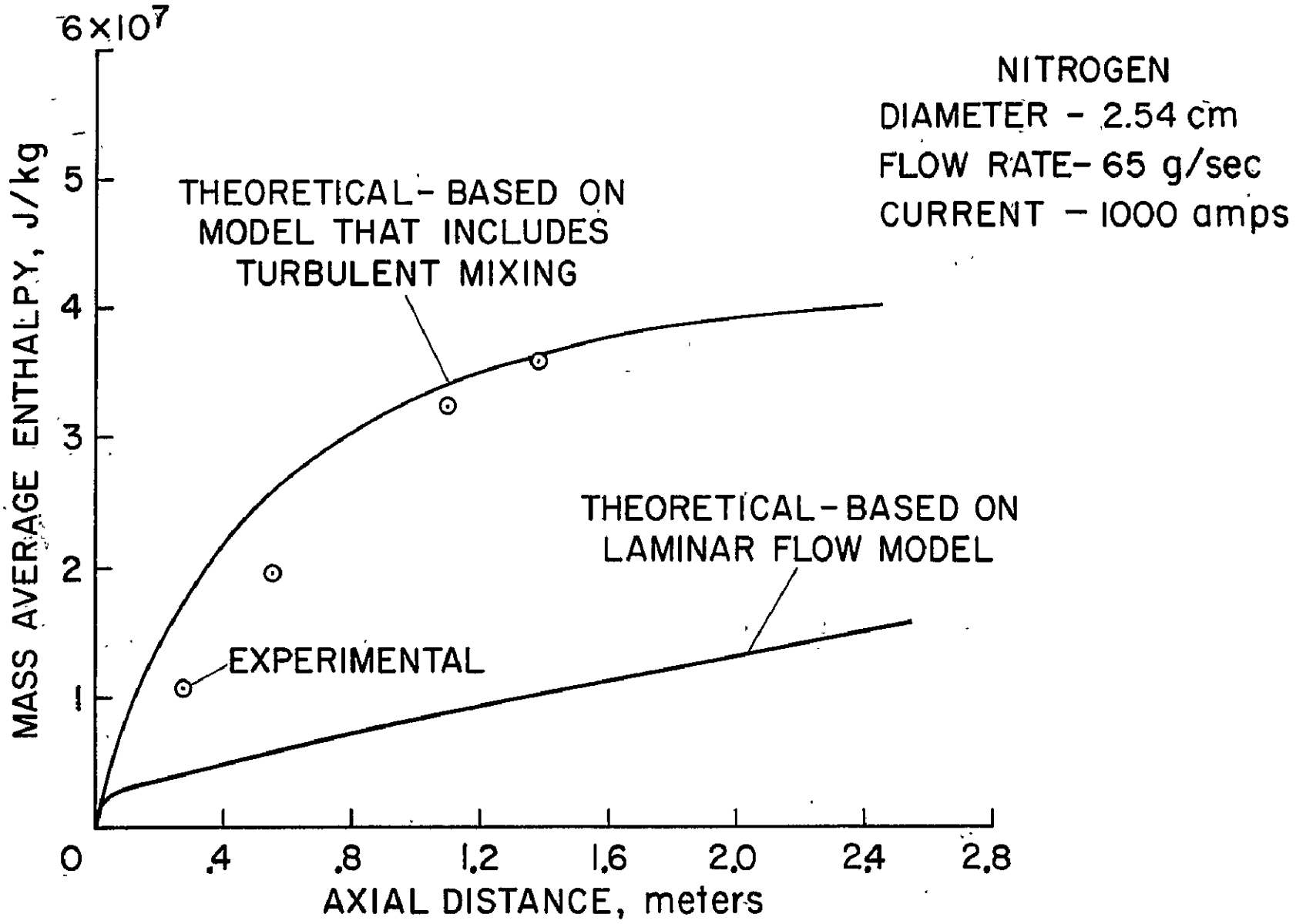

NATIONAL AERONAUTICS AND SPACE ADMINISTRATION
AMES RESEARCH CENTER, MOFFETT FIELD, CALIFORNIA

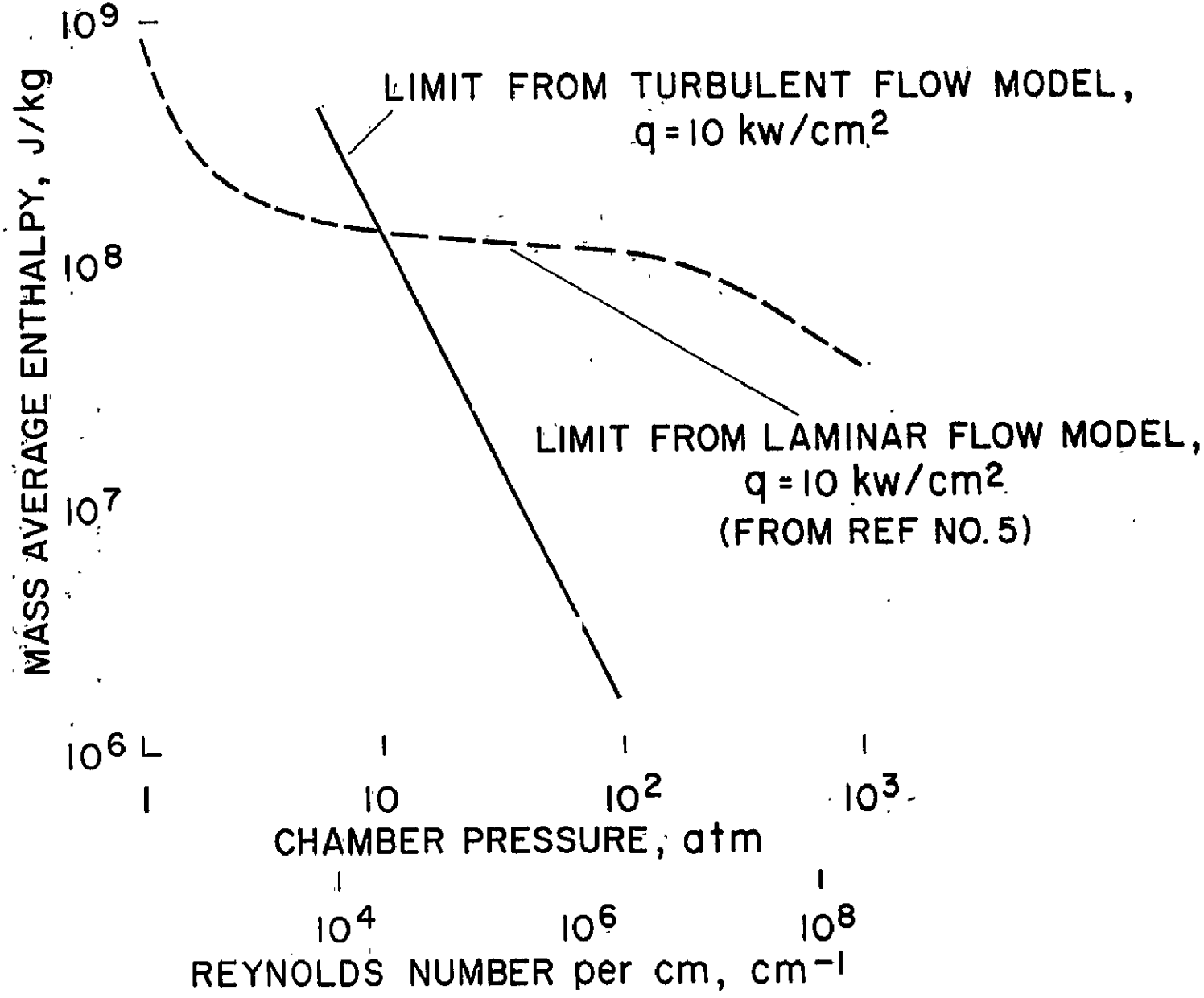

NATIONAL AERONAUTICS AND SPACE ADMINISTRATION
AMES RESEARCH CENTER, MOFFETT FIELD, CALIFORNIA

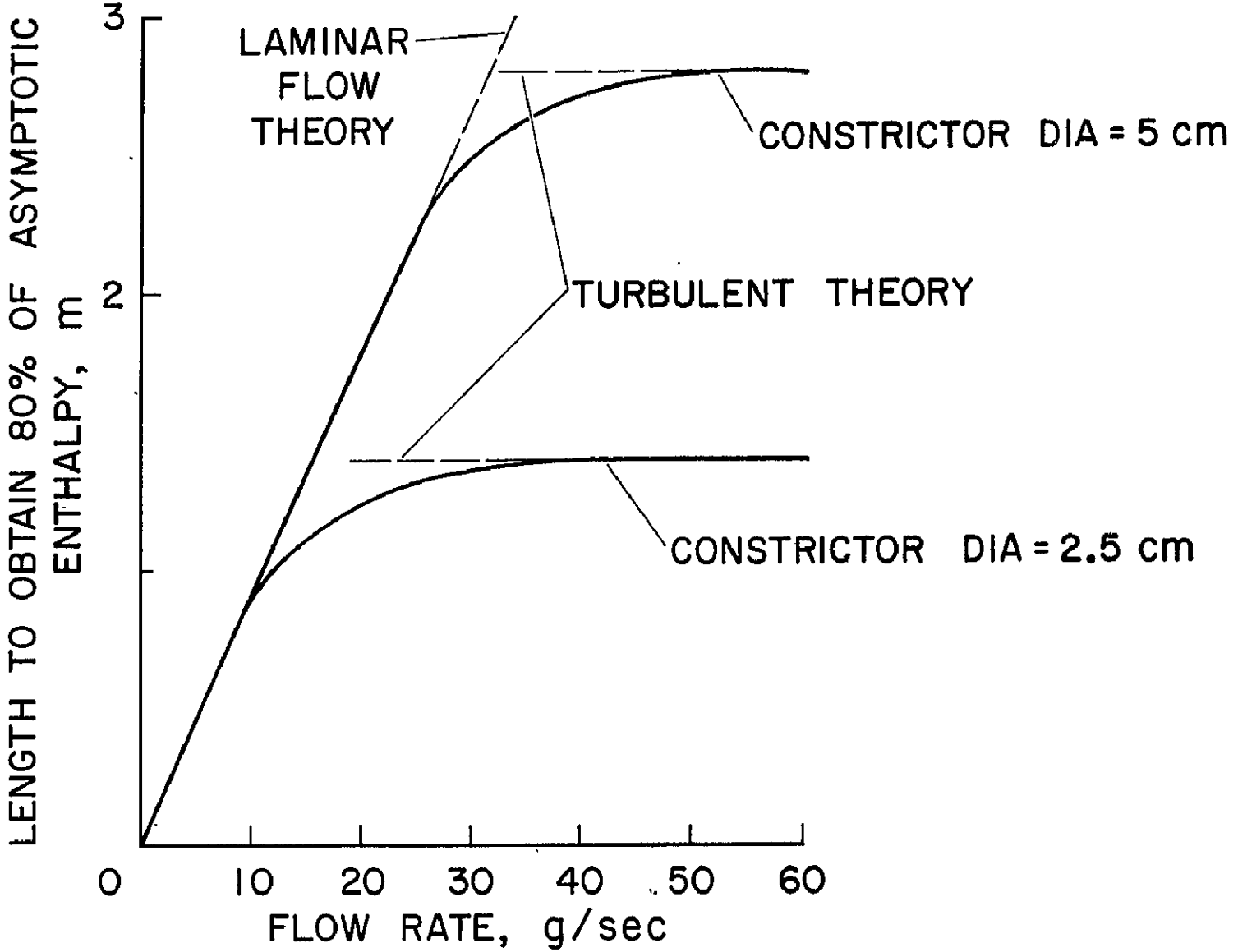

NATIONAL AERONAUTICS AND SPACE ADMINISTRATION
AMES RESEARCH CENTER, MOFFETT FIELD, CALIFORNIA

Abstract to be presented at

Fifth NASA Intercenter and Contractor

Conference on Plasma Physics

to be held at Washington, D. C.

May 24-26, 1966

BEHAVIOR OF FARADAY CUPS IN PLASMA BEAMS

By William C. Pitts* and Earl D. Knechtel*

National Aeronautics and Space Administration
Ames Research Center
Moffett Field, Calif.

Basically the Faraday cup is a very simple device for measuring the directed energy for a single species of charged particle. Essentially it consists of a flat-plate charge collector enclosed in a cup. The beam of ions or electrons to be analyzed enters an aperture at the open end of the cup where they are slowed down by a retarding potential on the collector plate. The energy distribution of the beam is obtained from a characteristic curve of the collector plate current as a function of the plate retarding potential. Ideally, for a monoenergetic beam, this characteristic curve should be perfectly flat until the retarding potential just equals the ion energy in electron volts, at which point the plate current should abruptly fall to zero. Many factors make it impossible to achieve a beam with this ideal energy distribution. In addition the Faraday cup itself may introduce varying effects on the apparent energy distribution. The present paper will discuss some of the problems encountered in using a Farday cup to determine energy distribution in a plasma beam of accelerated argon ions.

Briefly, the plasma device used in the present investigation consists of a plasma source, an ion accelerating system, and a source of electrons for neutralizing the space charge within the

---

*Research Scientist

accelerated ion beam. The ion beam is about 1 inch in diameter and has a number density of the order of 10^8 ions per cubic centimeter with directed energies variable between 10 and 250 ev. The beam consists of argon ions that flow through a background of argon gas at 2×10^{-4} Torr pressure.

A nonideal Faraday-cup characteristic along with the simple cup configuration used to obtain the curve is shown in figure 1. This cup consists of the collector plate and a grid (see inset) at negative potential to reject the electrons. Both are enclosed in a nonconducting cylinder. Several deviations from the ideal curve are evident. Near zero potential some low energy ions resulting from charge exchange appear. Above 150 volts the plate current is negative as a result of collecting secondary electrons from the electron filtering grid. The initial slope and the premature rounding-off of the curve are due to various forms of beam divergence, both real and induced by the above cup configuration. Since beam divergence has created the major difficulties, the remainder of the paper will concentrate on this problem.

The difficulty associated with divergence results from the ions approaching the Faraday cup with a component of velocity transverse to the axis of the cup as well as parallel to the axis. This transverse velocity component is not altered by the retarding plate potential so that the ions will follow a curving path toward the walls of the cup. The result is a washed-out Faraday-cup characteristic curve with an indicated ion energy that is more nearly associated with the axial velocity component than the total velocity.

Several factors can cause divergence of the ion beam. These include: (a) original plasma beam divergence due to imperfections in the accelerating system and natural repulsion of the beam ions, (b) scattering of ions by the neutral background gas, (c) interference of the plasma beam by the presence of the Faraday cup, (d) lens effect of the cup aperture, (e) nonuniform fields within the cup. The first two of these factors are not really attributable to the cup but must be considered in establishing the ultimate sharpness of the characteristic curve. The first difficulty inherent to the beam can be partially compensated for by using a small cup aperture and aligning the cup axis with the local velocity vector. The second can be eliminated if the background pressure can be reduced sufficiently. The cup interference problem can be minimized by maintaining the shell of the cup at the plasma potential. The lens aperture will always cause some divergence of the beam as it enters the cup but the effect can be minimized by reducing the potential gradients on both sides of the aperture. The problem of nonuniform fields within the cup is itself due to

to several factors: (a) wall effects, (b) fringing from element edges, (c) dirty surfaces, (d) poorly aligned elements. The wall effects can be a serious problem. As the ions are repelled by the plate a certain portion of them will go to the wall. If the wall is a nonconductor, a charge will accumulate until no more ions can pass through the resulting field to the wall. Entering ions will see this field and be deflected from the axial direction or if the cup diameter is sufficiently small, the field can close across the cup and prevent any ions from reaching the plate. A solution to this problem is to make the cup diameter large compared to the aperture and internal beam diameter and to make the wall area small by placing the elements close together. This modification will also help the fringing problem by removing the element edges from the beam region. Dirty surfaces can be a problem because they can sustain potential gradients even on supposedly conducting surfaces. The obvious solution is to maintain clean conditions and to use materials in the cup that do not contaminate easily. Another possible remedy is to use small apertures instead of wire mesh for the grids. This, however, leads to problems of optical element alignment since each aperture behaves as an electrostatic lens (see ref. 1).

On the basis of the preceding considerations, an improved Faraday cup was built and tested. The cup to aperture radius ratio was increased to 9, and the axial spacing of the elements was reduced to 1/4 the cup diameter. The electron filtering grid was made of very fine tungsten screen, 90-95 percent transparent to minimize secondary electron formation. The collector plate was surrounded by a guard ring which was maintained at the same potential as the collector for the purpose of minimizing fringing effects at the collector. A characteristic curve for this modified Faraday cup is shown in figure 2. The energy spread indicated by the modified cup is about 3.5 ev compared to between 20 and 25 ev for the original cup under similar plasma conditions. There was no evidence of secondary electron current to the plate and the low potential slope of the characteristic curve in the figure was eliminated.

References

Simpson, J. Arol: Design of Retarding Field Energy Analyzer, The Review of Scientific Instruments, Vol. 32, No. 12, Dec. 1961.

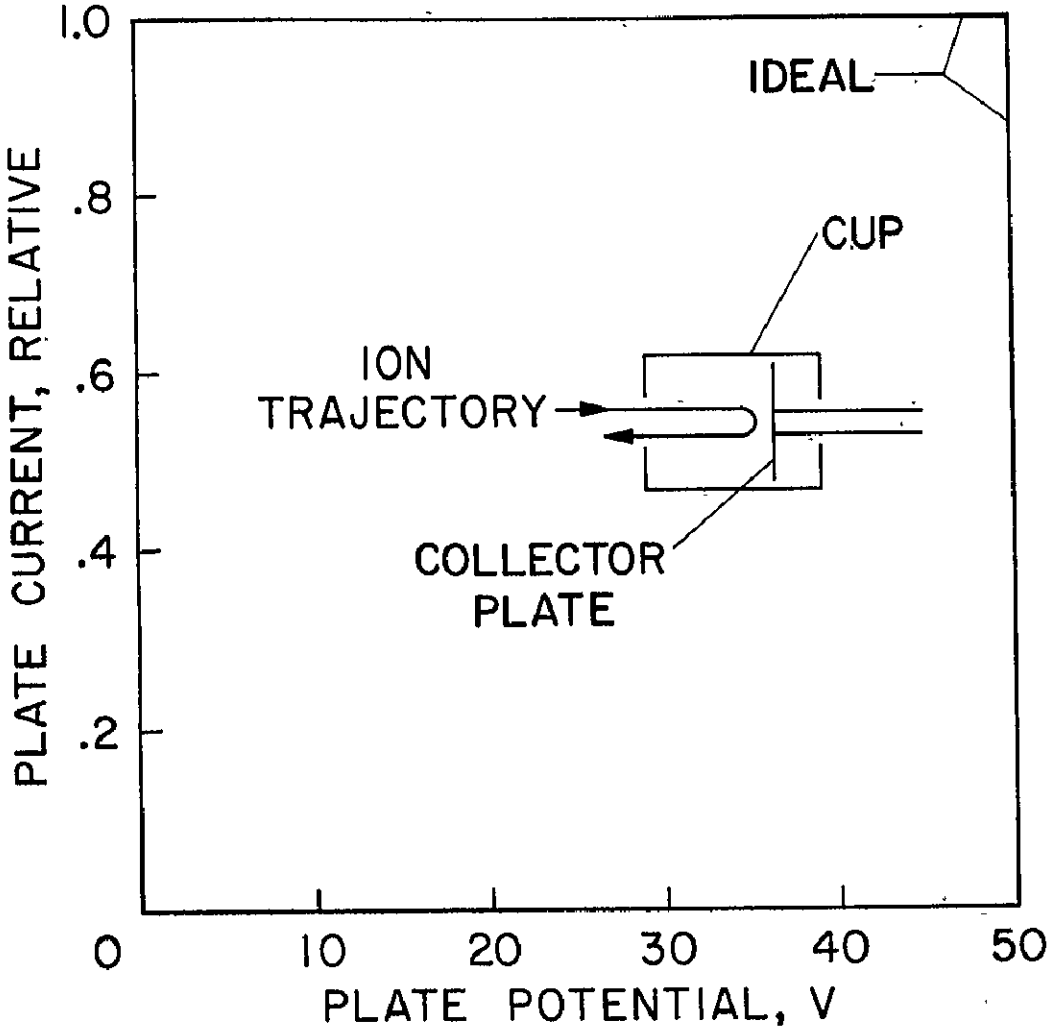

NATIONAL AERONAUTICS AND SPACE ADMINISTRATION
AMES RESEARCH CENTER, MOFFETT FIELD, CALIFORNIA

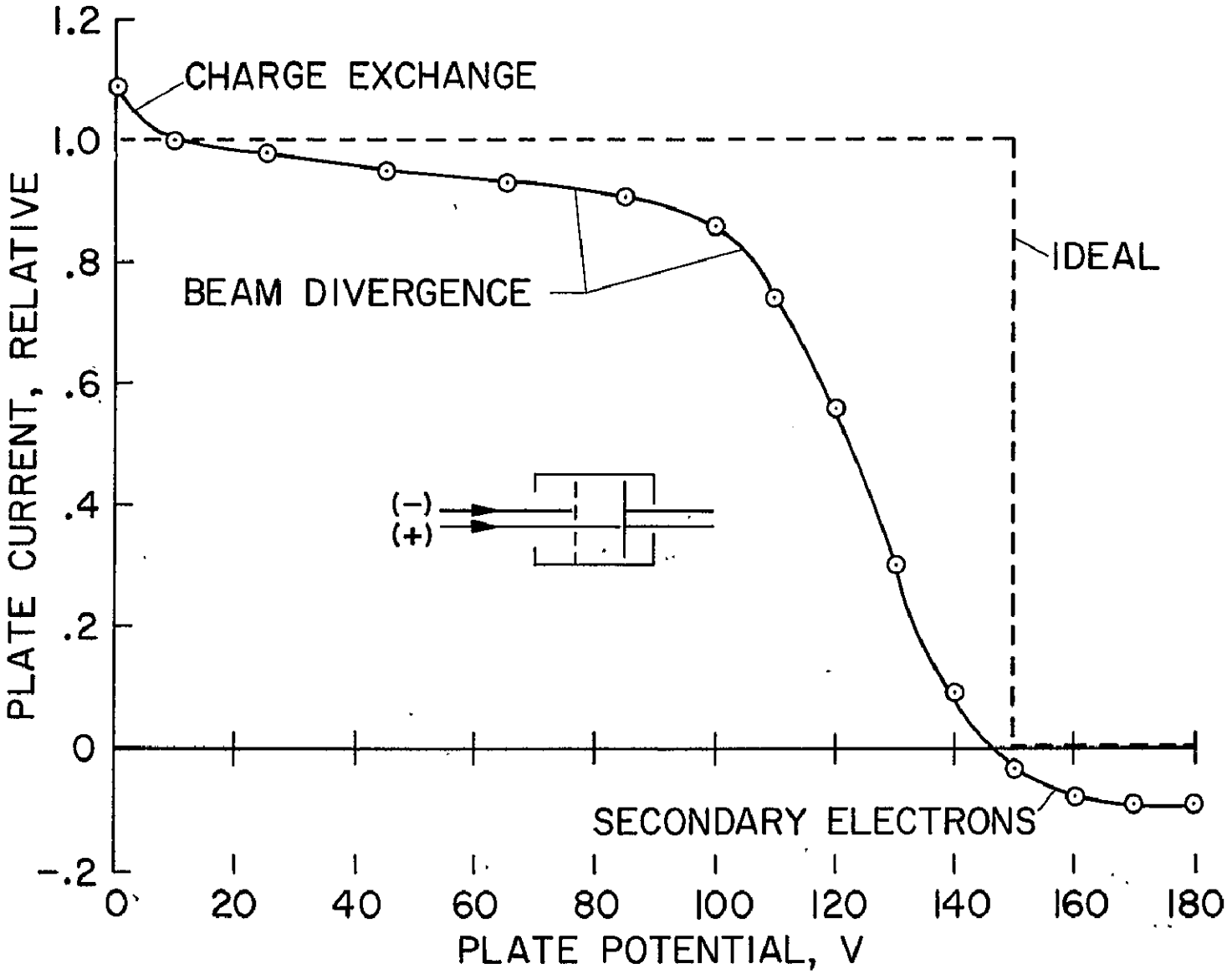

NATIONAL AERONAUTICS AND SPACE ADMINISTRATION
AMES RESEARCH CENTER, MOFFETT FIELD, CALIFORNIA

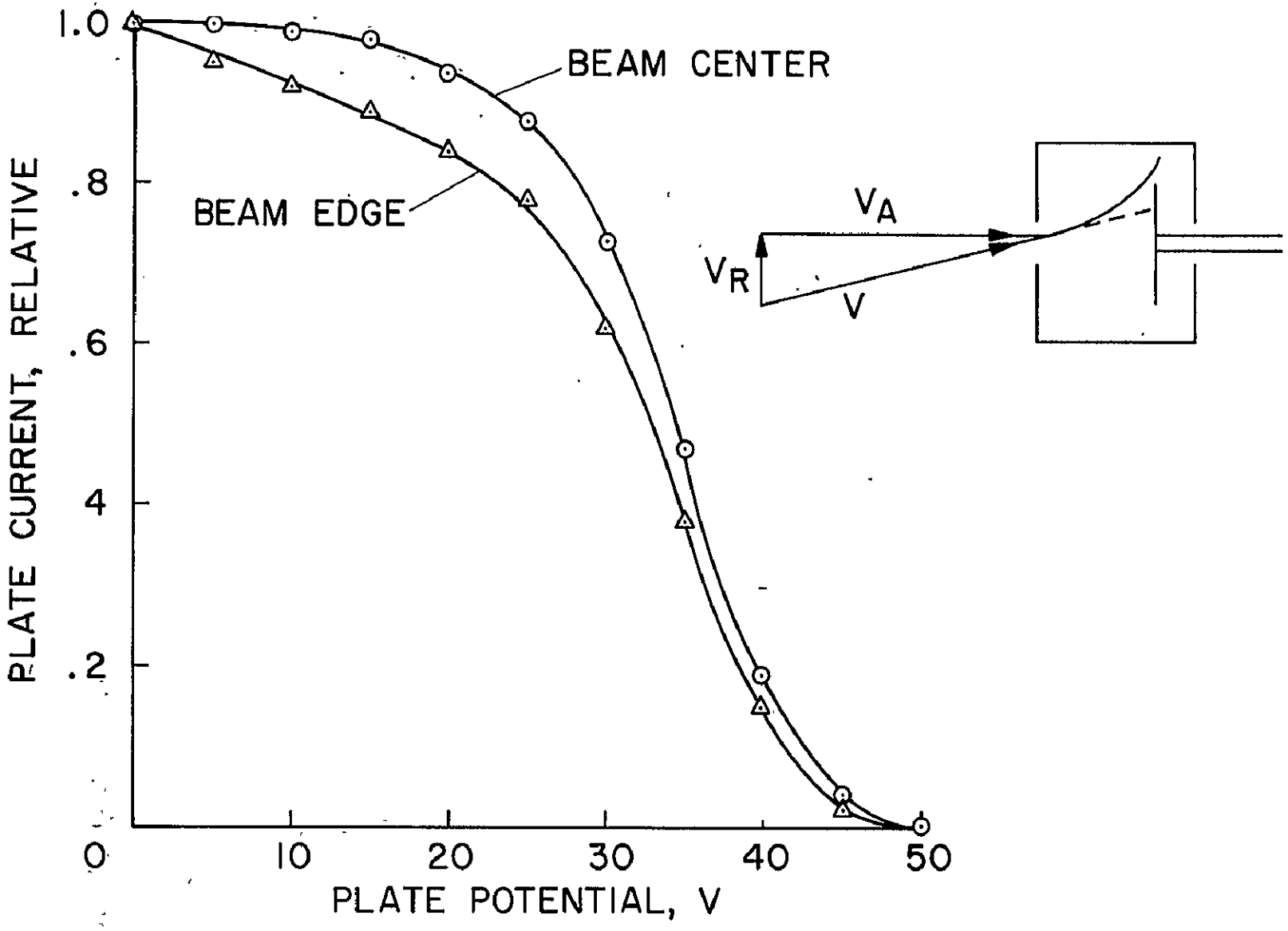

NATIONAL AERONAUTICS AND SPACE ADMINISTRATION
AMES RESEARCH CENTER, MOFFETT FIELD, CALIFORNIA

1. ORIGINAL PLASMA BEAM DIVERGENCE

2. SCATTERING OF IONS BY NEUTRAL BACKGROUND GAS

3. INTERFERENCE OF PLASMA BEAM BY CUP

4. CUP APERTURE LENS EFFECT

5. NONUNIFORM FIELDS WITHIN CUP

    a) WALL EFFECTS

    b) FRINGING FROM ELEMENT EDGES

    c) DIRTY SURFACES

    d) POORLY ALIGNED ELEMENTS

NATIONAL AERONAUTICS AND SPACE ADMINISTRATION
AMES RESEARCH CENTER, MOFFETT FIELD, CALIFORNIA

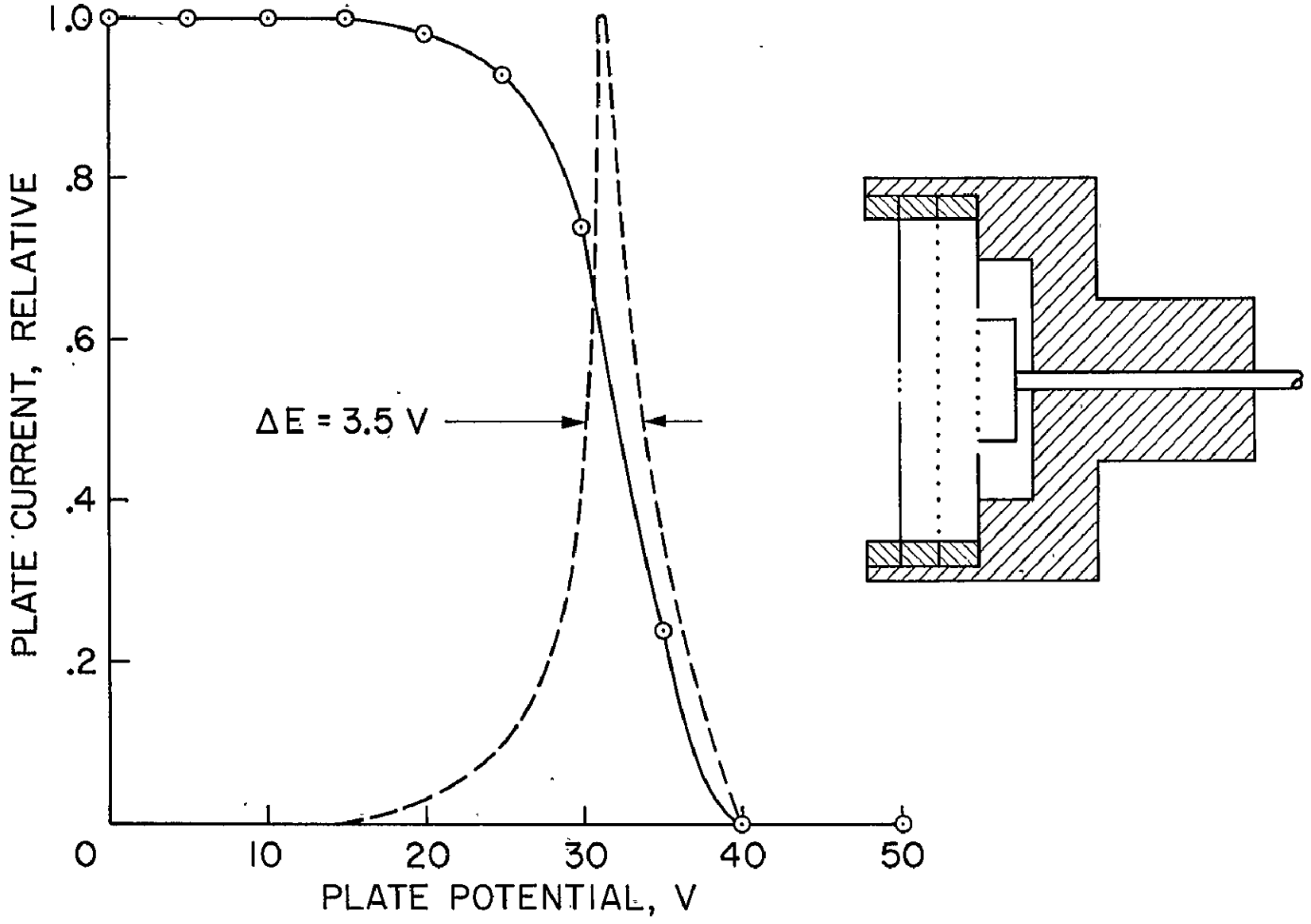

NATIONAL AERONAUTICS AND SPACE ADMINISTRATION
AMES RESEARCH CENTER, MOFFETT FIELD, CALIFORNIA

Abstract to be presented at

Fifth NASA Intercenter and Contractor

Conference on Plasma Physics

to be held at Washington, D. C.

May 24-26, 1966

FLOW-SWALLOWING ENTHALPY PROBES

By Lewis Anderson* and Robert Sheldahl*

National Aeronautics and Space Administration
Ames Research Center
Moffett Field, Calif.

Present plasma-generation facilities produce high-enthalpy, low-density plasma streams, but the local distributions of total enthalpy in the test region have not been determined accurately by direct measurement. The methods used presently to determine enthalpy are based on indirect measurements such as over-all heat and power balances on the system, heat-transfer rate and impact pressure measurements combined with heat-transfer theories to provide local enthalpy distributions, spectroscopic observations and related analytic assumptions, and combinations of these methods. Because of the many uncertainties in these determinations, a flow-swallowing method for directly measuring enthalpy in constricted-arc plasma jets is under development.

In the constricted-arc facility shown in figure 1, tangentially injected gas is heated by passing current through a constrictor to 23 anodes near the exit. The supersonic stream is expanded from a throat diameter 1.27×10^{-2} meters to an exit 15.5×10^{-2} meters through a 15° half-angle cone. The plasma is then discharged into a free-jet test chamber. The test chamber conditions are as follows: (1) a bulk stream enthalpy range from 7×10^{6} to 80×10^{6} Joules/kilograms, based on a heat balance for power input minus losses and gas flow rate, (2)

---

*Research Scientist

$2h_{av} < h_{\ell} < 4h_{av}$, based on heating rate and impact pressure profiles, (3) impact pressure range of 8×10^{-3} to 5×10^{-2} atms., (4) stagnation point heat-transfer rate up to 2 kw/cm^2.

Because of the uncertainties in the indirect measurements for determination of enthalpy, direct methods of sampling the plasma are under consideration. Although a number of "blunt body" or normal-shock-type flow-swallowing enthalpy probes are available, such probes have a number of disadvantages that limit their usefulness in a low-density plasma stream. Some of these disadvantages include: (1) a small captured mass which leads to inaccuracies in mass-flow measurements, (2) uncertainties in location of the dividing stream tube on the probe nose with respect to the sampling orifice and in determining the associated quantity of heat to be attributed to the captured plasma, (3) restrictions on the maximum heat-transfer rates that can be accommodated. To avoid these disadvantages, a probe is under study that promises to (a) capture two orders of magnitude or more mass than comparable blunt probes, (b) allow for accurate definition of the captured stream tube, and (c) consequently permit accurate determination of the heat content of the captured plasma.

The probe system differs from the available probes by utilizing a sharp leading edge as shown in figure 2. Two probes are to be programmed into the plasma in sequence. A water-cooled mass-flow measuring system, as shown in figure 2, will allow the captured plasma to be cooled to a reference temperature and the mass to be determined by using a venturi calibrated for low-density operation. The second probe, of identical aerodynamic shape to the first, is a transient heat-transfer calorimeter. The inner and outer walls are separated by a gap that is maintained at static pressure to minimize heat conduction. The lip is sharp, and the angles are designed so that inner and outer compression surfaces have the same heat-transfer rate. Thus a minimum of asymmetric thermal conduction occurs in the lip region. The leading edges and contraction region will be coated with a non-catalytic silicon monoxide surface to reduce the heat transfer due to heterogeneous surface reactions with the dissociated gas. Thus high local heat-transfer rates near the inlet will be suppressed until a downstream location is reached where the surfaces can be accurately instrumented for heat-transfer rate measurements. The inside dimensions of the probe are designed to position the terminal shock downstream of the contraction, and the subsonic downstream pressure approximates normal shock recovery for the free stream. The terminal shock can be located by adjusting the pumping pressure on the captured stream. By increasing this pressure in the subsonic

section, the length for complete atomic recombinations to occur is minimized.

The first requirement of this design was the survival of a sharp leading edge in the plasma stream. A 15° half-angle water-cooled wedge (shown in figure 3) was placed at the centerline of a plasma stream for 10 minutes duration. The leading edge of this wedge withstood the plasma environment at a heat transfer rate of 1.2×10^{7} watts/m^2 as measured at the stagnation point of a 2.5×10^{-2} m diameter hemisphere.

Preliminary tests of the flow-swallowing calorimeter probe have determined that the stream is captured, that an oblique shock originates at the lip, and that the sharp leading edge will also survive. In this test, the local pressures on the inside compression surface, and in the minimum area section, and the impact pressure of the stream were measured. The measured pressure ratio for the two inside surfaces with respect to impact pressure was 0.42, which indicates that the flow in the minimum section was supersonic.

Heat-transfer rates measured by the transient technique along the subsonic cylindrical portion of the diffuser have determined the length required to permit decay of all of the forms of energy into thermal energy. The results of these preliminary tests are shown in figure 4. The two charts, (a) and (b), illustrate the variation of heat-transfer rate with length for two values of mass flow for a fixed total power input to the plasma stream. Part (a) of this figure shows that heat-transfer rate decreased monotonically in argon. The nitrogen data, however, show a definite discontinuity at a position 0.3 meters from the upstream edge of the subsonic cylindrical section. The discontinuity indicates that atomic recombination is complete at this point, and that all the dissociated energy has been converted into thermal energy. It is interesting to note that the atomic recombination rate

$$N + N + N_2 \xrightarrow{C} 2N_2 + KE$$

can be obtained from the position of this discontinuity in the heat-transfer curve. Even an approximate solution,

$$C \approx \frac{u}{4x\rho^2} ,$$

derived by Dr. Chul Park, gives a reasonable recombination rate for nitrogen. If a mass-averaged velocity defined as

$$u = \frac{\dot{m}}{\rho A} ,$$

then

$$C = \frac{\dot{m}}{4xA\rho^3} \approx 3 \times 10^{15} \frac{(cc)^2}{mole^2 sec}$$

for an estimated terminal shock temperature of 5600°K and an assumed uniform stream mass flow ($\dot{m}$). Figure 4b verifies that for the lower enthalpy and higher mass flow, the axial location of the recombination zone moves upstream as expected, because the length x from the terminal shock is inversely proportional to the density cubed. The exit gas temperature was 380°K for the low flow rate and 520°K for the high flow rate. The exit temperatures were obtained on the axis by means of an unshielded thermocouple.

In conclusion, it appears feasible to operate an attached-shock flow-swallowing enthalpy probe, and therefore a more complete instrument is being designed.

FREE-JET TEST CONDITIONS NITROGEN ATM

$7 \times 10^6 < AV\ ENTHALPY < 80 \times 10^6\ J/km$

$2h_{AV} < h_{\mathcal{L}} < 4h_{\mathcal{L}}$

$8 \times 10^{-3} < P_{t_2} < 5 \times 10^{-2}$ atm

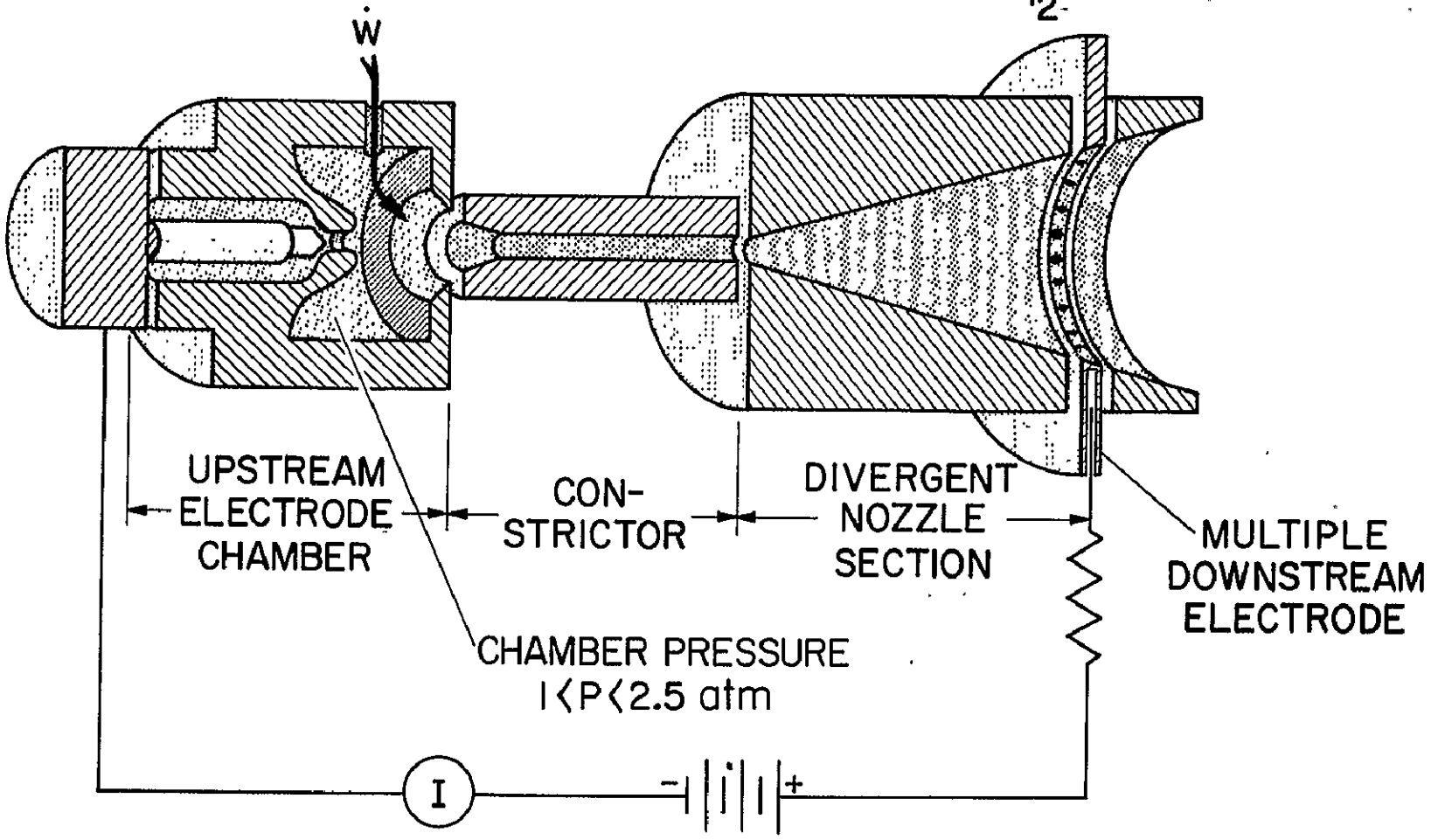

NATIONAL AERONAUTICS AND SPACE ADMINISTRATION
AMES RESEARCH CENTER, MOFFETT FIELD, CALIFORNIA

a. SCHEMATIC FOR THE TRANSIENT HEAT-TRANSFER MODEL
CONTRACTION RATIO = 1.17

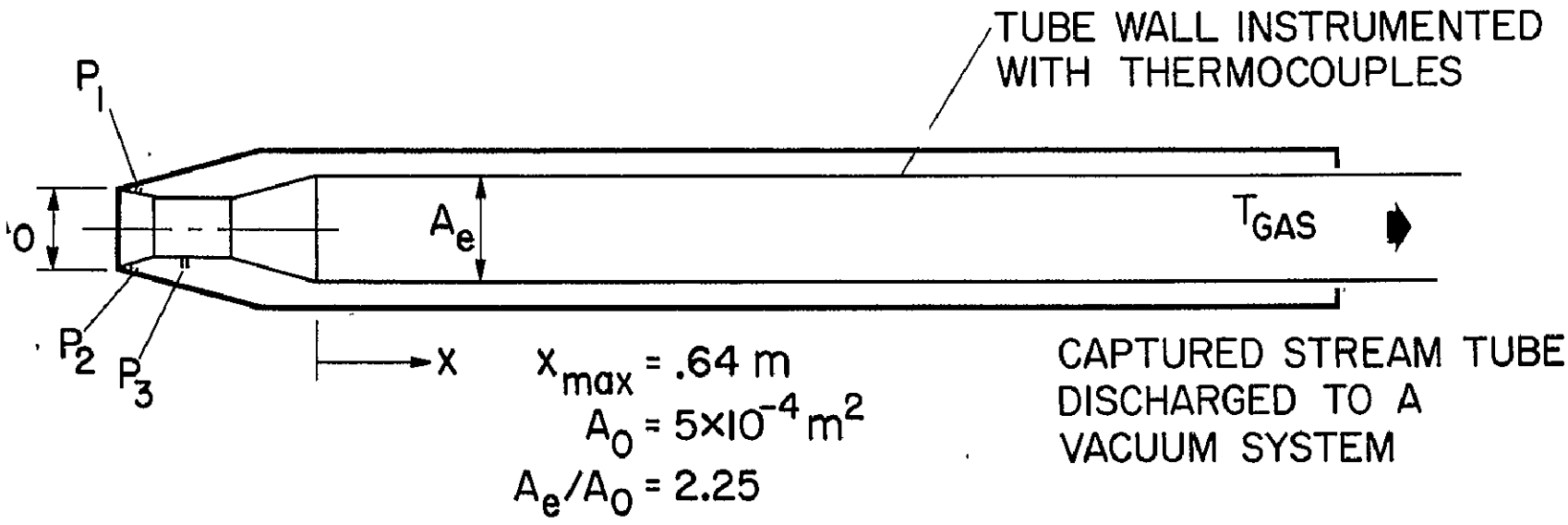

b. STEADY STATE MASS-FLOW MEASURING SYSTEM

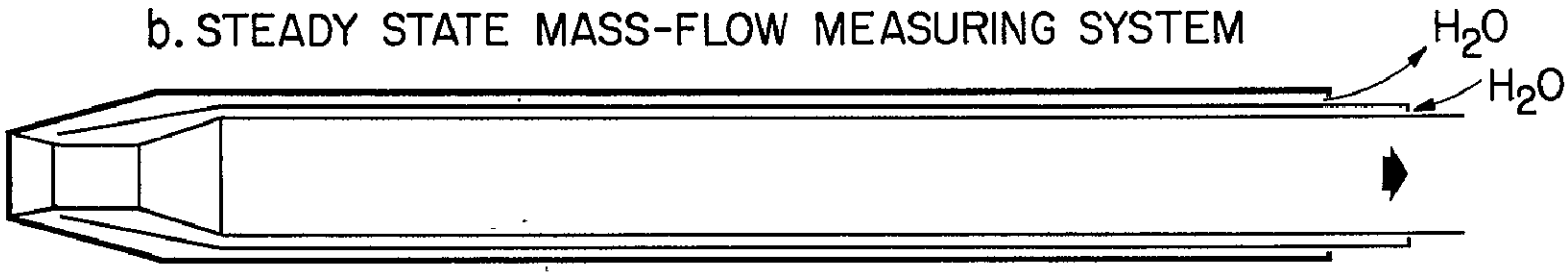

CAPTURED STREAM TUBE DISCHARGED THROUGH
A CALIBRATED VENTURI TO A VACUUM SYSTEM

NATIONAL AERONAUTICS AND SPACE ADMINISTRATION
AMES RESEARCH CENTER, MOFFETT FIELD, CALIFORNIA

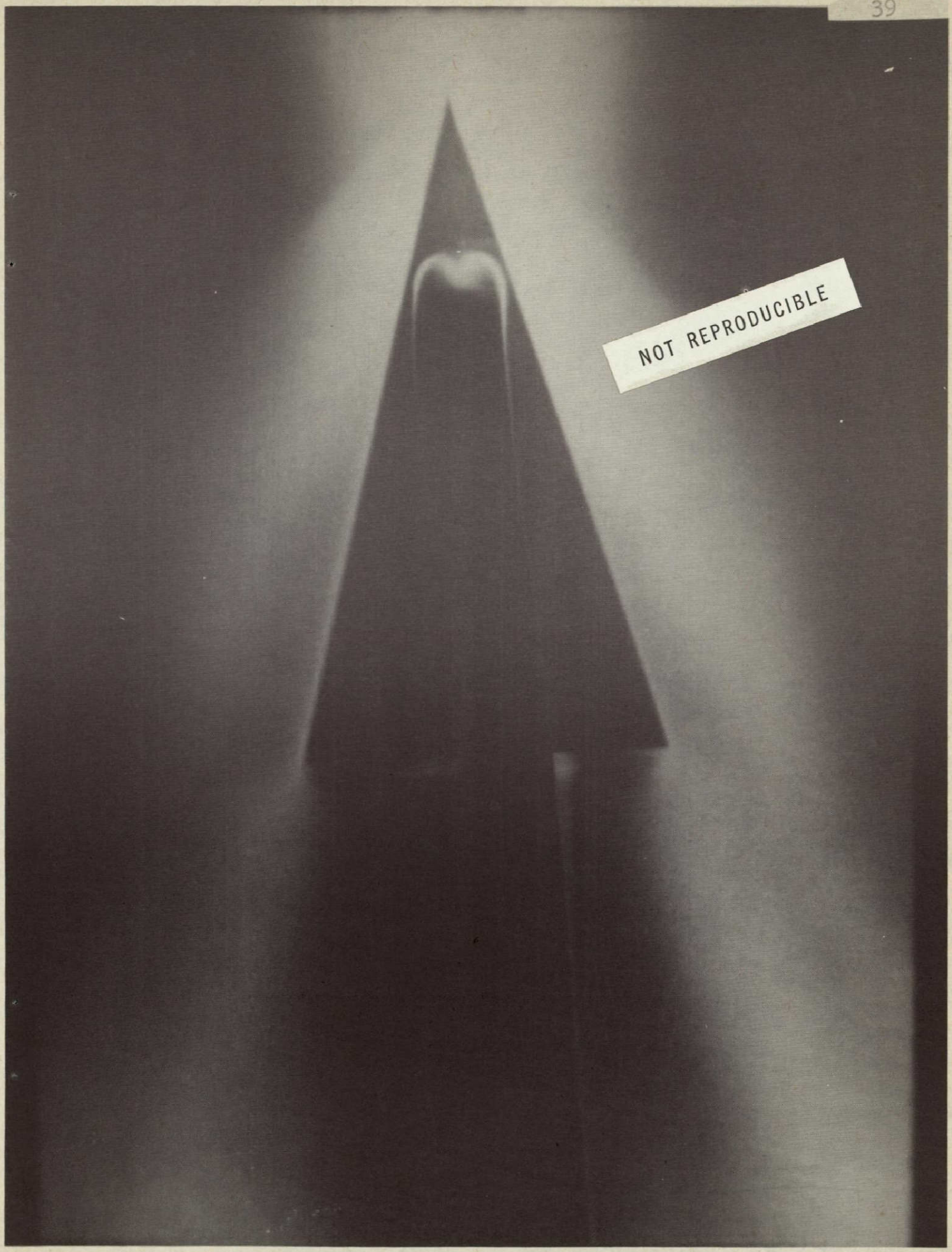
NOT REPRODUCIBLE

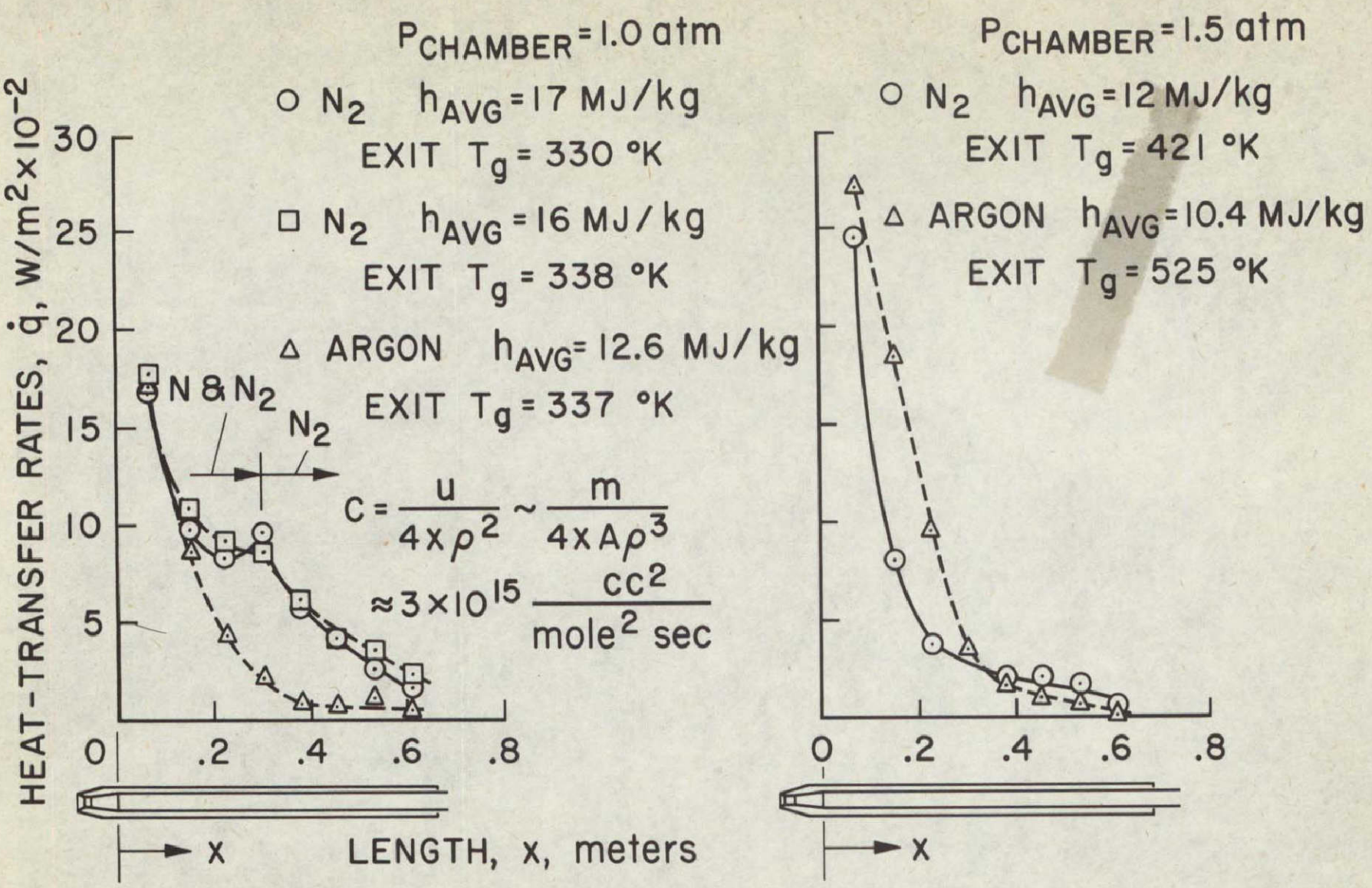

NATIONAL AERONAUTICS AND SPACE ADMINISTRATION
AMES RESEARCH CENTER, MOFFETT FIELD, CALIFORNIA

Abstract to be presented at

Fifth NASA Intercenter and Contractor

Conference on Plasma Physics

to be held at Washington, D. C.

May 24-26, 1966

CONSTRICTED ARC PERFORMANCE STATUS

By John W. Vorreiter

National Aeronautics and Space Administration
Ames Research Center
Moffett Field, Calif.

Since 1962 constricted arc heaters for wind tunnel applications have been built and tested at Ames Research Center. Very briefly, the constricted-arc units are constructed of stacks of water-cooled copper washers separated by boron nitride insulators and sealed by "O" rings. A cathode is located at the upstream end of the tube and a diverging nozzle at the other. A direct-current arc is established between the cathode and an anode array built into the nozzle wall. The working fluid is introduced near or at the upstream end of the constrictor. Further construction details can be found in reference 1.

To study the effects of size on constrictor behavior, the six constricted arc heaters that have been constructed to date ranged in diameter from 0.64 cm to 2.54 cm, and in length from 7.62 cm to 137 cm. Numerous evolutionary modifications of constrictor design details, gas injection arrangements, and electrode assemblies were introduced into each unit during the course of testing. Two devices having 1.27 cm diameter constrictors are presently operational in the power range from 0.2 to 0.8 MW. The other device currently in use is a unit having a 2.54 cm diameter constrictor that operates in the power range from 0.5 to 5.5 MW. It is the largest such device that has been constructed to date, and its behavior and performance will be the subject of the remainder of this discussion. A schematic drawing of this unit is shown in figure 1.

---

*Research Scientist

As is shown on figure 1, the constrictor has a length of 1.37 meter, and the total gap between electrodes is 1.70 meter. The supersonic nozzle has an exit diameter of 46 cm. Gas is injected through a series of gaps between constrictor elements along a 46 cm length of constrictor adjacent to the cathode.

The performance of the 2.54 cm constrictor diameter machine, over a range of pressure at the cathode and enthalpy of the nozzle exit can best be shown by a performance "map" (fig. 2). On this plot each point represents successful operation. One operational limit on these devices is set by the maximum heat transfer rate that can be accommodated. Therefore, superimposed on this chart are two estimates of the performance limit for a heating rate of 10 kw/cm^2. The limit for laminar flow (ref. 2) was calculated for the maximum enthalpy that could be contained at a given pressure. The limit for turbulent flow (ref. 3), again calculated for 10 kw/cm^2, is calculated for a 2.54 cm diameter constrictor as opposed to the laminar flow limit, which was calculated for a constrictor of variable size. Figure 2 shows the present operating range as compared with both these limits. Note here that the production of high enthalpy gas (satellite enthalpy $\approx$ 30 mj/kg) presents no formidable obstacles. However, to produce this gas at a respectable pressure, which is required for true Mach number simulation, forces operation near the limiting conditions. If these limits are correctly estimated, it would appear that the requirements for high model surface pressures, high enthalpy flow, and correct Mach number simulation are incompatible. However, high model surface pressures at high enthalpies can easily be obtained by employing a low area ratio nozzle at a sacrifice in test volume.

The flow emanating from the nozzle can assume a variety of forms depending on the ratio between constrictor current density and cathode chamber pressure. Two of these forms are shown in figure 3.

Shown in figure 3(a) is the behavior at a high ratio of current density to chamber pressure. Plotted on figure 3(a) are representative, measured flow profiles of heating rate and impact pressure. Note that both of these profiles have a parabolic shape. In figure 3(b) the behavior at a much lower ratio of current density to chamber pressure is shown. Here the heat transfer profile has retained essentially the same shape as before, but the impact pressure profile shows a severe depression in the core that probably results from the flow in the constrictor not being fully ingested into the arc column. This change in behavior shows that increasing the upstream pressure at constant current disproportionately increases the impact pressure at the edge of the flow, whereas the centerline impact pressure may even decrease.

The length-to-diameter ratio of the 2.54 cm diameter constrictor was selected to provide the same performance in terms of enthalpy and pressure as had been previously achieved in constricted-arc heaters having 1.27 cm diameter constrictors. According to elementary arc-column theory, the proper rule for effecting this scaling is to maintain the ratio of length to the square of constrictor diameter the same in both cases. Thus the L/D of the 2.54 cm diameter constrictor is twice that of the 1.27 cm diameter constrictors. This scaling procedure, indeed, provides over-all enthalpy-pressure performance to all intents and purposes identical to that achieved in the smaller units.

References

1. Vorreiter, J. W., and Shepard, C. E.: Performance Characteristics of the Constricted-Arc Supersonic Jet, Proceedings of the 1965 Heat Transfer and Fluid Mechanics Institute, June 21-23, 1965, page 42.

2. Cann, G. L., and Buhler, R. D.: A Survey and Prediction of the Performance Capability of Coaxial Arc Heaters, AGARDograph 84, Part 1, September 1964, page 277.

3. Watson, V. R.: Effects of Turbulence in Constricted-Arc Plasma Generators, NASA Intercenter and Contractor Conference on Plasma Physics, Washington, D. C., May 24-26, 1966.

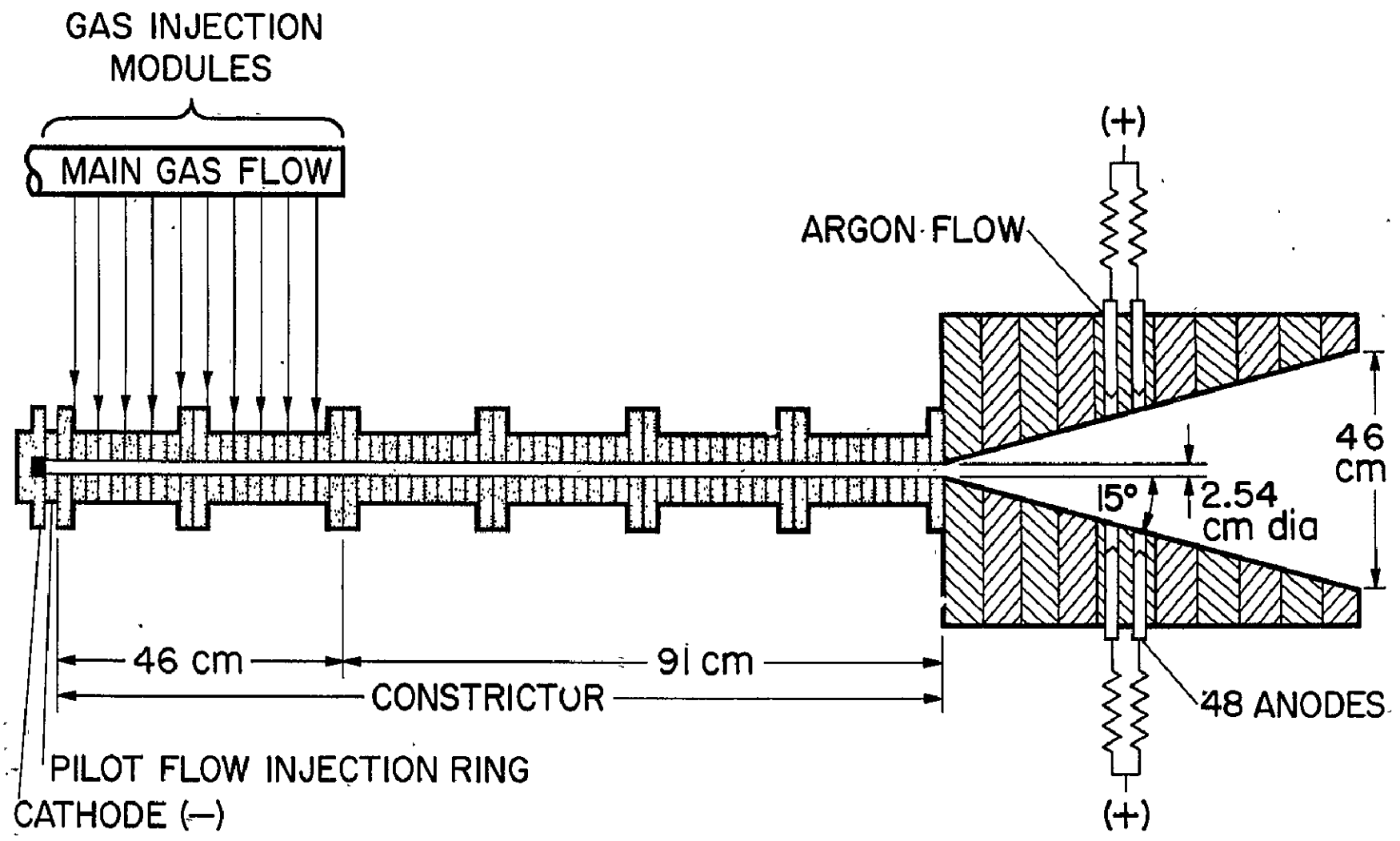

NATIONAL AERONAUTICS AND SPACE ADMINISTRATION
AMES RESEARCH CENTER, MOFFETT FIELD, CALIFORNIA

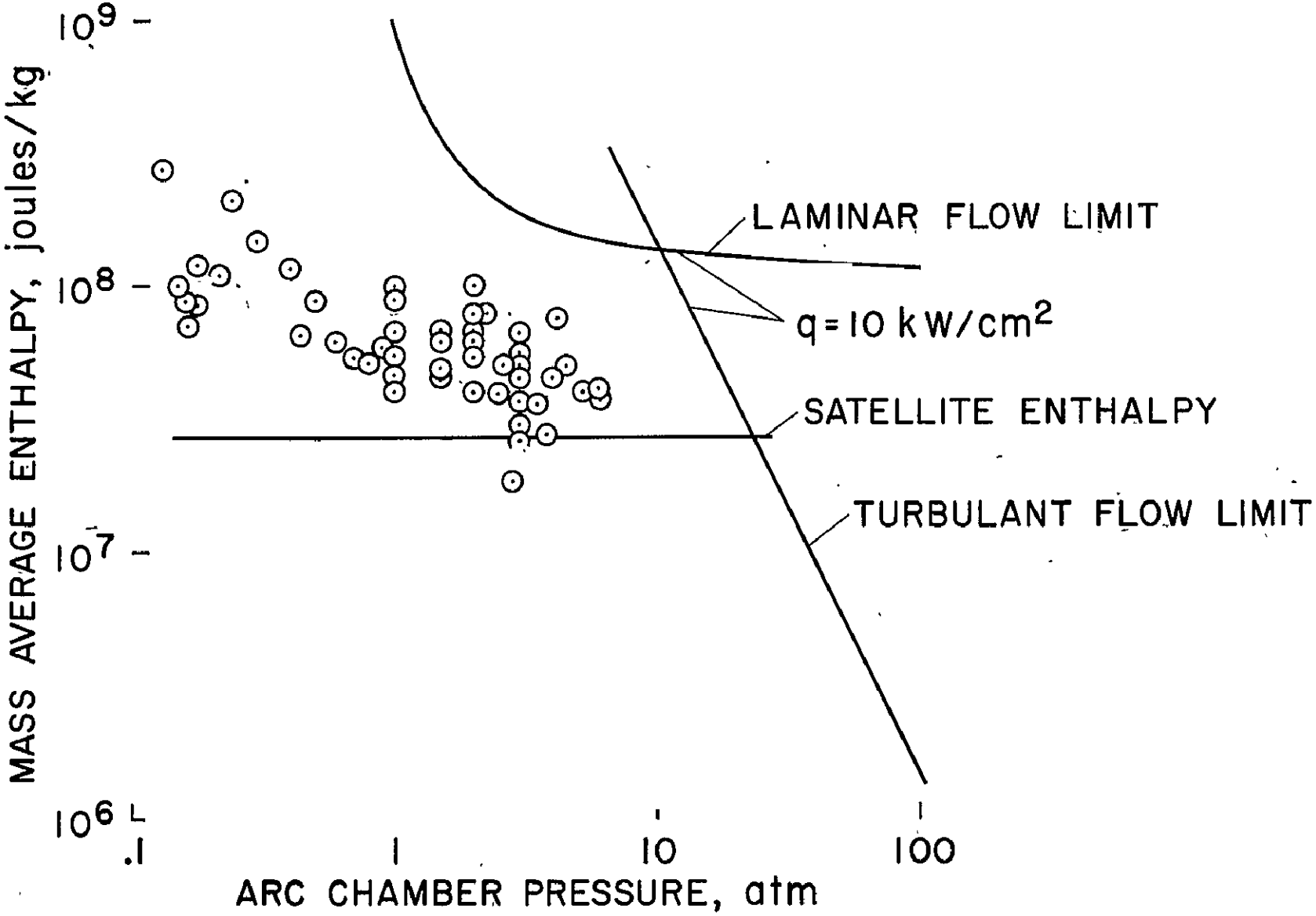

NATIONAL AERONAUTICS AND SPACE ADMINISTRATION
AMES RESEARCH CENTER, MOFFETT FIELD, CALIFORNIA

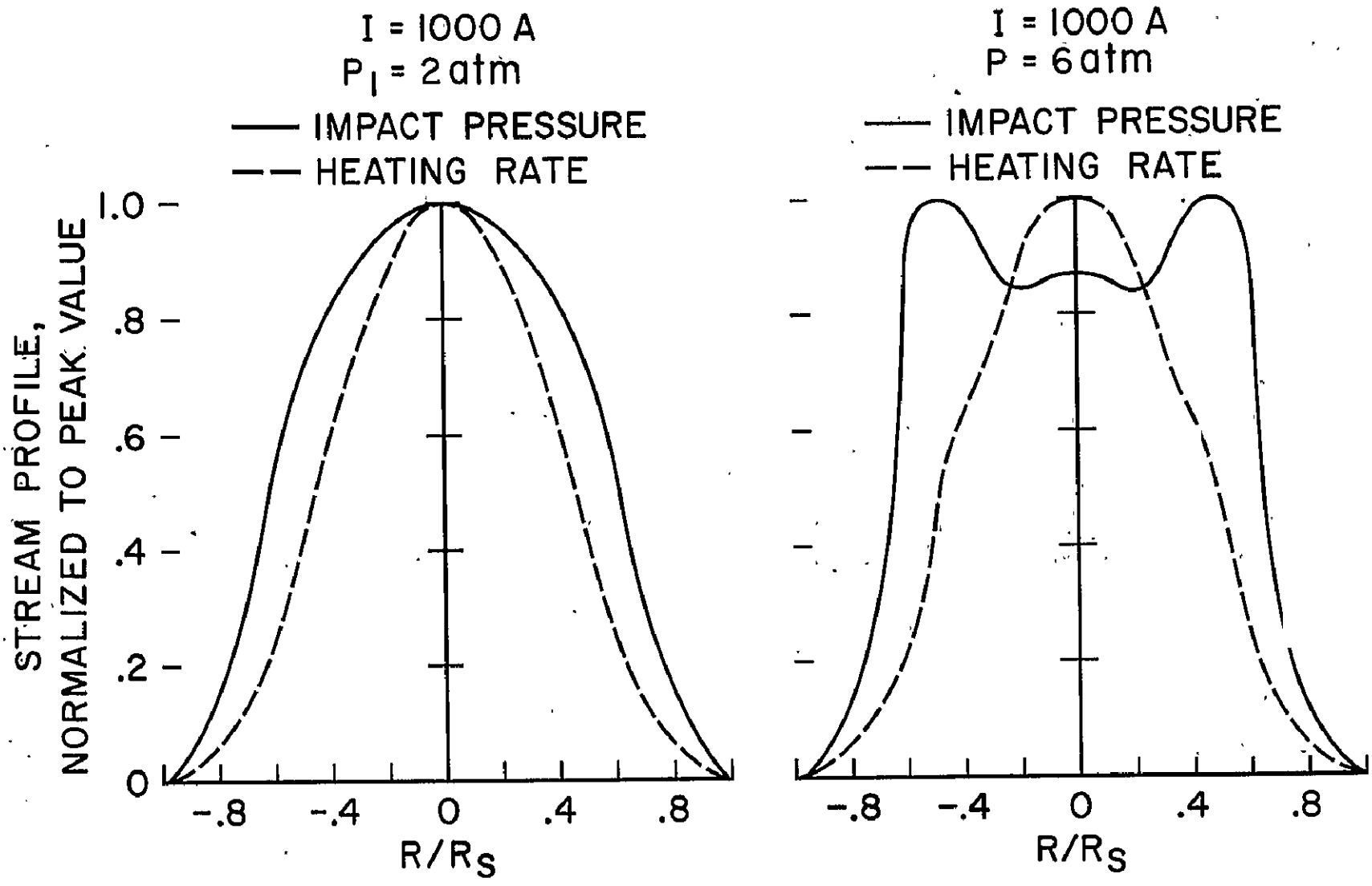

NATIONAL AERONAUTICS AND SPACE ADMINISTRATION
AMES RESEARCH CENTER, MOFFETT FIELD, CALIFORNIA

INTENTIONALLY

LEFT

BLANK

INTENTIONALLY

LEFT

BLANK

Abstract to be presented at

Fifth NASA Intercenter and Contractor

Conference on Plasma Physics

to be held at Washington, D. C.

May 24-26, 1966

IONIC RECOMBINATION RATE OF DISSOCIATED NITROGEN

By Chul Park*

National Aeronautics and Space Administration
Ames Research Center
Moffett Field, Calif.

The purpose of this investigation is to measure the three-body electron-ion recombination rate of dissociated nitrogen. Various tests have been made in the past with a similar purpose, but only molecular ion recombination has been measured, because the plasma temperature and density were not high enough.

The experimental setup for the present tests is shown in the first slide. The portion on the left represents a constricted arc heater with a diameter of 12.7 mm and a length of 30 cm. The nitrogen plasma flow is expanded to an area ratio of 10 and then shocked down to around 1/4 atm. stagnation pressure to produce a region in thermodynamic equilibrium. This equilibrium flow is then expanded through an area ratio of 2.25 by a second nozzle, and spectroscopic measurements are made along the constant-area region of the second nozzle.

Electron density is determined from the width of the hydrogen-beta line, and the temperature is determined from the line intensity ratio either of an ion-atom pair or an atom-atom pair. The content of hydrogen added for the purpose of electron density measurement was approximately 0.1 percent by volume.

The second slide shows how the electron density and the temperature are determined on the stream axis. The shape of the H_β

---

*NAS-NSF Fellow, Research Associate

line is taken at various positions away from the axis by means of a photomultiplier tube at the spectrograph exit plane. The resulting distribution is inverted by the Abel inversion formula, and from the widths of the H_β lines at the various radii, the electron density at each radial point is determined by the well-known formula: $n_e = 3.8 \times 10^{14} (\Delta\lambda)^{3/2}$ cm^{-3}. The intensities of selected line pairs are similarly measured as a function of distance from the axis and inverted by Abel inversion to get the intensities as a function of radius. Temperature is determined from their ratios. As indicated in this particular example, both the electron density and the temperature were almost constant over half the radius, and the centerline values were nearly equal to the integrated mean value across the horizontal plane through the centerline.

The third slide shows the measured electron density variation in the flow direction. Data were taken at six different conditions of pressure and enthalpy. As shown here, for low electron density cases, the electron density decreases steadily along the test length, indicating that at the first observation station the flow was far from equilibrium--that is, the production of ions was negligible. For the high electron density runs, however, the electron density gradient seems to level off downstream, indicating that even in the first test interval, the production term may not be neglected. From these data, rate coefficients can be determined if the velocity of the stream is known. For this purpose, the velocity was measured by means of a time-of-flight method, using a specially designed system which we call the "differentiated-delayed-correlation time-of-flight meter." This system gave typically around 7.5 km/sec stream velocity, a value which falls between the calculated frozen and equilibrium limits.

The temperature determined by the ion-atom line intensity ratio from the 3995Å ion line and the 4935Å atom line is around 11,000°K throughout the second nozzle for all cases, whereas the atom-atom line intensity ratio from the 4935Å atom line and the 5617Å atom line produces temperatures that vary from 8500°K to 11,500°K. A theoretical computation of the effect of nonequilibrium on spectroscopic temperature measurement has been carried out using the theory of Bates. It was found that the atom-atom line ratio method is unaffected by nonequilibrium for this temperature range, but the ion-atom ratio method yields doubtful results and is likely to overestimate the temperature. In the stagnation region, one is almost certain that equilibrium prevails, and the stagnation temperature determined from the ion-atom ratio is around 13,000°K. On the whole, therefore, the temperature

probably varies from 13,000°K in the stagnation region to around 10,000°K in the test region.

The next slide summarizes the measured values of the rate constant. The circled values are the measured values, determined from the approximate rate equation

$$\frac{dn_e}{dt} = - \kappa_r n_e^3$$

By integrating, one gets

$$\kappa_r = \frac{1}{2\tau} \left(\frac{1}{n_{e_2}^2} - \frac{1}{n_{e_1}^2} \right)$$

where τ is the time interval, n_{e_1} and n_{e_2} are the electron densities at the ends of the interval. Only the data from the interval formed by the first two viewing ports are used. As seen here, the rate constant for the high density runs is considerably lower than that for the low density runs indicating that a significant production of ions occurs between the viewing ports. To determine the contribution to the rate constant of ion production, a computer program was run to solve the nozzle flow relaxation problem for three arbitrary values of rate constant.

Since the exact rate equation is

$$\frac{dn_e}{dt} = \kappa_f n_e^2 n_a - \kappa_r n_e^3$$

the integration gives

$$\kappa_r = \frac{1}{1 - \epsilon} \frac{1}{2\tau} \left(\frac{1}{n_{e_2}^2} - \frac{1}{n_{e_1}^2} \right)$$

where

$$\epsilon = \frac{\kappa_f}{\kappa_r} \frac{n_a}{n_e} \simeq \frac{n_{eEq}}{n_e} < 1$$

is the ratio of the ion production rate to the ion recombination rate. This parameter ϵ is then computed for the different rate constants but for the same stagnation condition. The resulting recombination rate is shown by the cross marks in this figure.

When the rate was assumed to be 10^{-25}, the resulting rate from the calculation was onl6 0.6×10^{-25}. If the value of 10^{-26} is assumed, the calculations give 3×10^{-26}. The only compatible value is around 5×10^{-26}. When 5×10^{-26} is put into the program, the resulting ϵ value is such that the measured data would be interpreted as 5×10^{-26}. On the other hand, the case of low electron density shows that ϵ is negligible for all values of the recombination rate. Other effects such as radiation loss and diffusion are estimated to be very small, and so they were all neglected. In conclusion, therefore, one can quote the rate as 5×10^{-26} cm^6 sec^{-1} at 10,000°K.

The last slide compares the present results with existing data. Shown on the slide are the recombination rate for hydrogen, calculated by Bates; that for helium, measured by Hinnov and Hirschberg; and the theory of Bates carried out for nitrogen. As is apparent, the present experimental result lies well within the expected range, and is 7 orders of magnitude smaller than the molecular-ion recombination rate and 7 orders of magnitude greater than the atomic recombination rate.

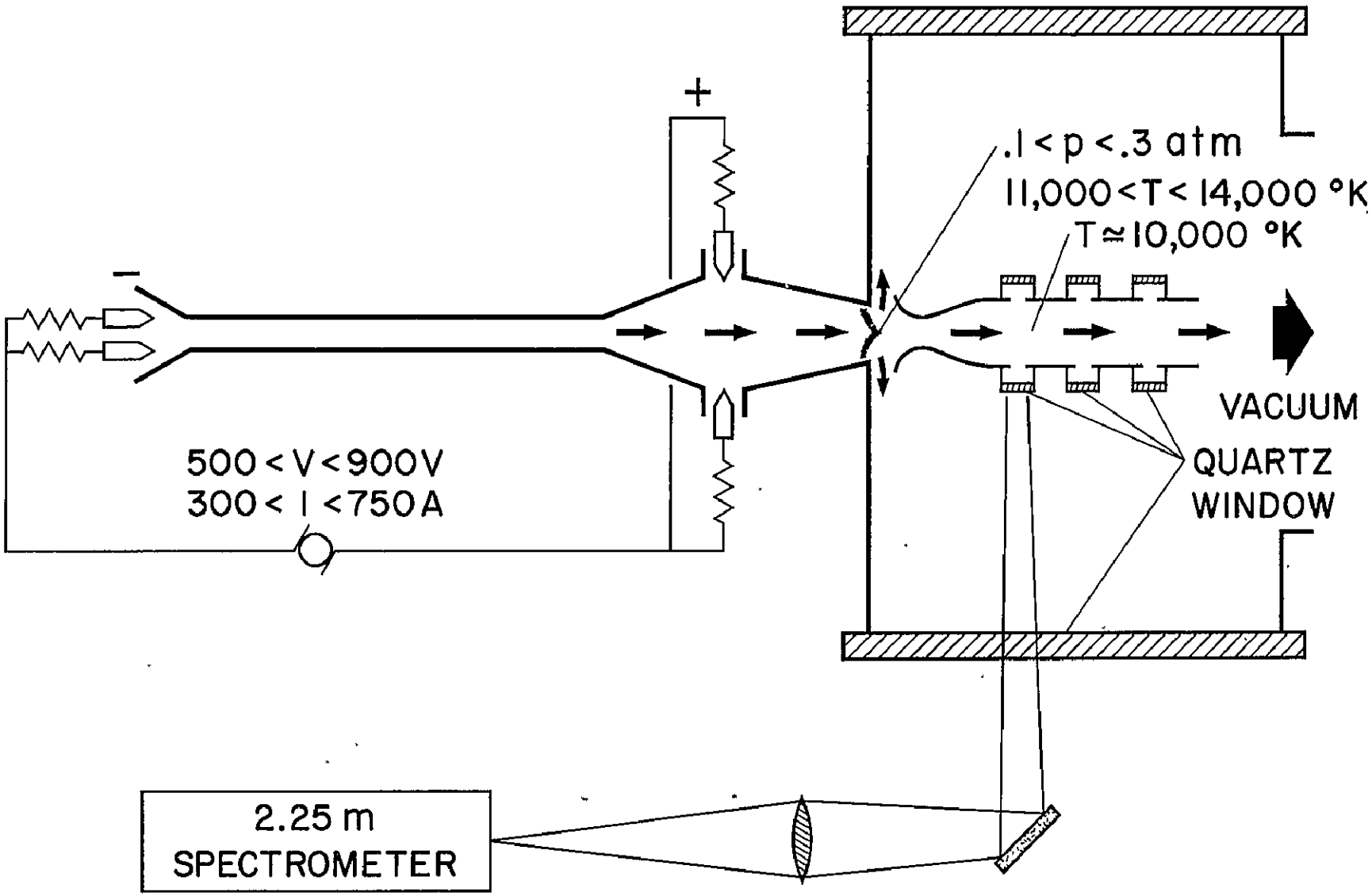

NATIONAL AERONAUTICS AND SPACE ADMINISTRATION
AMES RESEARCH CENTER, MOFFETT FIELD, CALIFORNIA

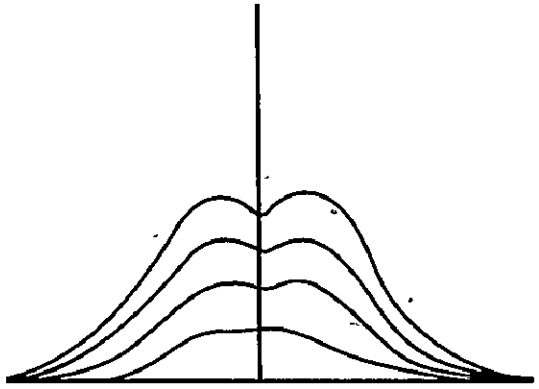

ORIGINAL H_β SHAPE

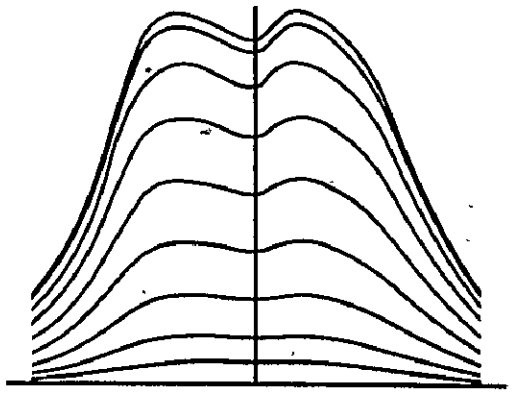

INVERTED H_β SHAPE

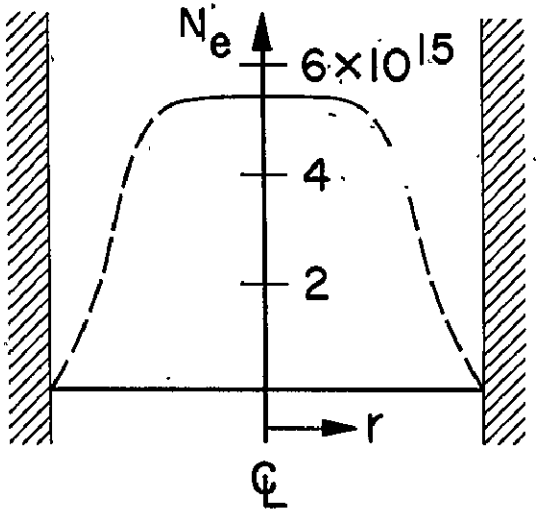

RADIAL DISTRIBUTION
OF ELECTRON DENSITY

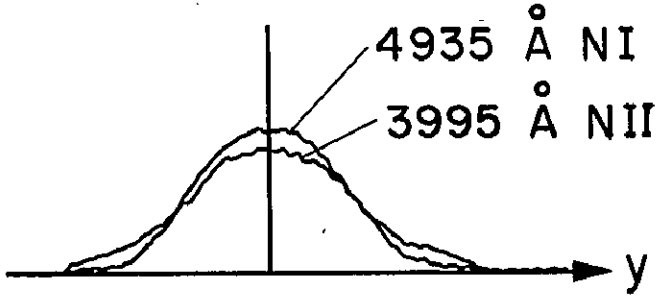

INTENSITY OF LINES

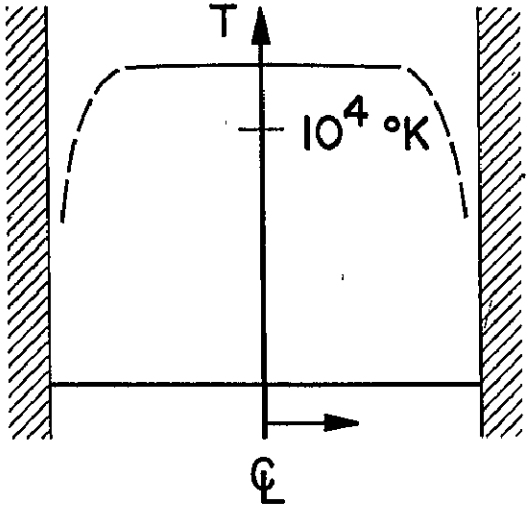

RADIAL DISTRIBUTION OF
TEMPERATURE (ELECTRON)

NATIONAL AERONAUTICS AND SPACE ADMINISTRATION
AMES RESEARCH CENTER, MOFFETT FIELD, CALIFORNIA

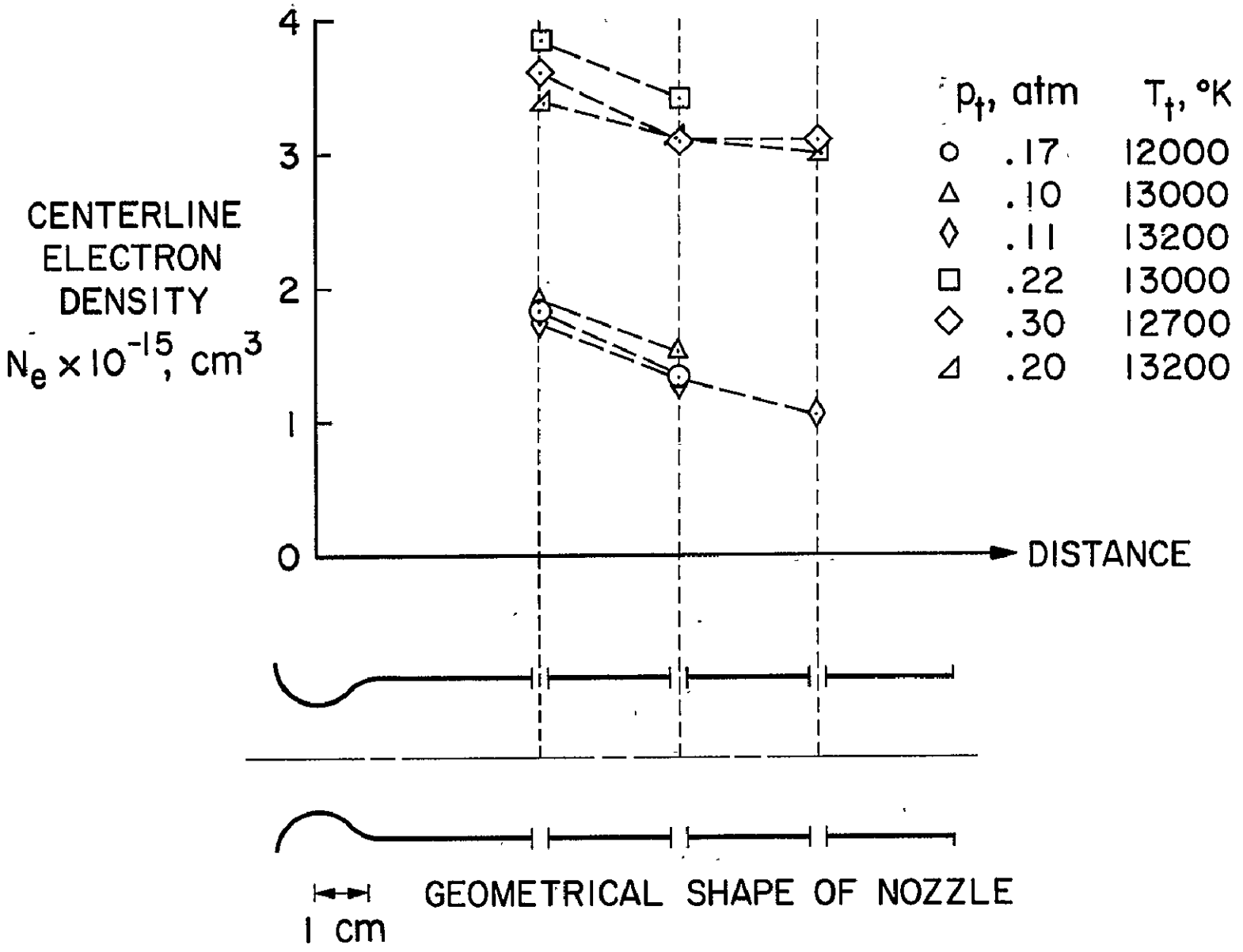

NATIONAL AERONAUTICS AND SPACE ADMINISTRATION
AMES RESEARCH CENTER, MOFFETT FIELD, CALIFORNIA

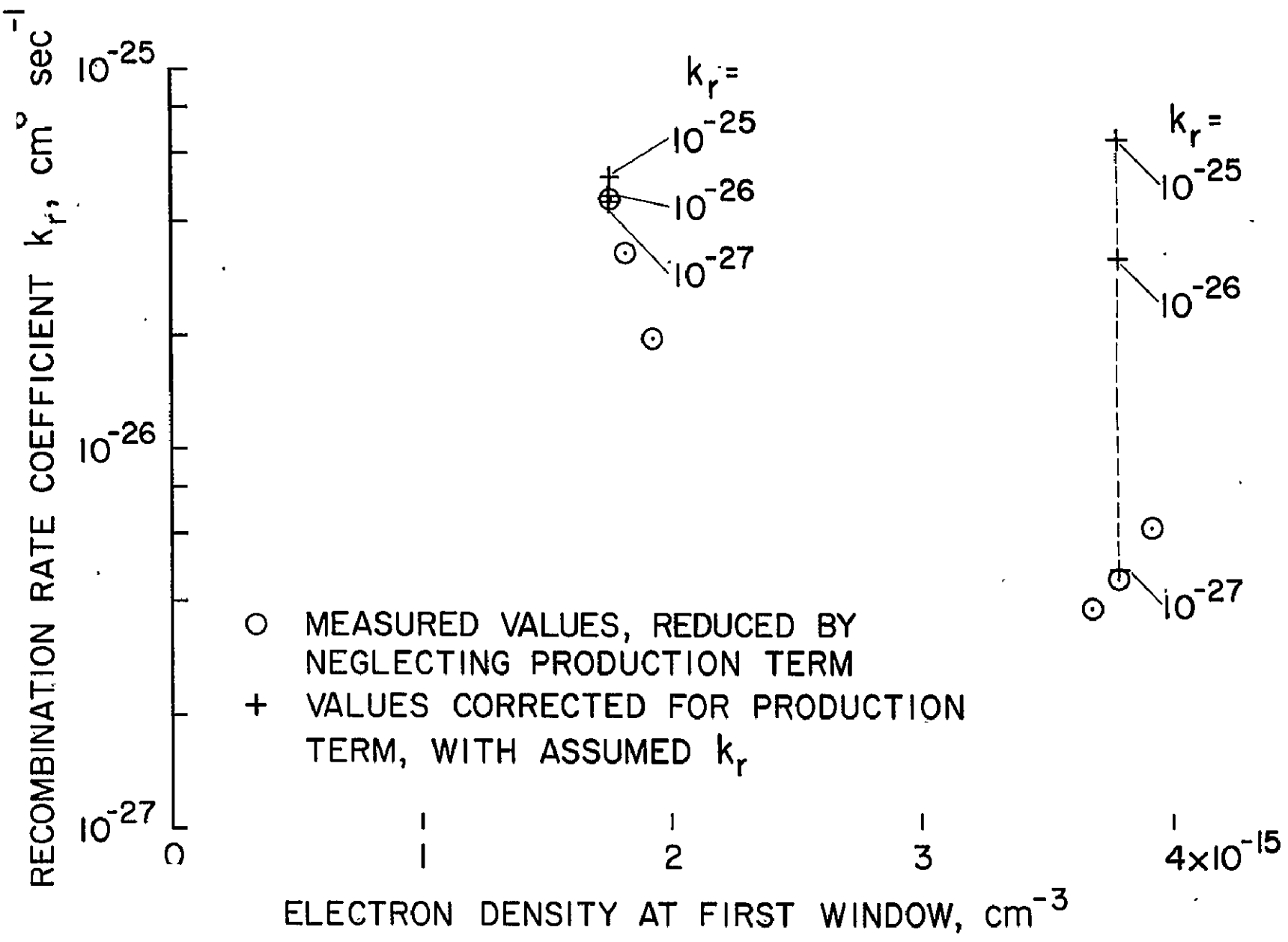

NATIONAL AERONAUTICS AND SPACE ADMINISTRATION
AMES RESEARCH CENTER MOFFETT FIELD CALIFORNIA

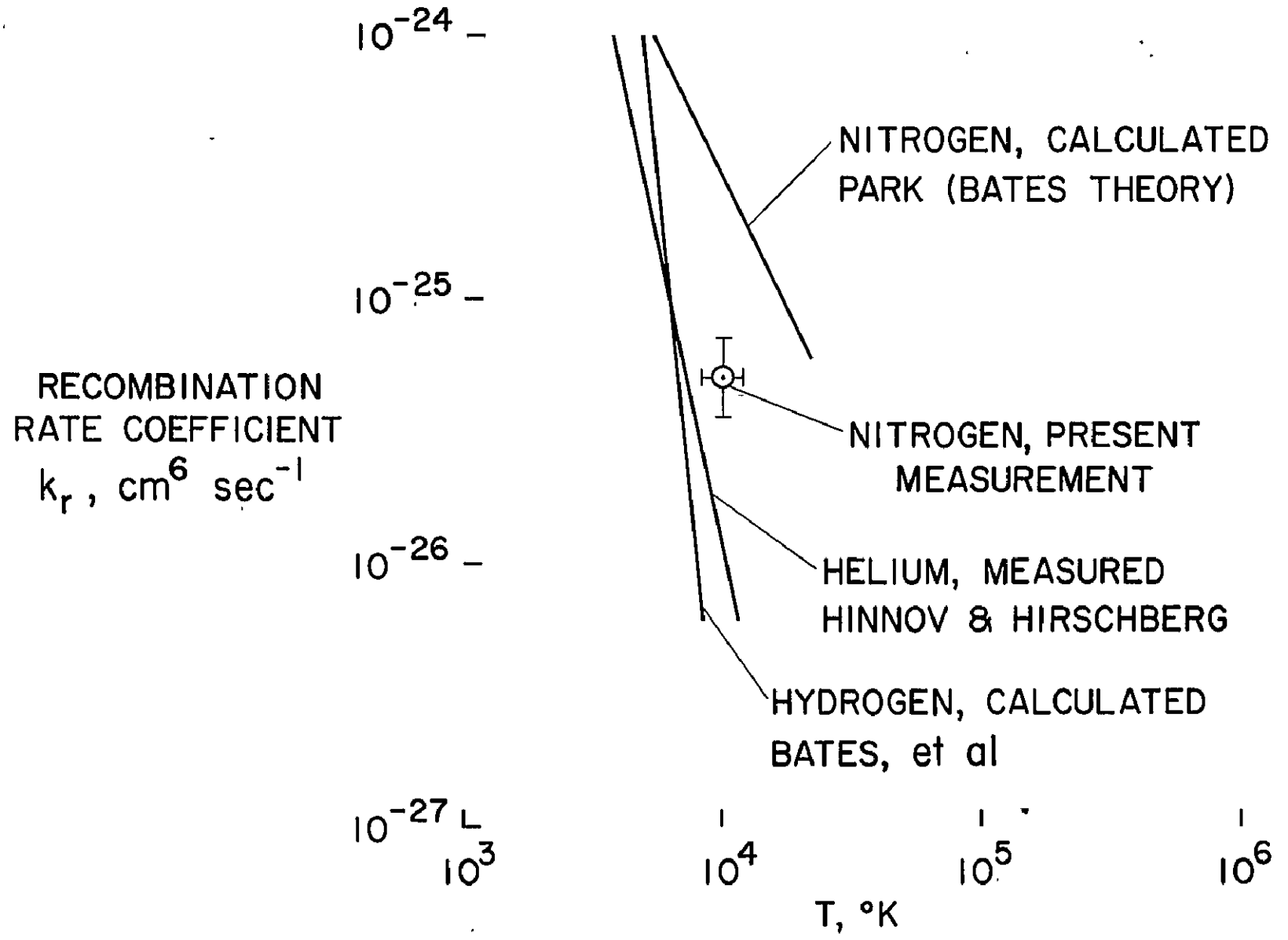

NATIONAL AERONAUTICS AND SPACE ADMINISTRATION
AMES RESEARCH CENTER, MOFFETT FIELD, CALIFORNIA

Abstract for presentation at the
Fifth NASA Intercenter and
Contractor Conference on Plasma Physics
to be held at NASA Headquarters
May 24-26, 1966

INVESTIGATION OF TRANSPORT PHENOMENA IN THE PHYSICS BRANCH

By Warren F. Ahtye*

National Aeronautics and Space Administration
Ames Research Center
Moffett Field, Calif.

ABSTRACT

A description will be given of the research being conducted in the Physics Branch which pertain to transport phenomena in partially and fully ionized gases. The first topic will be a discussion of Ahtye's derivation of an expression for the total thermal conductivity of partially and fully ionized gases. The present status of a general computer program for calculating transport properties of ternary gases to the third order in the Chapman-Enskog expansion will be described. Preliminary values of transport coefficients from this program will be compared with those using other theories. Stallcop's general technique for calculating differential cross-sections will be described. This technique is applicable to the case of elastic scattering between a neutral or ionized atom with another neutral atom and may be extended to the case of resonant charge exchange. The last topic will be a description of the low energy ion beam experiments of Witteborn and Nichols. Their present experiments to determine asymmetric charge-exchange cross sections, and future experiments to determine symmetric atomic charge-exchange cross-sections in the thermal range will be described.

---

*Research Scientist

Abstract for presentation at the Fifth NASA Intercenter and Contractor Conference on Plasma Physics, NASA Headquarters, May 24-26, 1966.

National Aeronautics and Space Administration
Ames Research Center
Moffett Field, Calif.

ELECTRODE PHENOMENA IN HIGH ENERGY DENSITY DISCHARGES AS APPLIED TO PLASMA ACCELERATION PROBLEMS

By Helmut R. Poppa, Research Associate *

Abstract

Plasma-electrode interactions were investigated, studying in detail microscopic and submicroscopic changes in electrode surface structures and morphology.

Transmission electron microscopy of crystallographically well defined thin foil electrodes showed that the orientation dependence of the sputtering yield is weak for low ion energies. Specifically, the difference in sputtering yield for (100) and (111) oriented gold foils (50 eV to 500 eV argon ion energy) is of the order of 15%; use of properly oriented single crystal discharge electrodes, therefore, will not reduce electrode destruction significantly, even if ion bombardment sputtering should be the major cause for electrode disintegration.

Transmission electron diffraction of Cu foils bombarded with 500 eV nitrogen ions (ion beam intensity ~ 0.07 mA/cm^2) revealed no sign of chemical corrosion attack, another possible mechanism of electrode disintegration. Reflexion electron diffraction of a bulk copper cathode exposed to a nitrogen discharge in a coaxial plasma gun confirmed the negative corrosion results.

Cathode morphologies of two plasma gun types (coaxial and pulsed arc gun) were studied by replica electron microscopy, as they developed during gun operation. Microscopic structure features found on electrode surfaces indicate the existence of small (5 to 50μ) areas of localized surface attack (cathode spots). The attack is so strong that localized melting of the cathode surface occurs. The melting hypothesis was verified by detecting changes in cathode surface crystallography caused by localized melting of cathode material. Future discharge electrode research should concentrate on investigating properties and function of cathode spots.

* Work done under NASA Contract NASW-1103 while at General Dynamics, Convair Division, San Diego, California (Report GDC-DBE-66-002).

Abstract for presentation at the Fifth NASA Intercenter and Contractor Conference on Plasma Physics, May 24-27, 1966

RESULTS OF THE PIONEER 6 AMES PLASMA PROBE EXPERIMENTS

John H. Wolfe, NASA-Ames Research Center, Moffett Field, California

Recent data on the plasma characteristics in the interplanetary medium as observed by the Ames Research Center plasma probe on Pioneer 6 are presented. In light of the preliminary results it has become clear that the previous assumptions of solar radial flow and thermal isotropy are inappropriate when the plasma is viewed with higher resolution instrumentation. The results show deviations from radial plasma flow of as much as 5° and reveal a high degree of thermal anisotropy in the plasma ions. Data indicate that the ion temperature parallel to the magnetic field may at times exceed the perpendicular temperature by an order of magnitude. In addition, evidence is presented which supports the presence of a third ionic species in the solar wind.

Abstract for presentation at the Fifth NASA Intercenter and Contractor Conference on Plasma Physics, May 24-27, 1966

PLASMA FLOW AROUND THE QUIET MAGNETOSPHERE

John R. Spreiter

Space Sciences Division
NASA Ames Research Center
Moffett Field, California

ABSTRACT

Analysis of the flow of solar plasma around the quiet magnetosphere requires consideration of a flow field having dimensions that are large compared with the fundamental lengths through observations made by instruments that are microscopic in comparison. In this paper, the large scale features of the flow are determined by use of the continuum equations of steady magnetohydrodynamic flow. The magnetosphere boundary is represented by a magnetohydrodynamic tangential discontinuity, and the bow wave by a fast magnetohydrodynamic shock wave. The connectivity of interplanetary and geomagnetic fields, and the asymptotic directions of the wake and shock waves at great distances from the earth are discussed in terms of properties of these discontinuities. It is shown that these considerations lead directly through approximations of good accuracy to the simpler equations of the classical Chapman-Ferraro theory for the shape of the magnetosphere boundary, and to those of nonlinear gasdynamics for the surrounding flow. These equations are solved numerically, and detailed results for the location of the bow wave and the bulk properties of the flow in the transition region are presented for several representative Mach numbers and ratios of specific heats. These results are combined with kinetic theory to determine specific numerical results corresponding to observations that would be made by a variety of idealized plasma probes on both oriented and spinning vehicles. Finally these results are compared with actual data obtained by plasma probes and proton analyzers on earth satellites that traverse the magnetosphere boundary and its bow shock.

PRINCIPLE PUBLICATIONS:

Spreiter, John R. and A. L. Summers - "On Conditions Near the Neutral Points on the Magnetosphere Boundary," (To be submitted to Planetary & Space Sciences).

Alksne, Alberta Y. - "The Steady-State Magnetic Field in the Transition Region Between the Magnetosphere and the Bow Shock," (To be submitted to Planetary & Space Sciences).

Spreiter, John R., A. Y. Alksne and B. Abraham-Shrauner - "Theoretical Proton Velocity Distributions in the Flow Around the Magnetosphere," (Submitted to Planetary & Space Sciences).

PUBLICATIONS CONTD.:

Spreiter, John R., A. L. Summers and A. Y. Alksne - "Hydromagnetic Flow Around the Magnetosphere," Plan. & Space Sci., Vol. 14, No. 3, 3-66.

Spreiter, John R. - "On the Maximum Magnetic Moment of Venus," JGR, Vol. 70, No. 17, 9-1-65.

Spreiter, John R. - "The Boundary of the Geomagnetic Field," I.C.S.U. Review, Vol. 6, 1964.

Spreiter, John R. and Wm. Prichard Jones - "On the Effect of a Weak Interplanetary Magnetic Field on the Interaction Between the Solar Wind and the Geomagnetic Field," JGR, Vol. 68, No. 12, 6-15-63.

Spreiter, John R. and B. R. Briggs - "Theoretical Determination of the Form of the Boundary of the Solar Corpuscular Stream Produced by Interaction with the Magnetic Dipole Field of the Earth," JGR, Vol. 67, No. 1, 1-62.

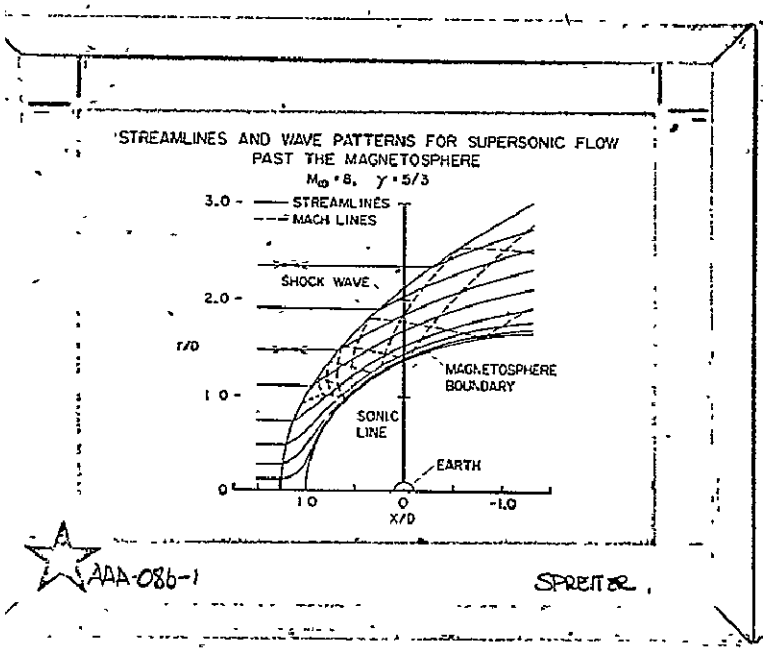

AAA-086-1 SPREITER.

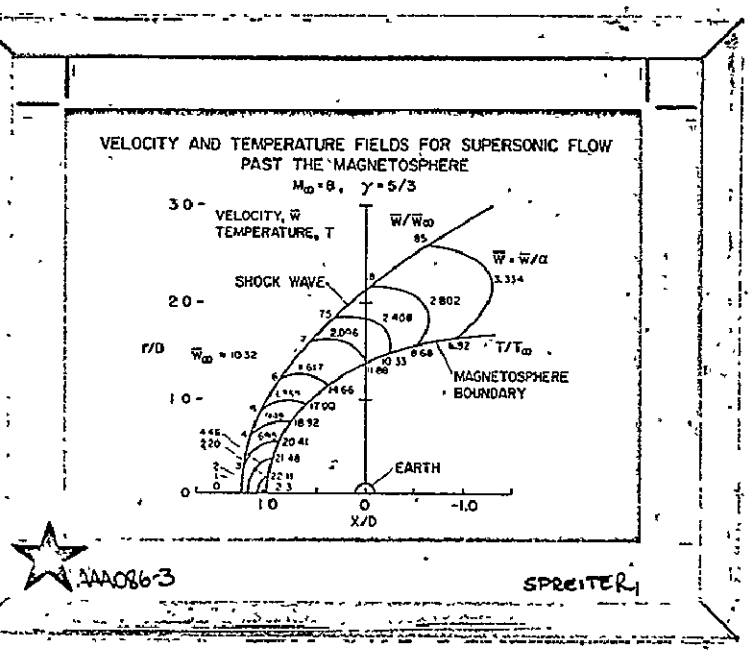

AAA086-3 SPREITER

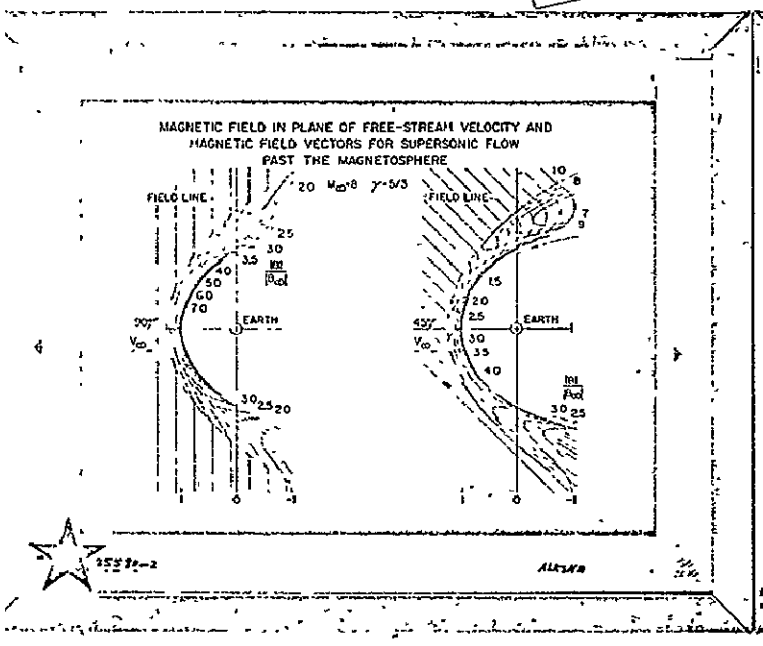

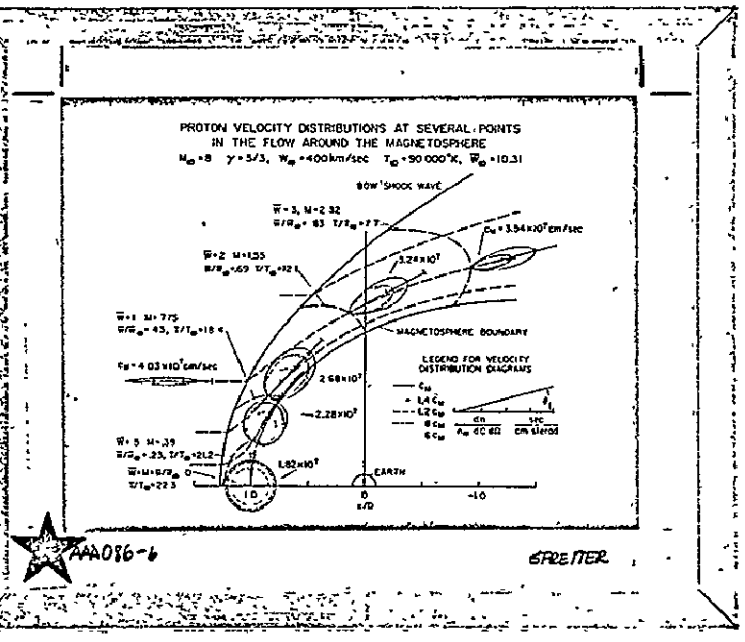

AAA086-6 SPREITER

National Aeronautics and Space Administration
Ames Research Center
Moffett Field, Calif.

COMPARISON OF EXPERIMENTAL WITH PREDICTED CONVECTIVE HEAT TRANSFER FROM A LAMINAR BOUNDARY LAYER OF THERMALLY IONIZED ARGON

L. H. Back, Jet Propulsion Laboratory

This paper describes some comparisons between predictionsand steady flow heat transfer measurements in a 1.95 in. diameter tube and in a 10° half-angle convergent-divergent located at the tube outlet. The laminar boundary layer convective heat transfer predictions (Ref. 1) are for a singly ionized monatomic gas with ambipolar diffusion by ion-electron pairs. Solutions from Ref. 1 for limiting cases of the diffusion rate assumed large compared to the net ion production rate and for assumed equilibrium indicate a predicted reduction in a heat transfer parameter below that for an un-ionized gas for Lewis numbers less than unity. This predicted reduction increases with ionization energy fraction. Predicted Lewis numbers based on the ambipolar diffusion coefficient are less than unity, being about 0.25.

Argon was heated upstream of the tube by an electric arc to average stagnation temperatures up to about 21,000°R, ionization energy fractions up to 0.5 and stagnation enthalpies up to 6800 BTU/lb. Semi-local heat flux measurements were obtained along the tube and nozzle by calorimetry in circumfrential water coolant passages with passage widths relatively small compared to the nozzle radius. The ratio of wall to total enthalpy is small, being less than 5%. As a result of the high gas temperatures and relatively low stagnation pressures (between 0.1 and 0.3 atm) Reynolds numbers are low and the boundary layers are laminar.

A meaningful representation of the heat transfer data requires a prescription of the core flow conditions. Mr. Massier, in the preceeding paper, described the core flow variables of interest - the mass flux $\rho_e u_e$, stagnation enthalpy H_{to} and static temperature - and various prediction methods by which these are obtained by utilizing the wall static pressure measurements. Experimental determination of the core flow requires either gas temperature or stagnation enthalpy measurement in addition to the measured wall static pressure distribution.

For the tests presented here, radiation from the gas is negligible compared to convection. By locating the electric arc around the corner from the tube radiation from the arc is essentially eliminated. With this arrangement better mixing is also achieved, but at the expense of secondary flows in the entrance region of the tube.

Local heat transfer coefficients along the tube and nozzle are presented in terms of a laminar boundary layer heat transfer group

$$\frac{q}{\left(H_{to} - H_w\right)\left(\rho_e u_e\right)_i} \left(\frac{\rho_e u_e}{\mu_e}\right)_i^{\frac{1}{2}} \qquad (1)$$

In this relation q is the heat flux to the wall, $\rho_e u_e$ is the local mass flux, $\rho_e u_e/\mu_e$ is a Reynolds number per unit length and $(H_{to} - H_w)$ is the driving

potential between the stagnation enthalpy and wall enthalpy. Properties denoted by i refer to the nozzle inlet condition. This representation should correlate data for un-ionized laminar boundary layers. Rather good agreement along the tube and nozzle is found between a relatively low stagnation enthalpy test (H_{to} = 1190 BTU/lb) for which the ionization energy fraction is negligible and the prediction from Ref. 2, except in the throat and divergent section of the nozzle where the data lie below the prediction. For tests at higher stagnation enthalpies up to 6800 BTU/lb and ionization energy fractions up to 0.5 the heat transfer group from Eq. (1) follows the trend indicated from laminar boundary layer predictions (Ref. 1) for a partially ionized gas where the group from Eq. (1) should decrease as the ionization energy fraction increases. However, the higher stagnation enthalpy results lie considerably below the predictions downstream of some point in the flow. This point moves upstream as the stagnation enthalpy is increased. This same trend is evident for other tests that spanned a range of stagnation enthalpies from 3000 to 6000 BTU/lb and corresponding ionization energy fractions from 0.25 to 0.5, but which were obtained with a shorter length of tube such that the length to diameter ratio was 2.5 instead of 4.7 for the previously mentioned tests.

To provide some insight on the relatively low values of the heat transfer group found for the higher stagnation enthalpy tests, values of stagnation enthalpy, temperature and ionization energy fraction $\alpha I/H_{to}$ are shown in Table I. The average stagnation enthalpies at the nozzle inlet as determined from overall energy balances are seen to be appreciably below the average stagnation enthalpies at the outlet of the electric arc heater. Spectroscopic measurements by the relative atom line intensity method just upstream of the nozzle inlet indicate temperatures appreciably above the average values at the nozzle inlet. Since these measured temperatures are nearer the average temperatures at the outlet of the electric arc heater, adiabatic core flow through the tube and nozzle was assumed in calculating the driving potential, $H_{to} - H_w$, in the heat transfer group of Eq. (1). However, as was noted, the variation of the heat transfer group along the nozzle indicates that as the stagnation enthalpy increases the point of deviation from the laminar boundary layer predictions for an adiabatic core flow moved upstream. This trend suggests that the lower values of the heat transfer group at the higher stagnation enthalpies may be due to non-adiabatic core flow downstream of some point in the flow where the thermal boundary layer may have reached the centerline. If this occurred the driving potential is less and the heat transfer is lower. Consequently, an appraisal of the effect of ionization on heat transfer that is indicated by theory is probably obscured by the large energy abstraction from the flow.

Mention should be made of previous comparisons between laminar boundary layers predictions and heat transfer data shown in Ref. 3 for negligible ionization energy fraction tests. In these previous results, obtained with the electric arc heater located axially upstream of the nozzle, the experimentally determined laminar boundary layer heat transfer group shown in Figs. 6, 7 and 8 of Ref. 3 would be lower if the average total enthalpy at the outlet of the electric arc heater were used in the driving potential rather than the average total enthalpy at the nozzle inlet which was used. Better agreement with the laminar boundary layer prediction (Eq. 10 in Ref. 3 which is essentially the same as that of Ref. 2) would be achieved, although the nature of the boundary layer at the nozzle inlet is not well known for these tests as a result of the separated flow region downstream of the step at the outlet of the electric arc heater.

To acquire further knowledge of heat transfer from high temperature partially ionized gases, core flow measurements are needed at various axial and radial locations. Additional spectroscopic measurements and cooled traversing probe measurements are planned. To enhance mixing an electric arc heater consisting of three circumfrentially spaced arc heads that discharge into a plenum chamber will be used. Heat transfer measurements in a sharp edged tube attached to the outlet of the plenum chamber and in a convergent-divergent nozzle are planned.

REFERENCES

1. Back, L. H., "Laminar Boundary-Layer Heat Transfer from a Partially-Ionized Monatomic Gas by the Similarity Approach," Technical Report No. 32-867, Jet Propulsion Laboratory, Pasadena, California, February 1, 1966.

2. Back, L. H. and Witte, A. B., "Prediction of Heat Transfer From Laminar Boundary Layers, with Emphasis on Large Free-Stream Velocity Gradients and Highly cooled Walls," Technical Report No. 32-728, Jet Propulsion Laboratory, Pasadena, California, June 1, 1965. To be published in the August 1966 issue of the ASME Journal of Heat Transfer.

3. Massier, P. F., Back, L. H., Witte, A. B. and Noel, M. B., "Heat Transfer From Ionized Gases," Space Program Summary No. 37-23, Vol IV, pp 109-118, August-September, 1963.

TABLE I

Ratio of Tube Length to Diameter, L/D = 2.5									
	TEST 112-24H P_t = 4.12 psia			TEST 112-26H P_t = 2.02 psia			TEST 112-30H P_t = 3.16 psia		
Location	H_{to} BTU/lb	T ^{o}R	$\frac{\alpha I}{H_{to}}$	H_{to}	T	$\frac{\alpha I}{H_{to}}$	H_{to}	T	$\frac{\alpha I}{H_{to}}$
Outlet of Electric Arc Heater: Energy Balance	3320	18,600	0.26	4770	19,500	0.42	5560	20,500	0.47
Nozzle Inlet: Energy Balance	1400	11,200	~ 0	1390	12,900	~ 0	1610	12,900	~ 0
From Spectroscopic Measurements at C_L just upstream of Nozzle Inlet	2680	17,500	0.17*	3550	18,300	0.32	7390	21,600	0.55

L/D = 4.7									
	TEST 112-34H P_t = 3.25 psia			TEST 112-35H P_t = 4.17 psia			TEST 112-36H P_t = 3.06 psia		
Location	H_{to}	T	$\frac{\alpha I}{H_{to}}$	H_{to}	T	$\frac{\alpha I}{H_{to}}$	H_{to}	T	$\frac{\alpha I}{H_{to}}$
Outlet of Electric Arc Heater: Energy Balance	1190	9,570	~ 0	3100	18,300	0.24	6790	21,200	0.52
Nozzle Inlet: Energy Balance	475	3,820	~ 0	1100	8,900	~ 0	1650	13,300	~ 0
From Spectroscopic Measurements at C_L just upstream of Nozzle Inlet		--			--		6400	21,000	0.52

* Calculated from Saha equation.

BEHAVIOR OF A MAGNETIC NEUTRAL LINE IN A PLASMA

A. Bratenahl

Jet Propulsion Laboratory
California Institute of Technology

ABSTRACT

The magnetic neutral line is a geometrical locus that occurs in a region where there is a hyperbolic arrangement of lines of force. The asymptotic lines of the hyperbolic arrangement generate two intersecting surfaces. The intersection of these surfaces is the magnetic neutral line. Although the neutral line is perpendicular to the field in its neighborhood, the field must vanish at all points on the neutral line itself. This is the usual definition of neutral line, but it is inadequate for our purposes. We now extend this definition by adding a field which, though otherwise arbitrary, must be tangent to the neutral line at all of its points. The original hyperbolic field, we now call $\vec{B}_\perp$, the added component, $\vec{B}_\parallel$. The topological significance of the neutral line is unchanged by the addition of the component $\vec{B}_\parallel$, and we assert in the light of this extended definition that: changes of magnetic flux between tubes belonging to different source systems, either "magnetic poles" or currents, can occur if and only if neutral lines are present. The proof of this theorem follows a topological argument in which it is seen that the change is merely a "severing and reconnecting" of lines of $\vec{B}_\perp$ at the neutral line. It is well known that this process of "severing and reconnecting" is nontrivial if the conductivity of the medium is large. The rate of reconnection in a conducting medium is controlled by the process of resistive diffusion, expressed by the equation,

$$\frac{\partial}{\partial t}\vec{B}_\perp = \frac{1}{\mu_0 \sigma}\nabla^2 \vec{B}_\perp , \qquad (1)$$

The above remarks make it clear that, for instance, no hydromagnetic dynamo (astrophysical dynamo) is possible without the presence of such neutral lines, and an understanding of the plasma behavior at such lines is therefore of great theoretical importance. Neutral lines are a topological property of a geometrical system of magnetic sources and are therefore in no way "destroyed" (as some people have said) unless the source geometry is destroyed or altered into some "degenerate" form. Theoretical study of the neutral point problem has a long history in which great emphasis has been placed on a search for mechanisms which provide a high rate of reconnection so as to account, for instance, for the solar flare. Prior to our experiment (which appears to be the first specifically undertaken for this purpose), the most successful theory from the point of view of fast rates would appear to be Petscheck's.**

---

* This paper presents the results of one phase of research carried out at the Jet Propulsion Laboratory, California Institute of Technology, under Contract No. NAS7-100, sponsored by the National Aeronautics and Space Administration.

** Petscheck, H. E., NASA SP-50, p. 425, U. S. Govt. Printing Office, 1964.

The experiment, as might be expected, has introduced a number of new concepts, and provides the basis for considerable extension of existing theory. Besides providing a remarkably good accounting for the solar flare (regarded as a characteristic group of related phenomena), we have at hand, I think, the ingredients for a completely new concept of hydromagnetic steady-state turbulence under conditions in which the mean magnetic pressure exceeds the gas pressure.

The experiment produces a neutral line at the line of first contact of two cylindrical shock waves (double inverse pinch apparatus), Figure 1. The gas is pre-ionized and the region behind the hydromagnetic shocks is highly conducting. After collision, and some initial diffusive interpenetration of fields, we have a configuration consisting of two parallel line currents at $x = \pm a$, a neutral line at $x = 0$, and a coaxial return path in the merged shocks now at larger radius, Figure 2. We have three flux linkages, one each around the two line currents, and one linkage about both. As the current continues to increase from I to $I + \Delta I$, the return path for the increase ΔI is found to lie entirely in the neighborhood of the neutral line, causing a pinch or compression of the gas into a sheet, Figure 3, along the $\pm$ y-axis and a closing of the angle between the asymptotic lines of the hyperbolic neutral point. These observations are best expressed the other way around: the gas, whose pressure is the lesser of the two principal stresses, retreats into the region of minimum magnetic pressure, the neighborhood of the neutral line. Only by this retreat can the gas acquire a pressure gradient that can oppose the gradient of the magnetic pressure. Since the current is concentrated in the magnetic pressure gradient, the concentration of current may be regarded as a direct consequence of the compression of the medium and would not occur otherwise. There is a simple relation between the current concentration, the current density at the origin, and the angle θ between the x-axis and the asymptotic lines of the neutral point,

$$(2) \qquad j_z(0,0) = \left[\int dx\, j_z(x,0)\right] \frac{\tan^2\theta - 1}{\tan\theta},$$

in which the integral is finite and is determined by the geometry and strength of the external current sources. We see that if θ approaches $\pi/2$, the current density at the origin approaches a Dirac δ-function. This, in fact, is exactly what does happen and it occurs in a time $T = a/V_\infty$, where V_∞ is the Alfvén speed. The physical reason for this is a rearrangement of the gas taking place in the pinch. The gas lying between the asymptotic lines and the y-axis is expelled at a velocity $B_x/\sqrt{\mu_0 \rho}$ by the magnetic force component $J_z B_x$. This ejection, which we call the "surge," takes place during ΔT and terminates this time interval by the removal of the internal gas and magnetic support so that the asymptotic lines can approach tangency at the origin. If the conductivity were infinite, the removal of support by the surge ejection would be complete; the resulting configuration would be a pinch of zero thickness at the origin, with infinite current density but no electric field and no flux change. We define this condition as the critical state. The rate of approach to this state, however, is controlled by dynamic forces and flows and so is independent of the conductivity. In actuality, the conductivity is never infinite and so the electric field can always reach sufficiently high values to "gate" through the neutral point

all the magnetic flux that has been accumulating during the time ΔT. This fact is guaranteed by the existence of the "virtual" critical state, and by the impulsive growth of $\vec{E}$ as the critical state is approached. We obtain the remarkable result that the resistive diffusion time becomes shorter the higher the conductivity. To understand this apparent paradox, note that equation (1) implies a scaling relation between the diffusion time Δt, the conductivity σ and the length ℓ on which diffusion is taking place, the familiar skin-depth relation,

$$\Delta t \cong \mu_0 \sigma \ell^2, \quad \Delta t < \Delta T \tag{3}$$

We have seen that the dynamics of ejection causes σ and ℓ to be inversely related on account of the existence of the critical state. Because of the exponent on ℓ in (3), t and σ become inversely related, and the reduction of thickness is greater than the increase in conductivity causing this reduction. The impulsive growth of $\vec{E}$ permits a corresponding impulsive rate of change of flux. This "flash phase" has been observed in our laboratory experiments. In fact it has been observed to repeat several times as a relaxation oscillation with the period $\Delta T \sim 2\mu$sec (under our conditions), and is accompanied by a corresponding flip-flop between the two configurations: curl-free neutral point, and sheet pinch, Figure 4.

We may expect, when we make the appropriate observations, that the residual gas remaining after the "surge" would be expelled at the much higher velocity E/B as a "spray" during this "flash phase" and the current carriers would enjoy the run-away process along the $\pm$ z-axis, reaching energies as high as eV. The fact is, the relaxation oscillation is a non-linear dynamic process that effects a trade-off which favors particle acceleration in place of ohmic dissipation as the preferred mode of energy dissipation.

In terms of the solar flare, taking 25,000 kilometers as typical of half the distance between relevant sunspots and dividing by the typical surge velocity 50 km/sec as representative of the Alfvén speed, we come out with 500 sec, or $8\frac{1}{2}$ minutes for ΔT, which, being the rise-time of our model flare, is seen to be in excellent agreement with observations. We see also three distinct particle energy spectra produced, the two most energetic of which occur during the violent "flash-phase." In addition, our flare can repeat since it is basically a relaxation oscillation.

Since we are discussing a special form of pinch, we give it the name hyperbolic pinch so that we may conveniently compare it with the more familiar elliptic pinch in which the field lines encircle the current, Table I.

TABLE I

		Elliptic Pinch	Hyperbolic Pinch	
1)	Number of Boundary Conditions	one	two	
2)	Hydromagnetic Stability	no	yes	
3)	Resistive Stability	yes	yes or no	Depending
4)	Ohmic Distruction of Flux	yes	yes or no	on 2nd
5)	Production of New Flux Linkage	no	yes or no	boundary
6)	Natural Occurrence Likely	no	yes	condition

Item (1) of Table I reveals an interesting property. The two opposing pairs of sectors separated by the asymptotic lines may be separately controlled; the added degree of freedom permits a wide and subtle range of effects. If the ejection on the y-axis is uninhibited, we say the y-boundary condition is "free." We have seen that relaxation oscillation is the preferred mode in this case since proximity to the critical state is controlled by the conductivity. If, however, conducting rods are introduced on the y-axis, at say $y = \pm a$, the field due to the induced currents in them will interfere with the flow so that proximity to the critical state is now controlled by this interference. The relaxation oscillation is blocked, and a mode resembling Petscheck's steady-state solution is observed. We propose this to be the process taking place in quiescent prominances. If currents in these rods are externally driven exactly out of phase with those on the x-axis, the y-boundary condition is "rigid," the flow completely inhibited, and we have Harold Grad's cusp geometry. Some of these effects have been observed and studied in our experiments.

Item (6) of the table is of great significance. The elliptic pinch requires the inward flow of energy from a continuous sheet current surrounding the pinch. If the continuity of this sheet is broken, there will also be hyperbolic pinches present. This seems to be a complicated and unrealistic boundary condition to expect to find occurring in a natural system. On the other hand, the minimum requirement for a hyperbolic pinch is two parallel line currents, or a dipole field interacting with almost any other kind of field. The relative simplicity of the latter requirement is obvious. Item (6) is strongly supported by Item (2).

Item (5) relates the hyperbolic pinch to the dynamo. It also provides a much needed mechanism for maintaining a minimum time-average of the total magnetic field energy compatible with steady state but random change taking place in the source distribution (the turbulence problem). It must be emphasized, the hyperbolic pinch can only occur if the magnetic pressure exceeds the gas pressure in the mean.

During the coming year, we hope to investigate this pinch with the use of a ruby-laser Schlieren system employing the technique developed by Ralph Loveberg at U. C. San Diego. We also expect to apply these results in considerable detail to a number of processes taking place in the solar atmosphere.

Two papers have been presented on this subject:

1. Bratenahl, A., and Hirsch, W., Paper X-8, Plasma Phys. Div., A.P.S., November 8-11, 1965, San Francisco, Calif.

2. Bratenahl, A., and Hirsch, W., Paper 66-152, AIAA Plasmadynamics Conference, Monterey, Calif., March 2-4, 1966.

STRAIGHT ARROWS: CURRENT FLOW
CURVED ARROWS: MAGNETIC FLUX
STIPPLE: LUMINOSITY
ENERGY SOURCE: TWO 135-μf
CAPACITOR BANKS, 5-15 kv

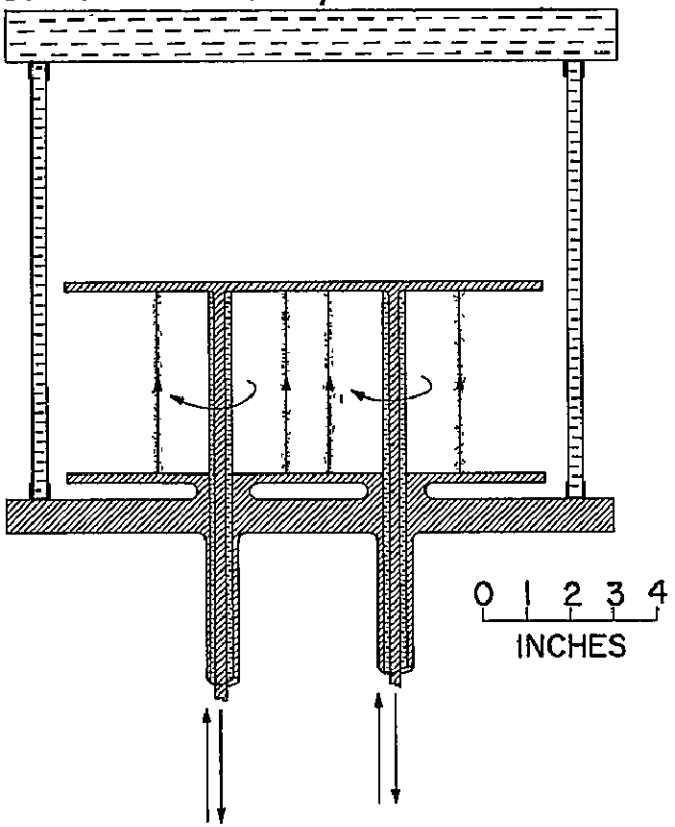

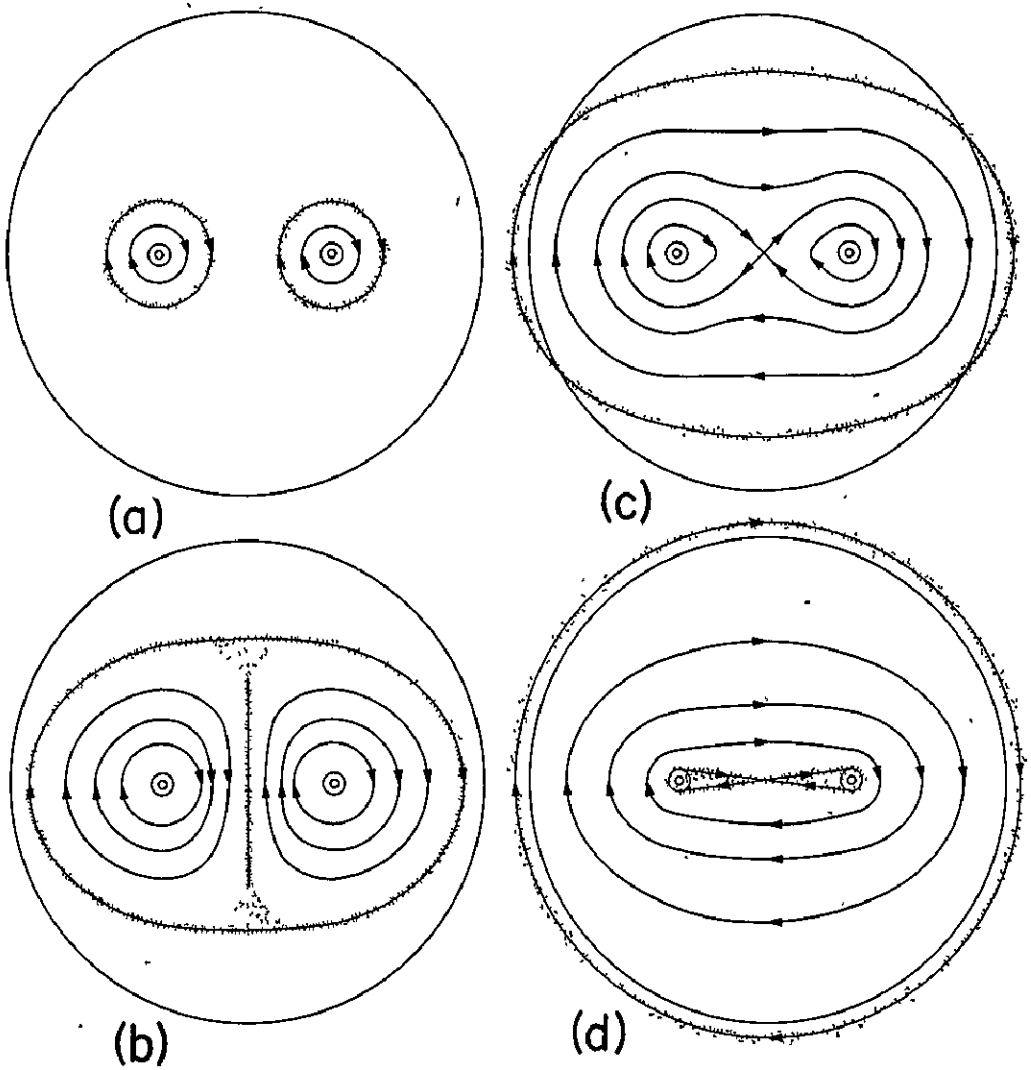

DOUBLE INVERSE PINCH:
(a) BEFORE COLLISION; (c) CURRENT MAXIMUM;
(b) AFTER COLLISION; (d) FIRST CURRENT ZERO

Figure 1

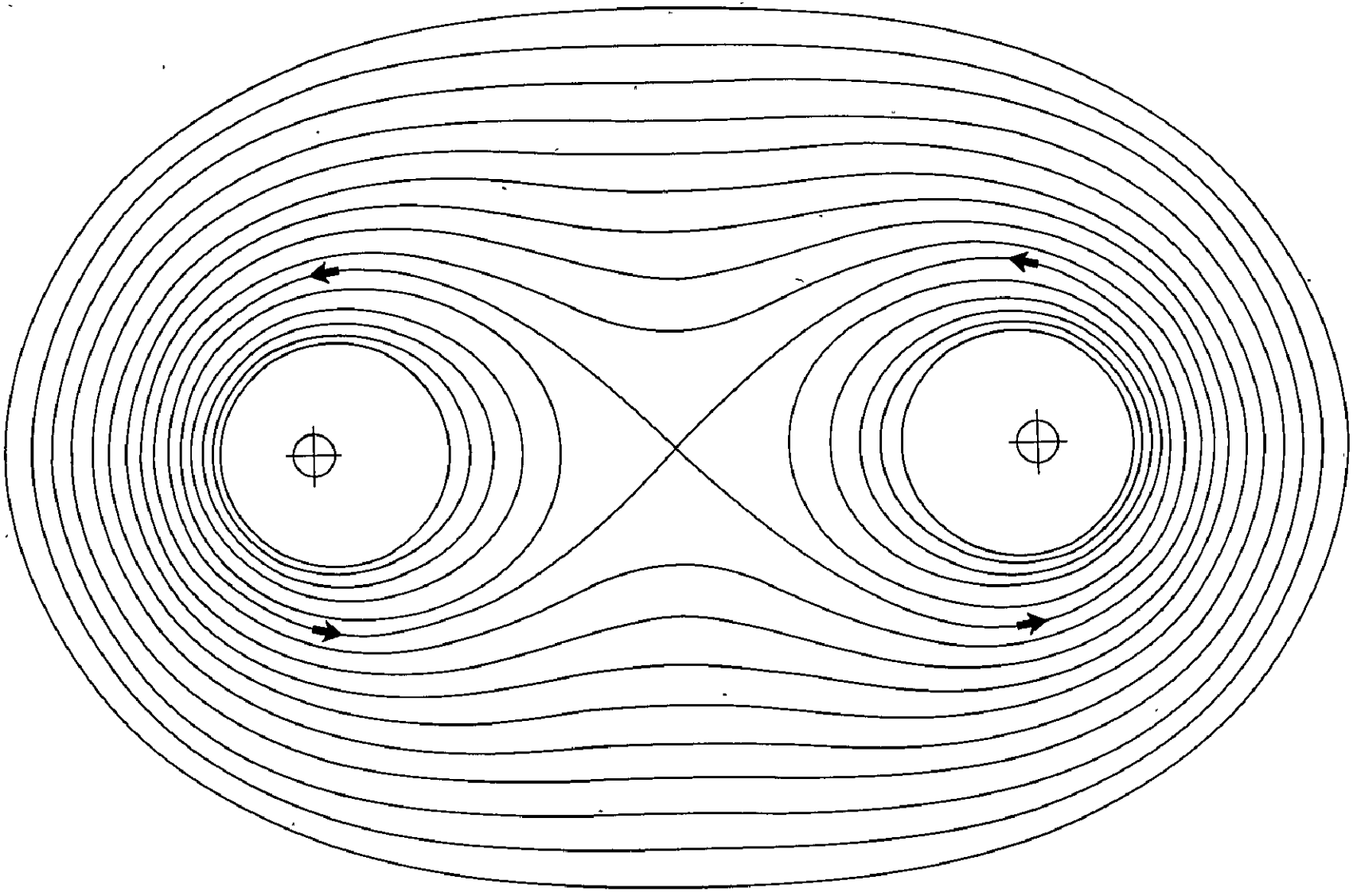

Figure 2 The basic neutral point configuration. Line spacing is 0.1 the value of the vector potential at the neutral point.

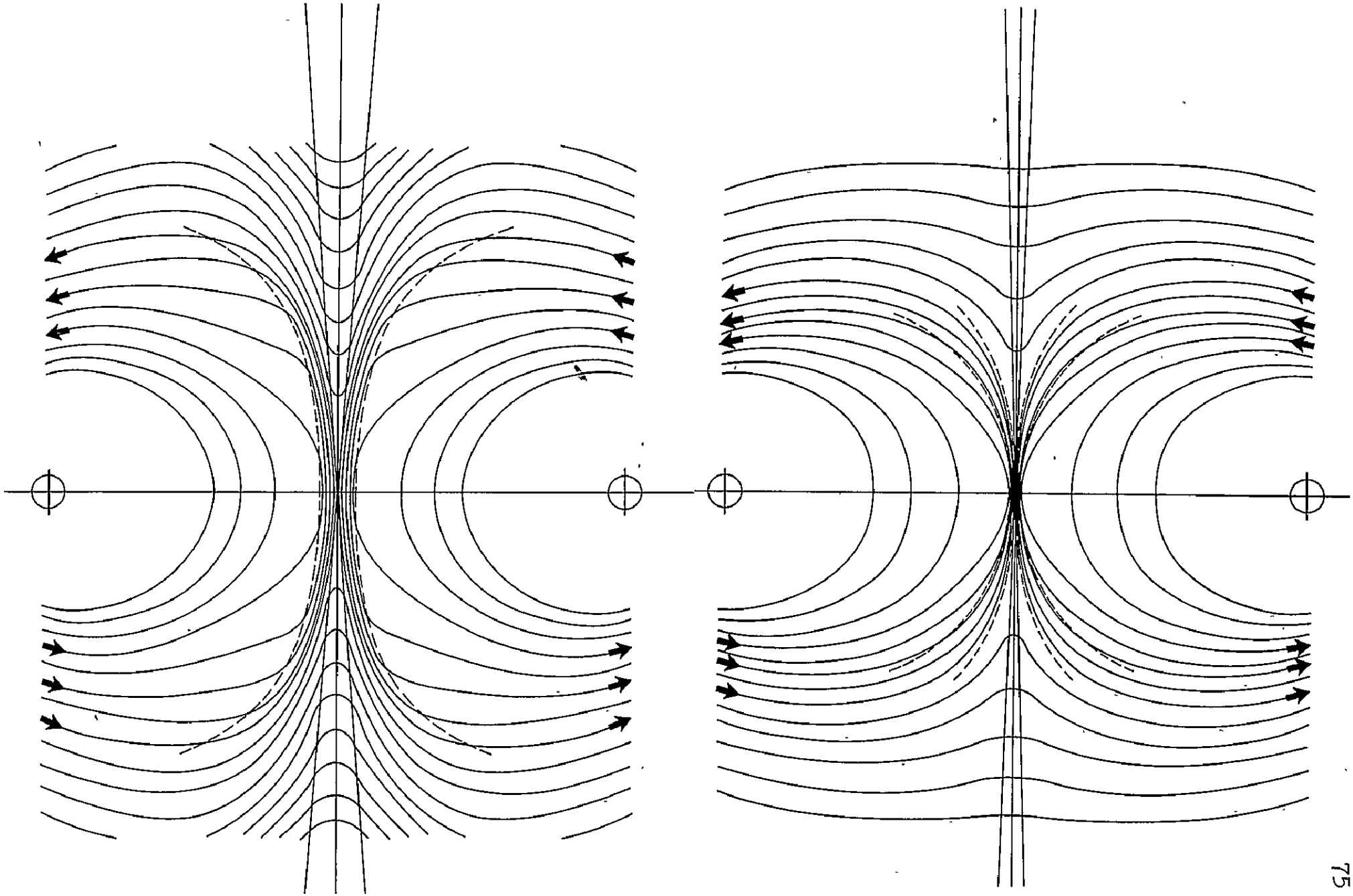

Figure 3 The sheet pinch. Current distribution bounded approximately by dotted lines. Difference between (a) and (b) shows effect of expulsion of gas at Alfvén speed on the angle between asymptotic lines.

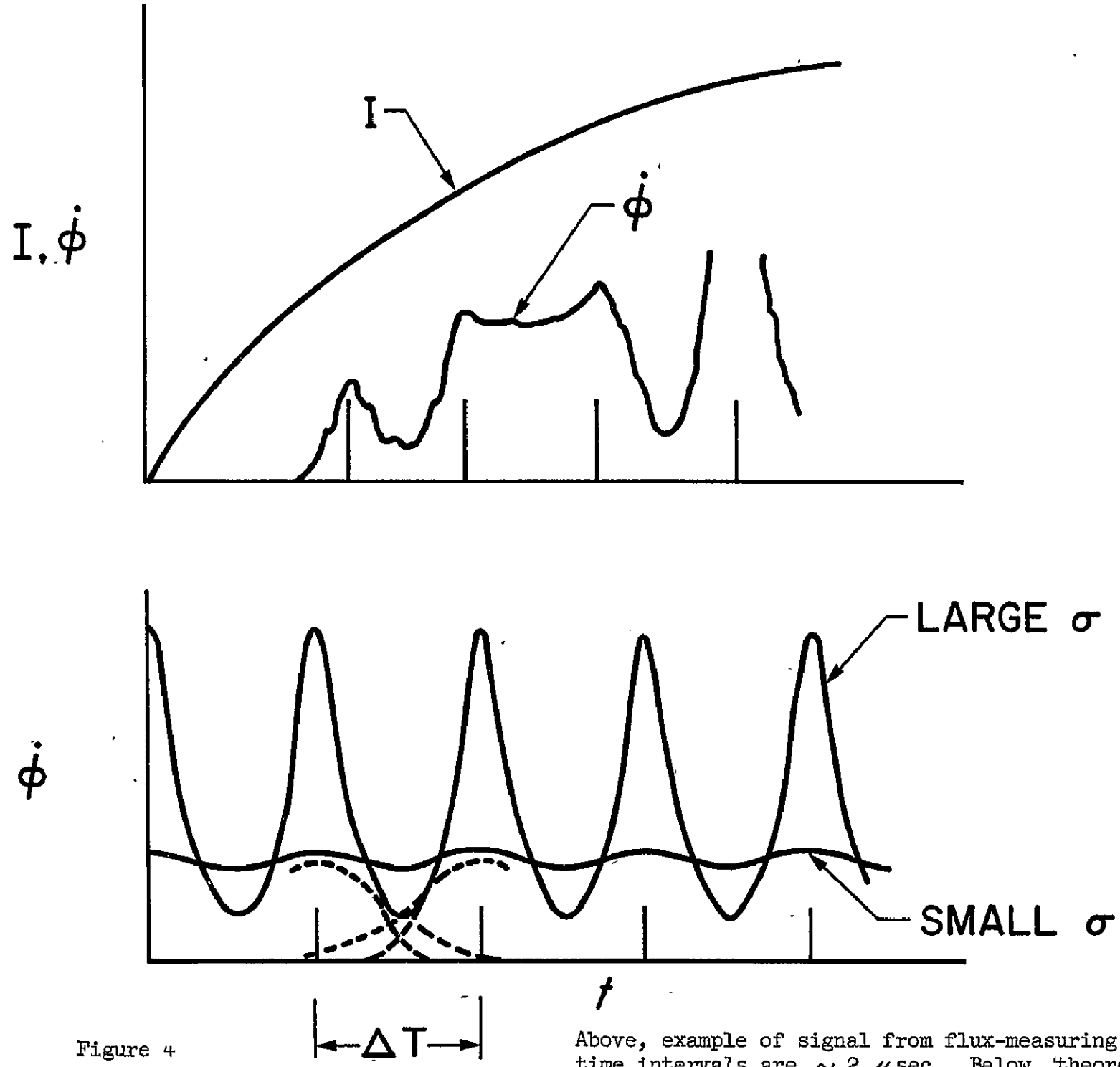

Figure 4

Above, example of signal from flux-measuring probe; time intervals are ~ 2 μsec. Below, theoretical expectation, showing qualitatively effect of σ on $\dot{\phi}$

LASER INDUCED BREAKDOWN, ELECTRON RECOMBINATION AND SHOCK WAVE STRUCTURE IN PARTIALLY IONIZED GASES

Che Jen Chen, Jet Propulsion Laboratory

I. RECENT RESULTS

A. Experimental evidence of inverse Bremsstrahlung and electron impact ionization in low pressure argon ionized by a giant-pulse laser

The generation of plasma in different gases by a giant pulse Ruby laser beam has been reported by several authors. Mechanisms responsible for the ionization of the gas have also been advanced. The following mechanisms have been proposed; multiphoton ionization, microwave breakdown, tunnel auto-ionization, and inverse Bremsstrahlung. In this report experimental evidence is presented which shows that the most probable mechanism for electron production is due to inverse Bremsstrahlung and subsequent electron impact ionization.

A Q-switched giant pulse Ruby laser (6943Å) capable of delivering up to 100 megawatts is focused at a focal point by a lens in an argon atmosphere of pressure from a few milimeters of mercury up to one atmosphere. The gas breakdown at the focal point is observed by an electrostatic probe. The number density of the charged particles produced as a function of time at different pressures is obtained by measuring the conductivity of the plasma drop produced at the focal point of the laser beam. The energy of the electrons in the plasma drop is obtained from the measurement of the time rate of growth of the size of the plasma drop.

An estimation of the ionization has also been made based upon the assumption that some pre-existing electrons gain energy from the laser radiation through inverse Bremsstrahlung processes and ionize the gas by excitational collisions with the gas atoms. By using the concept of the mutual absorption coefficient for the photon-electron interaction given by Wheeler and Wildt, the elastic and excitational collision cross-section given by Petschek and Byron and assuming the rate of ionization to be limited by the rate of excitation to the first excited state, the electron density has been computed for the same conditions as in the experiment. The experimental data agree quite well with the theoretical calculations. Both the experimental and theoretical results indicate that at lower pressures a large fraction of the electrons is produced after the cessation of the laser pulse which is about 20 n sec. An estimation of the time required for the electron to break through the atomic potential barrier indicated that this time is about 5×10^{-14} sec. This time interval cannot account for the lag of production of charged particles behind the laser pulse. Therefore, the possibility of multiphoton absorption and tunnel auto-ionization as a main mechanism responsible for the production of charged particles behind the laser beam can be excluded. The microwave breakdown theory is equivalent to Compton absorption in the quantum mechanical sense. The rate of energy absorption of the electron by this mechanism is estimated to be several orders of magnitude less than the observed values. Therefore, the microwave breakdown mechanism also can be excluded. The possibility of production of a small amount of high energy electrons by photo-ionization which ionizes the gas by impact without the inverse Bremsstrahlung process, can be excluded by cross-section considerations. It is therefore concluded that the ionization process in the gas irradiated by a laser beam is inverse Bremsstrahlung and electron inelastic collisions.

B. Velocity profile measurement in plasma flows using tracers produced by a laser beam

Since a plasma drop is composed of a highly luminous and almost fully ionized gas, the motion of the drop can be detected by the electrostatic probe, drum camera and other techniques. Furthermore, the velocity of the drop will follow the velocity of the flow accurately. Therefore, the drop can be used as a tracer for a flow velocity measurement. The following two methods are used to detect the motion of the plasma drop produced by the laser beam.

1. Electrostatic Probe Method

An electrostatic probe is located at a known distance ($\sim$ 5 mm) downstream of the focal point of the laser beam in a plasma flow. The time required for the drop to travel from the focal point to the probe is measured by the time elapsed between the initiation of the laser pulse and the point of the maximum signal from the probe. The velocity of the flow is thus obtained from the time and distance data.

2. Drum Camera Method

A drum camera having film traveling at speeds up to 100 m/sec is focused at the vertical plane of a plasma flow containing the path of the plasma drop. The velocity of the flow is obtained from the angle between the direction of film motion and that of the streaks formed by the luminous plasma drop.

The plasma tracer method of measuring flow in the present set-up has an accuracy better than 3%. New features of the method are: (a) high spatial resolution--it can give an average velocity over a volume less than $10^{-3}cm^3$; (b) minimum disturbance in the flow.

The drum camera technique has been used successfully to measure velocity profiles in supersonic free jets. The results of this experimental study are summarized in Ref. 1.

C. Partition of Recombination Energy in an Argon Plasma

In the collisional-radiative electron-ion recombination regime, the energy liberated from each recombination is partly carried away by the third colliding free electron and partly transformed into radiation. The partition of the energy among the electrons and radiation is predicted by comparing the probability of the collisional de-excitation at different energy states in the atoms, calculated using Gryzinski's formulation, and the spontaneous transition probability of the bound electron to all lower states evaluated by using the central field approximation. A recombination-dominated decaying plasma is produced by a discharge tube energized with a capacitor bank. After cessation of the discharge current the electron density, electron temperature and atom temperature are measured by using both microwave and electrostatic probes, the spectral line ratio method, and a fast rise-time resistance thermometer, respectively. The partition of the recombination energy under different conditions is determined from a solution of the electron energy equation. The experimental results are in good agreement with the theoretical predictions.

II FUTURE PLANS

A. Study of the partition of recombination energy for other gases than argon: He, Ne, etc.

B. Measurement of the rate of dissociative recombination of an inert gas by using a decaying plasma produced in a DC discharge tube with a mass spectrometer, microwave diagnostics, spectroscope and electrostatic probes.

C. Refine the measuring technique to study the production of plasma by a laser beam including electron density and temperature measurements using spectral line broadening with time resolving spectroscopic techniques utilizing a STL converter camera.

D. Investigation of shock structure in a partially ionized gas utilizing laser scattering techniques.

REFERENCES

1. Chen, C. J., "Experimental Study of Breakdown Phenomena in an Argon Gas by a Laser Beam at Low Pressures," AIAA Plasmadynamics Conference, Monterey, California, March 2-4, 1966, AIAA Paper No. 66-176.

MEASUREMENTS NEAR A SHOCK WAVE IN A SEEDED-GAS PLASMA*

W. H. Christiansen

Jet Propulsion Laboratory
California Institute of Technology

ABSTRACT

A cesium-seeded argon gas stream has been used for plasma studies in a low-density wind tunnel. The device[1] is briefly described and some results of measurements near a plasma shock wave are presented.

Spectroscopic methods and free-molecule Langmuir probes were used to measure electron number density and temperature profiles in front of a flat disk in a supersonic plasma. The region of interest extends from the disk surface, through the shock, and several body diameters upstream of the disk. The measurements are compared with each other, and in turn compared with plasma shock wave theory for a free-stream electron density of approximately $10^{12}/cm^3$. The measurements show a nearly constant electron temperature through the shock wave, a result which is compatible with energy relaxation times at these densities. However, the same measurements also indicate an electron density behavior that is not in accordance with plasma shock wave theory.

---

* This paper presents the results of one phase of research carried out at the Jet Propulsion Laboratory, California Institute of Technology, under Contract No. NAS7-100, sponsored by the National Aeronautics and Space Administration.

1 Christiansen, Walter, Rev. Sci. Instr. 36, 71-75, January 1965.

HIGH PURITY SHOCK TUBE IONIZATION STUDIES

A. J. Kelly, Jet Propulsion Laboratory

The design of a high purity shock tube has been essentially completed and the preliminary phases of construction initiated. This shock tube has been designed specifically to provide information on the initial, atom-atom and electron-atom, ionization relaxation processes which occur behind strong (M_s>6) shock waves in the noble gases. Of particular interest is the delineation of the various inelastic and elastic interactions which influence both the electron density and the electron temperature profiles.

When a strong shock wave propagates through a body of gas, ionization relaxation occurs, i.e. the electron density of the body of gas behind the shock increases. This ionization process can be roughly divided into two stages. Immediately after the passage of the shock front the electron density builds up, as a linear function of time, the predominant ionization reaction being the electron temperature independent atom-atom two-step excitation-ionization process. When a sufficiently large number of electrons have been produced by this process the more efficient electron-atom ionization process becomes dominant. During this phase the electron generation rate is a function of the electron density and temperature.

The first stage (i.e., atom-atom ionization has been studied, the reaction delineated and the cross-sections for Ar, Kr and X_e determined.[1] Calculations by Petschek and Byron[2] concerning the onset (i.e., transition from atom-atom to electron-atom dominated ionization), of electron-atom ionization predicted transition electron densities which are a full order of magnitude higher than were observed in the studies of Ref. 1. This indicated that a reaction hitherto unaccounted for in any analysis of the post shock ionization process was operative, viz. evaluation of electron temperature by atom-atom ionization collisions. This interesting reaction is now being studied analytically and with the completion of the shock tube will be experimentally investigated as well.

In order to accomplish these ionization studies, which involve only weakly ionized gases, i.e., gases with ionization levels of $< 10^{-4}$, it is mandatory that the impurity level of the test gases be restricted to levels of the order of 10^{-6}(1-PPM) or less. Previous experiments[3] have demonstrated that, should the level of contamination exceed this level by a factor of 10 or more, spurious results could be expected. Consequently, the shock tube is being designed to be baked and permit evacuation to pressures below 10^{-6} torr. As a consequence, the combined leak and outgassing rates are anticipated (on the basis of previous work[1]) to be such that, the overall impurity level will meet requirements. The test gas flow system allows a flow of the pre-shock test gas (at pressures around 10 torr) to sweep out and dilute contaminants present from outgassing and leaks.

There will be three major diagnostic systems employed on this experiment. Atom temperature will be inferred from shock velocity data gathered by shadowgraph shock position indicators and recorded on a high precision

oscilloscope raster display. The electronics, for the majority of this system, have been well proven in previous applications[1]. This system will permit not only the mean shock velocity to be measured but also shock attenuation. A knowledge of shock attenuation is necessary, as any small variation in atom temperature due to variation in Mach number along the slug of heated gas passing the observation station would have a large effect upon the ionization rate in the atom-atom regime. The effects of shock attenuation have to be accounted for in both the atom-atom and the electron-atom regime, as electron generation rates can be increased by a factor of 2 or more above the zero attenuation case by modest levels (2%/meter) of shock attenuation in argon.

Electron densities in the range $10^{11} \leq N_e \leq 10^{14}$ will be measured by two independent microwave systems mounted so as to be transverse to the shock tube, the microwave beams propogating through the quartz diagnostics section of the tube. One system will operate at a nominal frequency of 24 GHz and provide electron density information over the range $10^{11} \leq N_e \leq 10^{13}$. This system will monitor the measurable phase and the amplitudes of the signals transmitted through and reflected from the shock generated plasma. The circuitry for this system[4] and the procedures for its proper adaptation to the shock tube[1,4] have been well tested and shown to be adequate. A similar, 90.0 GHz, system is in the process of being assembled. The power generation and modification portion of the circuitry have been completed. The 24 GHz system is available and requires only very minor modification for application to the tube.

The third diagnostic tool will be the high resolution spectroscopes available to this project (Jarrell-Ash 3M, ARL 1.5M). These devices will be employed to determine the electron temperature history of the gas behind the shock and to provide an insight into the manner in which the excited stages are populated and de-populated, in an effort to refine our understanding of the influence that radiative processes have upon the ionization reactions.

It is anticipated that once the main task of the investigation of the ionization transition region is completed, that a study of the degree to which resonance radiation trapping contributes to atom-atom ionization will be undertaken. This study will require the use of vacuum ultra-violet spectroscopic techniques as the resonance radiation from the noble gases of interest occur at ~ 1000 A°. Future work will include the study of the atom-atom, and electron-atom ionization processes under the influence of electric and magnetic fields to contribute to our knowledge of these more generalized non-equilibrium processes. To pursue these studies the shock tube proper (exclusive of the dielectric diagnostic section) will be constructed of non-magnetic metal tubing.

REFERENCES

1. Kelly, A. J., "Atom-Atom Ionization Mechanisms and Cross Sections in Noble Gases and Noble Gas Mixtures," Ph.D. Thesis, California Institute of Technology (1965).
2. Tetschak, H. E. and Byron, S., Ann. Phys. (N.Y.) 1, 270 (1957).
3. Harwell, K. E., Jahn, R. G., Phys. Fluids 7, 214 (1964).
4. Kelly, A. J., JPL TR-32-835, "An Experimental Feasibility Study of Injectant Materials to Alleviate Mars Entry Communications Blackout" (1965).

HEAT TRANSFER FROM STEADY INTERNAL FLOWS OF A THERMALLY IONIZED GAS - CORE FLOW ANALYSIS

P. F. Massier, Jet Propulsion Laboratory

The objectives of this investigation are to determine the influence of ionization, acceleration, and applied magnetic and electric fields on heat transfer and fluid dynamics of steady internal flows of partially ionized gases. Both the analytical and the experimental work conducted thus far has been concentrated on the effect of thermal ionization and acceleration, particularly for argon.

The investigation was initiated as a consequence of the interest and the limited understanding of the heat transfer and the fluid flow phenomena associated with steady-flow electrical propulsion and power generation devices and plasma test facilities. The containment of high-temperature thermally ionized gases and the expansion of the flow to supersonic velocities impose severe cooling requirements on mixing chamber and nozzle walls as well as on the anode. Experiments conducted thus far pertaining to the influence of ionization and acceleration on heat transfer from argon have ranged between 0.1 and 2.0 atmospheres pressure. The ratio of the ionization energy to total energy content of the gas as determined by energy balance has ranged from essentially zero to about 0.5.

Approximate radiative heat transfer from subsonic non-accelerating flows of argon have been determined by calculation as well as experimentally by means of a circumfrential cavity used as a segment of the flow passage. For pressures in the vicinity of 0.2 atm., at which the cavity results were obtained, it was found that the radiative heat flux is less than 2% of the convective heat flux. A sketch of the test apparatus with the cavities is shown in Figure 1.

Several models of the fluid flow have been selected to aid in the analysis of the experimental data and to provide boundary conditions for making theoretical heat transfer predictions. These models are differentiated by assumptions which include: equilibrium flow, nonequilibrium flow, adiabatic core flow with a non-adiabatic laminar boundary layer, and non-adiabatic uniform flow. The need for a variety of models is a consequence of the high enthalpies encountered, the recombination effects, and the ranges of operating conditions. For an equilibrium adiabatic core flow without viscous effects or radiation, the equations of motion contain the following variables:

Entrophy:

$$S_s = f_1(\alpha_s, T_s, p_s) \tag{1}$$

Saha:

$$\alpha_s = f_2(T_s, p_s) \tag{2}$$

State:

$$p_s = (1 + \alpha_s)\ \rho_s R T_s \tag{3}$$

Continuity:

$$\dot{m} = \rho_s V A_c \tag{4}$$

Enthalpy:

$$H_{t_o} = 5/2\ (1 + \alpha_s)RT_s + \alpha_s I_o + \frac{V^2}{2} \tag{5}$$

Momentum:

$$\frac{1}{\rho_s}\ \frac{dp_s}{dx} + V\frac{dV}{dx} = 0 \tag{6}$$

The flow variables obtained by measurement are the wall static pressure p_s, the mass flow rate $\dot{m}$, the flow cross sectional area A_c, and from an energy balance the inlet stagnation enthalpy H_{t_o}. In a constant-diameter section the flow is one-dimensional and the flow variables are obtained by using equations (1) - (5) in which there are 5 unknowns: the velocity V, and static values of the entropy S_s, the ionization fraction α_s, the gas temperature T_s, and the density ρ_s. Stagnation values are obtained by setting V = 0 and equating the stagnation and static entropies, i.e., $S_s = S_t$. In addition Equations (1) - (3) are used replacing the static values with stagnation values. The unknowns are α_t, T_t and ρ_t.

In an accelerating flow, Equation (4) is replaced with Equation (6) which allows the flow to be quasi two-dimensional. For this case there are again 5 equations with 5 unknowns.

For nonadiabatic uniform flow, allowance is made for the heat transferred to the wall. This is of significance as a limiting case to allow for the thermal boundary layer thicknesses that extend to the centerline of the passage. To account for the heat transfer, Equation (7) is added.

Energy:

$$H_t = H_{t_o} - \Sigma \frac{Q}{\dot{m}} \tag{7}$$

One additional unknown is introduced by Equation (7) which is the local stagnation enthalpy H_t. Q represents the heat transfer which is determined from calorimetric measurements obtained in numerous coolant passages along the test apparatus. For an accelerating flow the equations for this case are (1), (2), (3), (5), (6) and (7).

For a nonequilibrium accelerating flow additional equations are needed to account for the recombination rates and the consequent influence of the recombination on the electron temperature.

Results obtained from the experiments coupled with the adiabatic core flow analyses establish the flow variables that are essential for making comparisons with boundary layer predictions. The important variables at the free stream edge of the boundary layer are the mass flux, $\rho_s V$, the stagnation enthalpy, H_{t_o}, and the static temperature T_s. Experimental results will be discussed in the following presentation by Dr. Back.

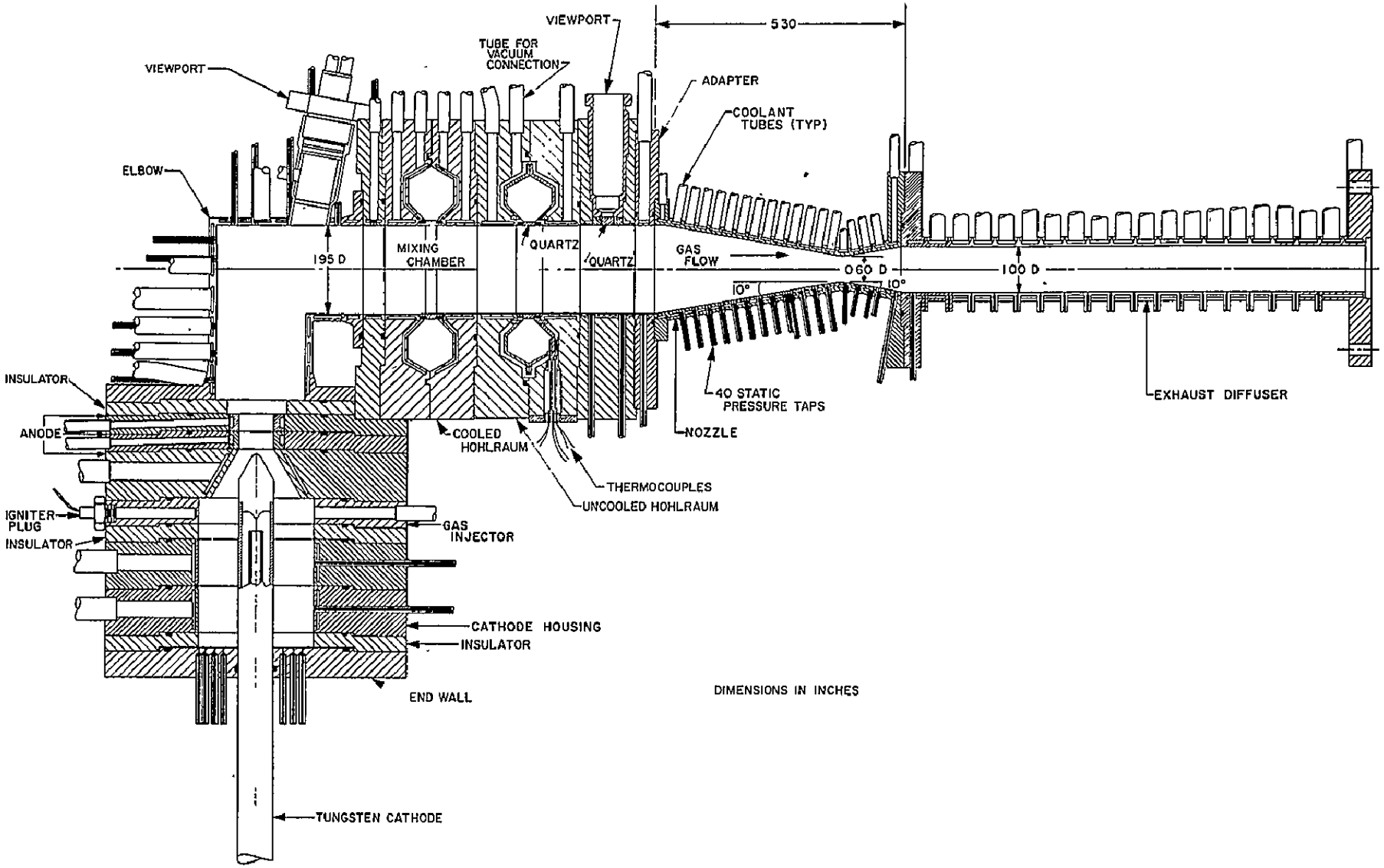

IONIZED GAS HEAT TRANSFER TEST APPARATUS

Figure 1

MAGNETO-FLUID DYNAMIC FLOW OVER BLUFF BODIES*

T. Maxworthy and G. Yonas

Jet Propulsion Laboratory
California Institute of Technology

ABSTRACT

We are measuring the character of the flow of a conducting fluid as it passes over a bluff body suspended in an aligned magnetic field. A flow tunnel which pumps liquid sodium (at 135°C) around a closed loop is used for this purpose and is shown in Fig. 1. The nature of the flow through the test section has been determined and found to be suitable for aerodynamic testing except under the most adverse circumstances (very strong magnetic fields and very low flow rates).

Three types of test have been used to look at the flow field:

i) Drag measurements. Using a three-wire suspension system and conventional high-temperature strain gauge techniques, the drag of spheres and disks of various sizes has been measured. Typical results are shown in Fig. 2, where the drag coefficient is plotted against the interaction parameter N (ratio of Lorentz force to inertia force). As N becomes large $C_D \sim \sqrt{N}$ and is the same for disks and spheres.

ii) Pressure distribution measurements. A special rotating sphere mechanism allows us to measure the distribution of static pressure as a function of angular position around a sphere. Again at large N the distribution has the character shown in Fig. 3. The large increase in drag is seen to be due mainly to a large increase in the suction pressure behind the sphere and, secondarily, to a more uniform distribution of the stagnation pressure over the front of the sphere.

iii) Wake measurements. Using slightly modified Pitot-static probes, it is possible to probe the velocity and pressure distribution field behind the sphere. Attempts are being made to measure these quantities in front of a sphere but with limited success so far. Immediately behind a sphere, at large N, a stagnant region of fluid is formed. At distances larger than the sphere radius, the axial velocity is considerably in excess of the free stream velocity. A very intense shear layer joins these two regions.

A composite picture of the flow at large (but not infinite) N is shown in Fig. 4, and this includes all of the reliable information available on such flows.

* This paper presents the results of one phase of research carried out at the Jet Propulsion Laboratory, California Institute of Technology, under Contract No. NAS7-100, sponsored by the National Aeronautics and Space Administration.

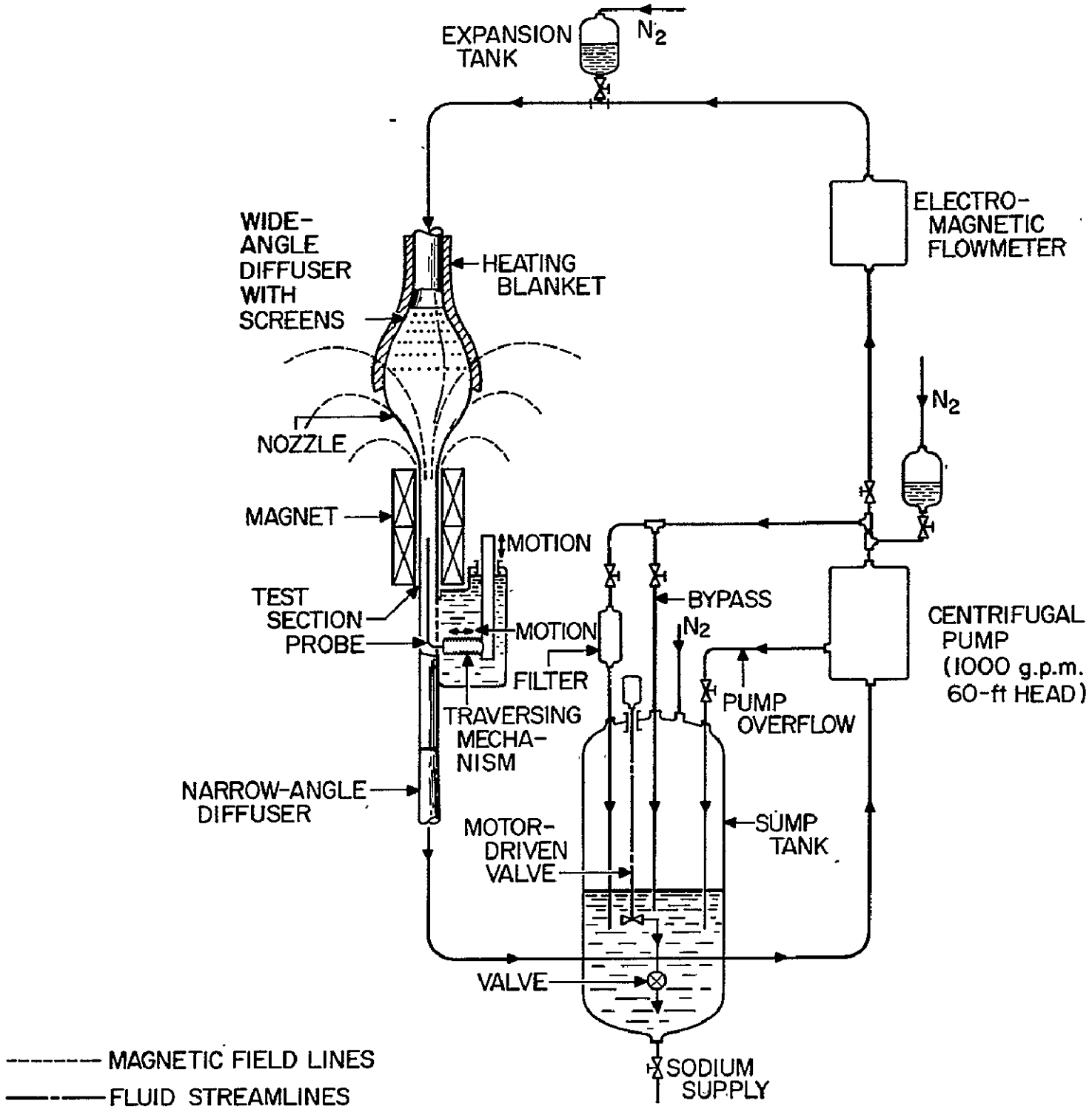

FLOW DIAGRAM FOR THE J.P.L. LIQUID SODIUM TEST FACILITY

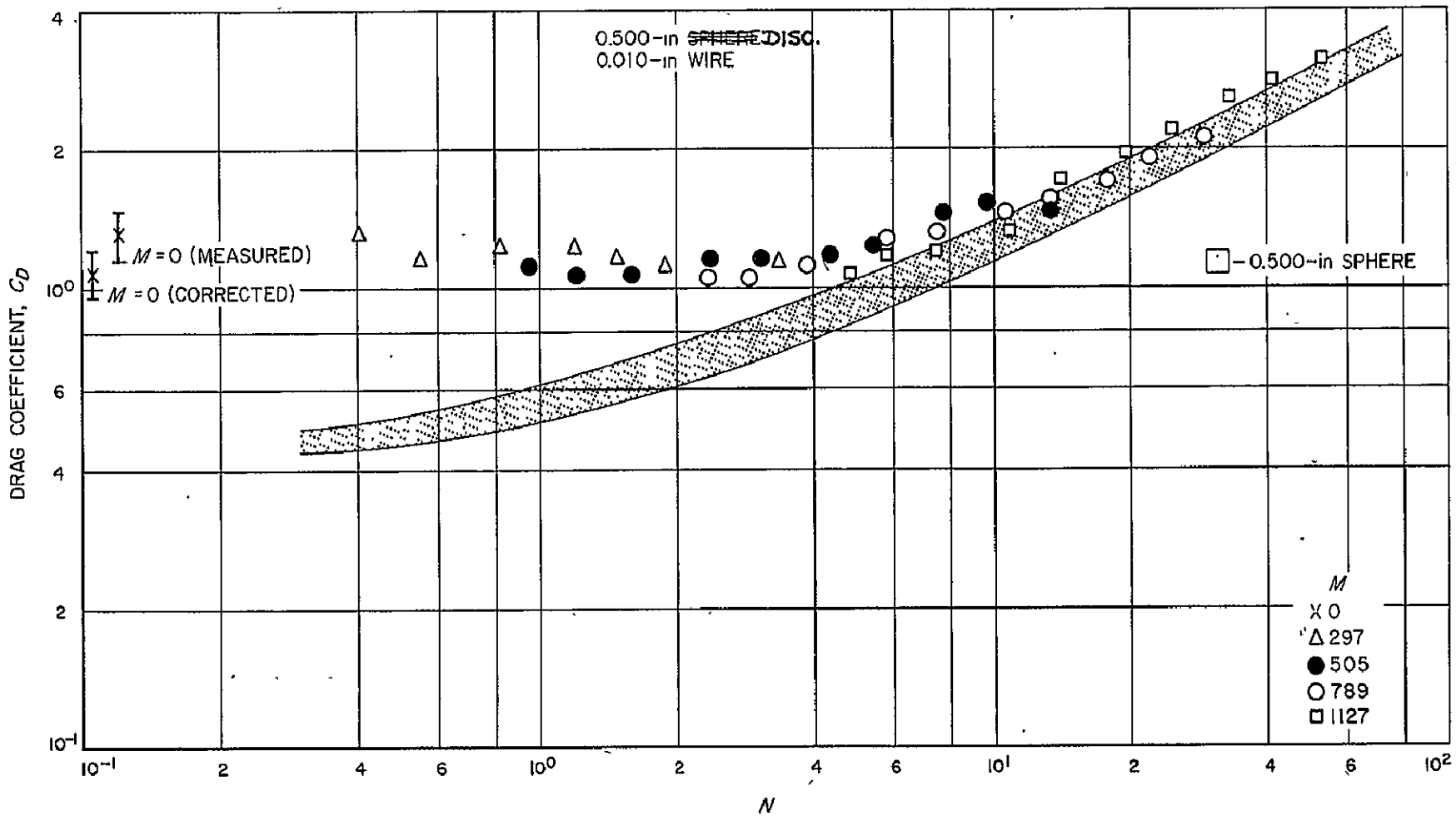
0.500-in ~~SPHERE~~DISC.
0.010-in WIRE
M = 0 (MEASURED)
M = 0 (CORRECTED)
0.500-in SPHERE
M
0
297
505
789
1127
DRAG COEFFICIENT, C_D
N
4
2
10^0
6
4
2
10^{-1}
10^{-1}
2
4
6
10^0
2
4
6
10^1
2
4
6
10^2

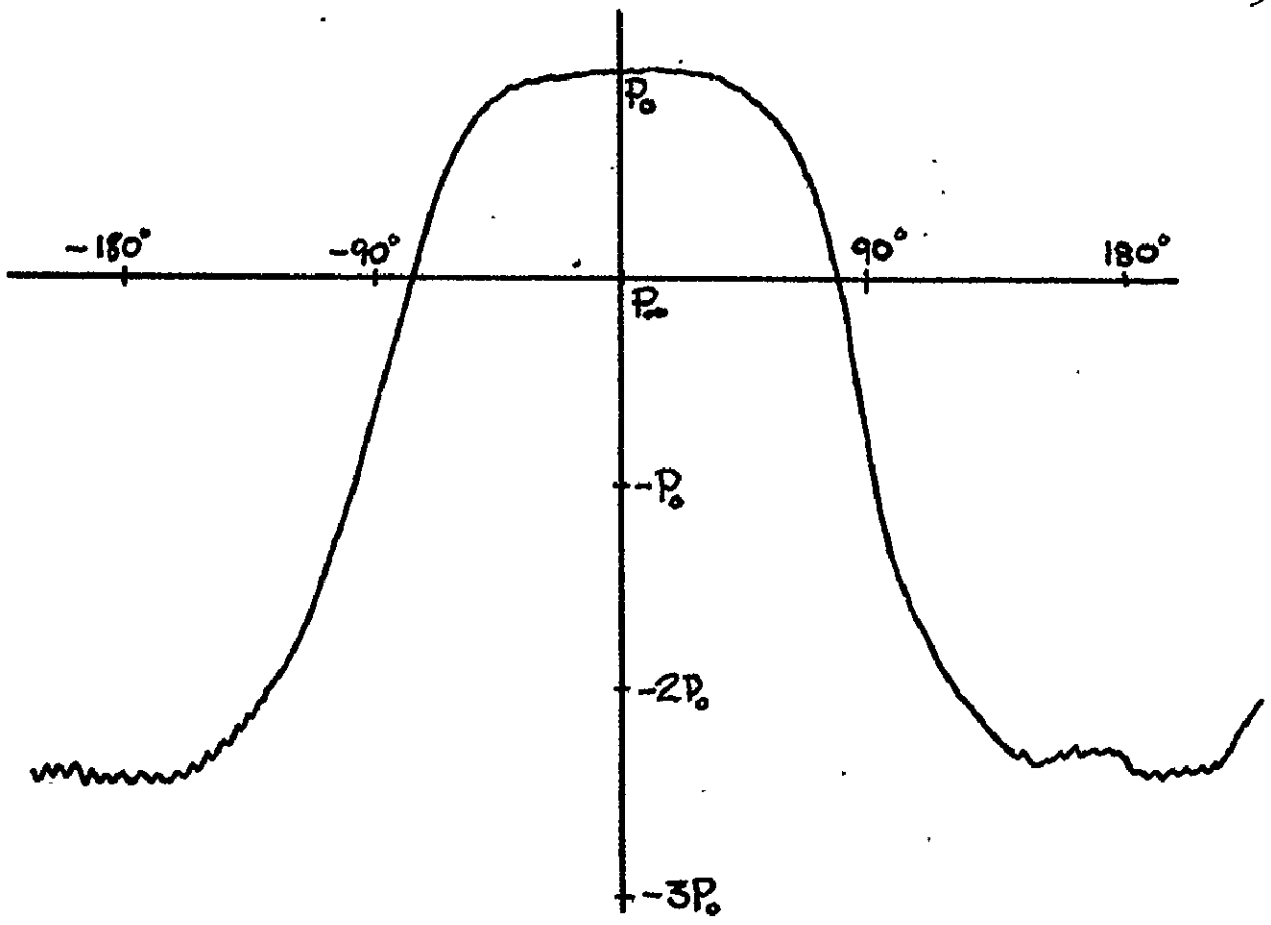

PRESSURE DISTRIBUTION for N=40.

P_∞ = Upstream Static Pressure.

P_0 = Upstream Stagnation Pressure.

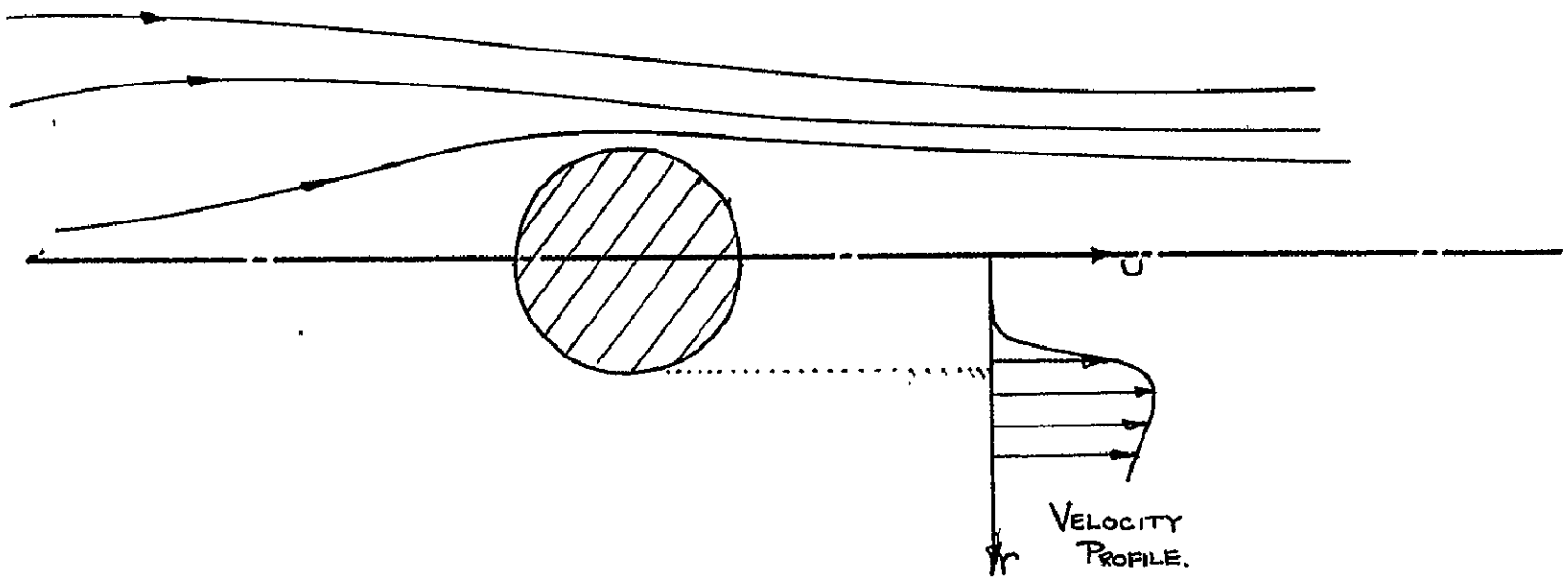

FLOW FIELD for N~40

MEASUREMENT OF ELECTRON TEMPERATURE AND DENSITY PROFILES IN AN MPD ARC

N. M. Nerheim, Jet Propulsion Laboratory

Early results obtained from MPD thrustors showed great promise for their use as efficient, high specific impulse engines. However, as investigations continued at lower test pressures and smaller propellant feed rates, inconsistencies in the data, such as impossibly high thrust efficiencies, became apparent. These inconsistencies are as yet unsolved, and as a consequence the actual capability of the MPD engine is seriously questioned, particularly at low feed rates. Although the level of effort devoted to detailed diagnostics is increasing, the emphasis has been placed on the development of increased efficiency and lifetime with fuels compatible with long-term space missions. The theories that have evolved are based largely on visual observations and the observed trends of thrust, arc voltage and, to some extent, current paths in the exhaust as a function of the operating conditions. Unfortunately, the interactions of the electromagnetic and fluid dynamic forces are very complicated, and a consistant theory of the major thrust producing mechanism has not been formulated.

One of the areas that has not been adequately investigated is the inter-electrode region where most of the ionization occurs. Detailed information on the state of the plasma before it becomes fully ionized and highly accelerated may help explain the reasons for some of the observed behavior. For example, it is possible that rate processes should be considered in the design.

One of the objectives of the present investigation will be to measure the electron density and temperature in the inter-electrode region by spectroscopic methods. An existing MPD source will be modified to allow observation of this region. The initial experiments will use argon. Line broadening measurements, with hydrogen or helium trace elements, will be used to determine electron densities and standard spectroscopic methods will be used to determine the temperature.

Our past work[1,2] in plasma spectroscopy has been largely concerned with temperature determinations of the exhaust plume of an MPD source operated on argon. A 0.5 meter Ebert-mounted plane grating monochromator and a RCA 7265 photomultiplier tube were used to make the measurements. The temperature was determined from the relative intensities of fourteen argon ion lines for which Olsen[3] has published values of the transition probabilities. All measurements were taken near the exit of the plasma source where the intensities of the ion lines were high. Radial intensity profiles were obtained for each line by inverting the measured lateral profiles with Abel's transformation. The temperature at a number of points along the plume radius was then found by a least-mean-square fit of the data which are displayed in the usual manner on a Boltzmann plot.

The relative-line-intensity method was used for the temperature determination. It is less accurate than some other methods of spectroscopic temperature measurements, but it was the only useable method for the plasma conditions that existed. The more reliable Larenz method is based on the

principal that, at a fixed pressure, the intensity of every spectral line from an equilibrium plasma reaches a maximum at a certain temperature that is called the normal temperature. Its use requires that the intensity of the line radia- have a maximum at some off-axis position at which point the plasma is at the normal temperature. The temperature profile of the MPD plume was found to be nearly constant at about 18,000°K. This is above the normal temperature of the atomic line and below that of the ion lines. Another condition that precluded the use of the Larenz method was that the pressure across the exhaust was not constant because of shock formations.

A major factor that limits the accuracy of the relative-line-intensity method, in addition to the errors in the transition probabilities, is the small difference in the upper energy levels of the lines observed. For the ion lines used in this work, the difference is about 2 eV. If the relative intensities of both the atom line and the ion line could be compared, the energy level difference would be increased to about 8 eV and the uncertainty in the temperature correspondingly decreased. The use of both species requires that atom and ion concentrations be related through equilibrium relationships. The range of conditions at which both species radiate with sufficient intensity for accurate measurement is limited. The atom lines in the MPD exhaust are very weak.

Recent published analysis[4] of the maximum errors that can occur, if only two lines are used, have shown that it is possible for the accuracy to be so poor that the method would be worthless. However, if a large number of lines are used, and if the errors in the relative values of the published transition probabilities are randomly distributed the errors will be much smaller than those estimated for the two-line method. A standard calculation, that is based on the least-mean-square fit of the data and relates an error to the amount of data scatter, has been used in this work to obtain an estimated error of approximately 7% on the jet centerline.

The correlation between the spectroscopically measured excitation temperature and the electron temperature is not generally known if the plasma departs from local thermal equilibrium (LTE). The two temperatures are identical if the population levels of the excited states are controlled by collisions with electrons that have a Maxwellian velocity distribution. How well these conditions are fulfilled as the plasma departs from LTE is not well known. Part of the planned work will be to obtain an experimental correlation between the excitation temperature and the electron temperature as a function of the arc operation conditions by comparing the spectroscopic measurements with Langmuir probe measurements. The MPD source has been operated from low pressures (~ 100 micron) up to atmospheric pressure; therefore, it will be possible to examine the plasma in regimes where LTE may reasonably be expected to exist and where both the atom and ion line can be measured. The relation between the radiation from the two species will be investigated and compared to the probe results as a function of the ambient pressure and total enthalpy. Because of the large amount of data that must be handled in performing the Abel inversion for each line, some effort will be devoted to recording the data in digital form.

REFERENCES

1. Kelly, A. J., Nerheim, N. M., Gardner, J. A., "Electron Density and Temperature Measurements in the Exhaust of an MPD Source," AIAA Second Annual Meeting, San Francisco, Calif., July 26, 1965, AIAA Paper No. 65-298.

2. Nerheim, N., "Spectroscopie Measurement of Plasma Electron Temperature Using The Relative Intensities of Argon II Lines," JPL Space Programs Summary No. 37-35, Vol. IV, p. 174 (1965).

3. Olsen, H. N., "The Electric Arc as a Light Source for Quantitative Spectroscopy," J. Quant. Spectrosc. Radiat. Transfer, Vol. 3, p. 305, Pergamon Press, Ltd., 1963, Great Britain.

4. Chuang, H., "Uncertainties in the Measurement of Helium Plasma Temperature by the Relative Intensity Method," Applied Optics, Vol. 4, p. 1589, Dec. 1965.

STUDY OF A NONEQUILIBRIUM MHD GENERATOR UTILIZING INERT GASES AND INERT GAS MIXTURES

Gary R. Russell, Jet Propulsion Laboratory

A study has been initiated at JPL to determine the feasibility of operating a nonequilibrium MHD generator utilizing inert gases without the addition of metalic vapor seeding. Both theoretical and experimental work are included in the program.

Normally, in the theoretical treatment of nonequilibrium generators, it is assumed that a steady state has been attained where electron elastic energy losses and possibly radiative losses are exactly balanced by the energy addition from the magnetically induced electric field. Usually, it is assumed that the Saha equation is valid and that the electron density is in equilibrium with the free electron temperature. The transient problem of how this energy balance is established, or whether it can be established at all, has received relatively little attention. Comparisons of inert gases and inert gas mixtures with alkali-metal seeded inert gases to determine optimum working fluids for nonequilibrium generators should include the complete transient flow problem for both cases. Here, solutions are obtained only for pure inert gases and inert gas mixtures to determine the feasibility of achieving nonequilibrium operation, without the addition of metalic vapors, where the degree of ionization at the generator entrance is extremely small.

A computer program has been generated to determine nonequilibrium MHD generator plasma properties considering simultaneously the electron heating, ionization and subsequent energy extraction from the plasma. The generalized macroscopic equations describing a quasi-one-dimensional flow of a compressible multi-component plasma with different species temperatures are solved utilizing the transport theory of Zhadanov[1] to obtain a generalized Ohm's law and electron energy equation. In addition to the tensor electrical conductivity, radiation, electron thermal conductivity, thermal-electric effects, and finite electron ionization and recombination rates are included in the analysis. A three level hydrogen-like model is used to calculate the rate of change of the population of the first excited state, the free electron density, and the radiation associated with the ionization process. It is shown that continuum radiation is always negligible compared with the elastic energy losses from the electron gas and, therefore, can be neglected in the electron energy equation. The ionizing radiation is not always negligible, and particularly at the end of the ionization period when excited state populations are relatively large, the radiation must be included in the electron energy equation.

Constant pressure and variable area solutions can be obtained from the computer program. Pure argon, pure xenon and argon-xenon and helium-xenon mixtures have been studied as working fluids. For the case of the supersonic generator, the expansion in a supersonic nozzle is also analyzed with a computer to determine the entrance conditions of the generator--principally the degree of ionization and nozzle induced electron temperature elevation.

The principle results of the computer program obtained thus far are the following:

1. Generator operation can be attained utilizing inert gases and inert gas mixtures without metalic-vapor seeding at stagnation temperatures attained in nuclear reactors.

2. The electron temperature elevation is achieved before appreciable ionization commences. Thus, the flow consists of three approximately separate regions--an entrance region where only the electron temperature changes, an ionization region where the electron density increases at an elevated electron temperature, and an energy extraction region where all the plasma variables can change rapidly along the duct length.

3. Saha equilibrium at the electron temperature is rarely achieved. Generally, adjacent to the generator entrance the electron density appreciably lags the electron temperature. After the start of appreciable energy extraction and a subsequent decrease in the plasma velocity, electron recombination is not fast enough to maintain equilibrium, so that the electron density and electrical conductivity tend to remain elevated as the electron temperature decreases.

4. The generator length is determined almost exclusively by the rate of ionization of the gas with the lower ionization potential in a gas mixture. This length may be increased appreciably by radiative depopulation of excited states at low electron densities.

5. Because the energy necessary for ionization is supplied by the electron gas the inelastic losses in the electron energy balance can cause the electron temperature to be reduced appreciably below the value determined by elastic collisional losses, thereby reducing the ionization rate and increasing the generator length. This reduction in the ionization rate fixes an upper bound for a given Hall parameter on the atom density and gas pressure which, if exceeded, will result in excessive generator lengths. For example, in a 2% xenon-98% helium mixture, for atom densities greater than about $10^{18} cm^{-3}$, the generator length would exceed ten meters.

An experimental MHD generator is now under construction and should be completed in a few months. The generator is designed to operate in the supersonic range at constant pressure. Other types of operation are possible, but operation at constant pressure may minimize the possibility of shock waves forming in the flow in regions of rapid energy extraction[2]. Also, there is some experimental evidence obtained with cross-field accelerators indicating that electrode and insulator reliability can be attained much more readily in free jets than with flows constricted in a duct[3].

The test apparatus consists of a plasma heater powered by three MPD arcs, an uncooled tantalum supersonic nozzle, and a constant pressure uncooled test section employing tungsten segmented electrodes. The generator test section is about 50 cm in length and has a cross sectional area of about 16 cm^2, depending on the test section Mach number. There are 80 pairs of tungsten wire electrodes with an electrode spacing of 0.76 cm.

Although most of the inert gases and inert gas mixtures can be used successfully as working fluids over a wide range of generator sizes,

consideration of dimensional and vacuum pump restrictions in this experiment indicate that the helium-xenon mixture appears to be the best working fluid. The helium--xenon mixture is particularly attractive because the induced generator voltage can be made large compared to the boundary layer and electrode sheath voltage.

Initially, attention will be focused on the measurement of the degree of electron temperature and density elevation along the generator duct length. Electron temperatures and densities will be measured with Langmuir probes, microwave diagnostics, and spectroscopic techniques. Use of both a 24 GHz and 90.9 GHz microwave system will make it possible to measure electron densities in the range $10^{11} \leq ne \leq 10^{14}$ cm^{-3}. The actual range of electron densities expected in the experiment is $10^{9} \leq ne \leq 10^{15}$ cm^{-3}

REFERENCES

1. Zhadanov, V. M., "Transport Phenomena in a Partly Ionized Gas," (PPM Vol. 26, No. 2, 1962, pp 280-288) pp 401-418 Applied Mathematics and Mechanics (Translation).

2. Louis, J. F., Gal, G., and Blackburn, P. R., "Detained Theoretical and Experimental Study on a Large MHD Generator," AVCO Research Report No. 174, March 1964.

3. Russell, G. R., Byron, S., and Bortz, P. I., "Performance and Analysis of a Crossed-Field Accelerator," AIAA Electric Propulsion Conference, Colorado Springs, Colorado, March 11, 1963.

RESEARCH IN PLASMAS IN THERMIONIC DIODES

Katsunori Shimada

Jet Propulsion Laboratory, California Institute of Technology
Pasadena, California

The Thermionics Research Group in the Guidance and Control Research Section at the Jet Propulsion Laboratory is conducting research work in plasmas such as are found in thermionic-energy converters.

The goals of our research are twofold. The first is to understand the physical properties of plasmas existing in small gaps of the order of 1/1000 inch, between electron- and ion-emitting electrodes. The second goal is to utilize such understanding in improving the performance of existing thermionic-energy converters by reducing plasma losses.

In order to attain such goals, we have investigated, during the past two years, (1) low-frequency oscillations in cesium diodes, and (2) charge transport in neutral and non-neutral plasmas. The experimental phase of task (1) was completed and our current efforts are directed toward task (2). The study of charge transport is intended to improve our understanding of the current conduction through plasmas, the plasma formation, and the plasma-sheath interactions. This work will be extended to a plasma immersed in an external magnetic field. A mathematical formulation of charge transport has been completed for an electrically neutral plasma as well as for a non-neutral plasma. Subsequently, the results will be presented at this meeting.

Our research group also works very closely with the Power Sources Section at the Jet Propulsion Laboratory. Consequently, the properties of plasmas in prototype thermionic-energy converters can be obtained as required.

Low-Frequency Oscillations in Cesium Diodes

The initial intent of this work was to investigate the possibilities of generating and sustaining magnetosonic oscillations of large amplitude in thermionic diodes. However, the scope of this work was reduced to the study of the natural oscillations occurring in cylindrical cesium diodes without the application of an external magnetic field.

Several cesium diodes having cylindrical geometry were fabricated in glass envelopes. The results obtained from these diodes showed that the oscillations occurred in the plateau region of the volt-ampere

curves when the diodes were operated in an unignited mode with the ratio of emitter temperature to cesium reservoir temperature nearly equal to, or slightly larger than, the value required for neutral emission. Although the amplitude of the oscillations depended on the circuit resistance in series with the diode, it reached a characteristic value when this resistance was reduced below a threshold value which was of the order of an ohm. This characteristic amplitude (peak-to-peak) may be as large as the dc current through the diode. The peak value of this oscillation current closely followed the theoretically expected saturation current available from the emitter, whereas the minimum value was substantially smaller. A block diagram of the experimental setup is shown in Fig. 1. This setup enabled us to make measurements of the volt-ampere curves, the waveforms, and the frequency of oscillation under various operating conditions of a diode. The results are presented in Fig. 2. The period of oscillation (the reciprocal of frequency) was proportional to the pressure and was approximately proportional to the interelectrode distance.

It was concluded that the oscillations occurring in cesium diodes operating in an unignited mode are the result of space-charge oscillations about the average space-charge density which yields neutral emission.

Charge Transport in Plasmas

Theoretical studies of charge transport in plasmas were initiated as part of our efforts in finding means for reducing plasma losses in thermionic-energy converters. Our future effort will be directed toward utilizing a magnetic field in increasing the efficiency of ionization in thermionic diodes.

The spatial distribution of charge particles was calculated for an electrically neutral plasma, assuming that the plasma is strictly neutral and that the sourceless and sinkless condition holds only for the net current density. The charge density was found to be a superposition of two parts; one was invariant in the space coordinate, and the other varied exponentially with distance. The constant part described the net current through the plasma, and the exponential part followed the Boltzmann distribution. The result obtained above for a non-zero electric-field condition also included a solution for the zero-field condition as a limiting case. The solution in the latter case had a linear dependence on the space coordinate. Furthermore, such quantities as the characteristic length, the time constant, and the generation or the recombination rate were calculated. They are summarized in Figs. 3 and 4.

An analysis of charge distribution in a non-neutral plasma was also made. A system of equations was reduced in such a way that the

electron density and the excess charge density (the difference between the positive and the negative charge) could be determined independently of each other. Our future work will be to integrate these solutions with a solution for the plasma sheath adjacent to the electron- and ion-emitting electrodes so that the external volt-ampere characteristic of a cesium diode can be obtained.

An in-house design of a test vehicle having a metal-ceramic structure has been completed and its fabrication is in progress. This diode will be used in the experimental phase of our research on charge transport.

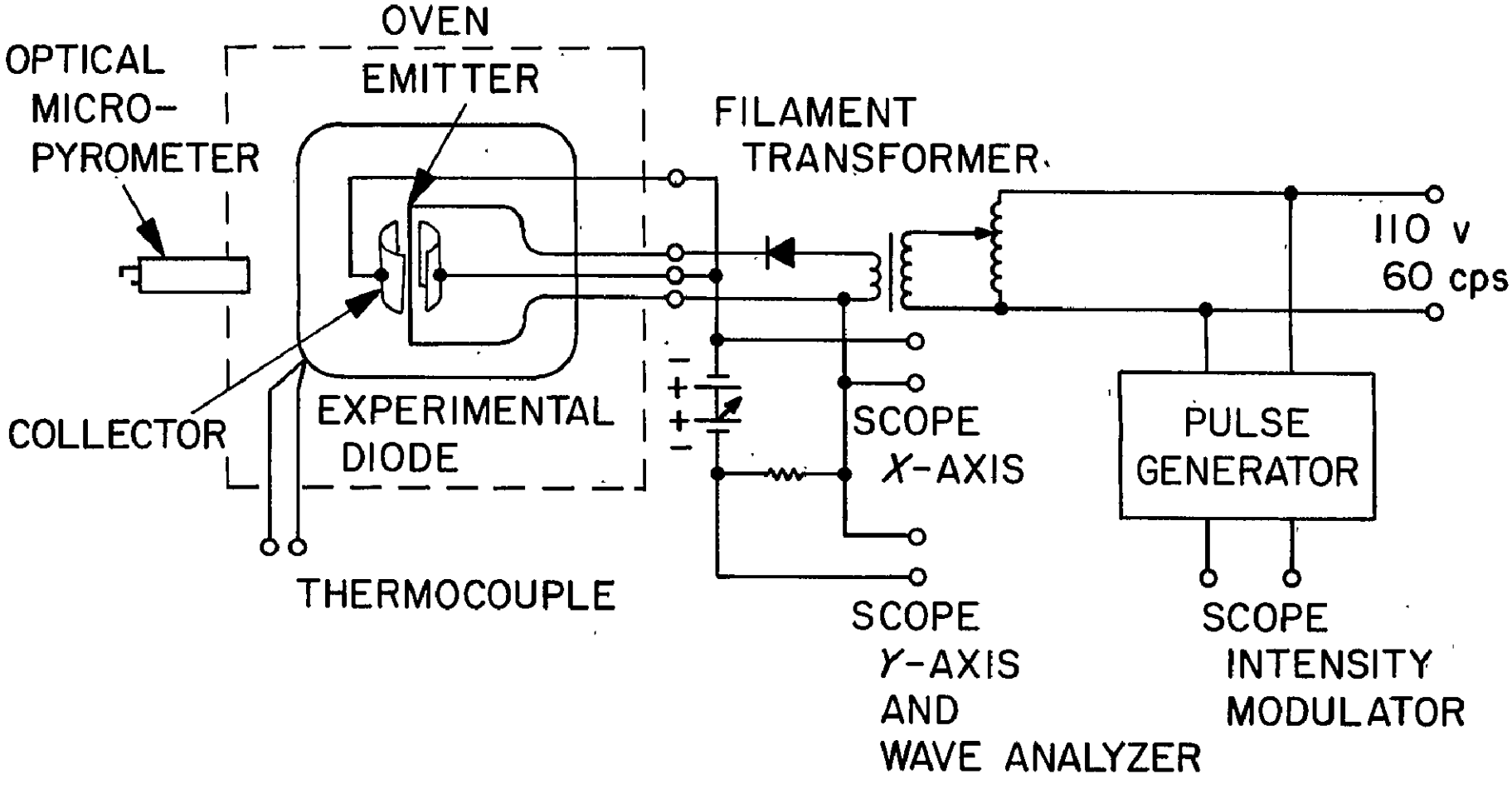

FIG. 1. SCHEMATIC DIAGRAM OF MEASURING CIRCUIT

FIG. 2. AMPLITUDE OF OSCILLATION
W – Ta SMALL DIODE

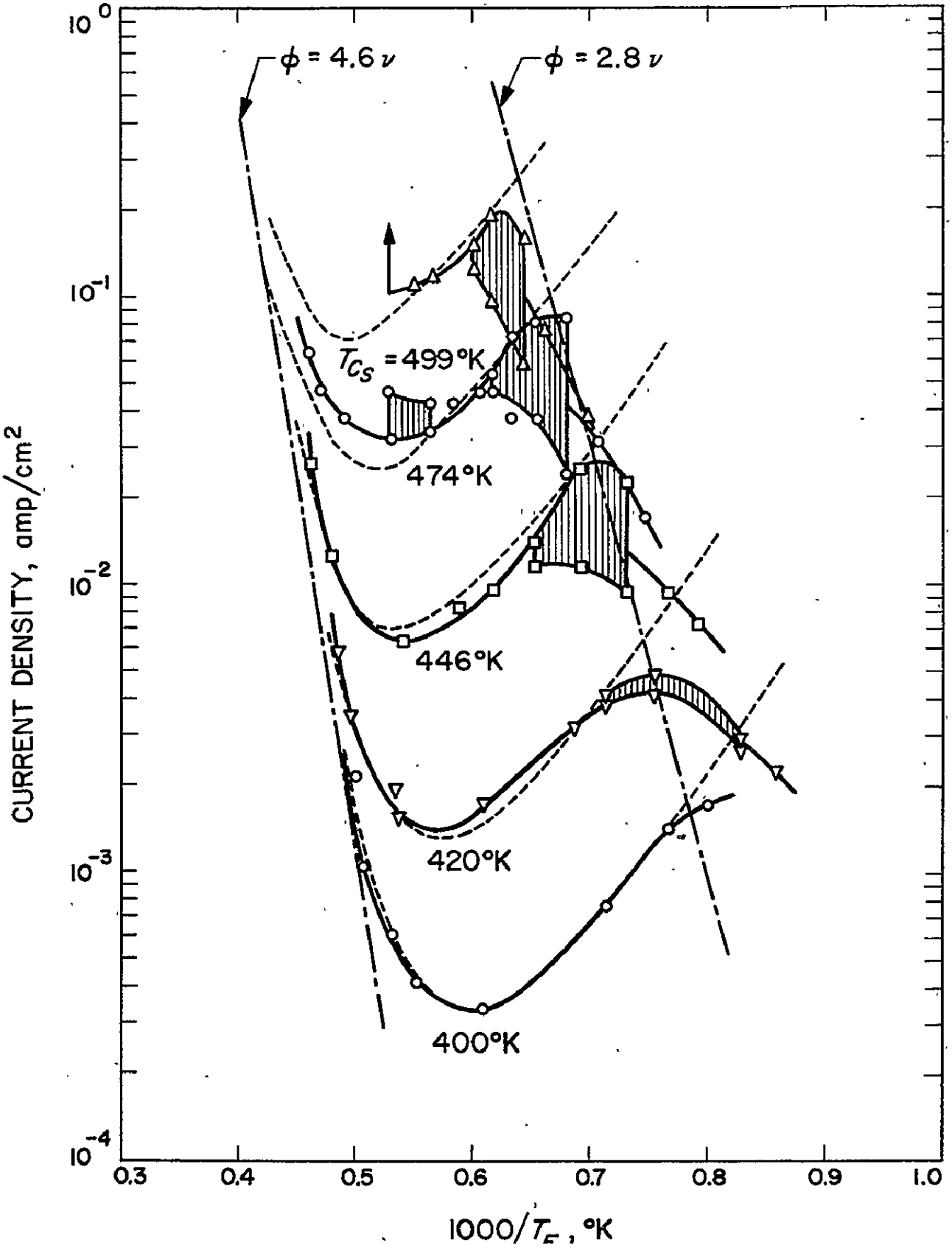

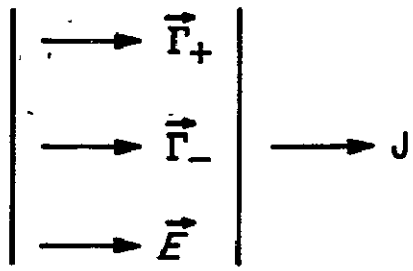

$x = 0 \qquad x = d$

$$\vec{\Gamma}_+ = \mu_+ \vec{E} n_+ - D_+ \nabla n_+ \tag{1}$$

$$\vec{\Gamma}_- = -\mu_- \vec{E} n_- - D_- \nabla n_- \tag{2}$$

$$n_+ = n_- = n \tag{3}$$

$$\nabla \cdot \vec{E} = \frac{e}{\epsilon_0}(n_+ - n_-) = 0 \tag{4}$$

$$\nabla \cdot \vec{J} = e\, \nabla \cdot (\vec{\Gamma}_+ - \vec{\Gamma}_-) = 0 \tag{5}$$

$$\vec{E} = \vec{i} E_x \tag{6}$$

$$E_x \frac{dn}{dx}(\mu_+ + \mu_-) - (D_+ - D_-)\frac{d^2 n}{dx^2} = 0 \tag{7}$$

SOLUTION: CASE (1), $E_x \neq 0$, $D_+ \neq D_-$

$$\boxed{n = n_1 e^{-\frac{x}{L_a}} + n_2} \tag{8}$$

$$L_a = \frac{D_- - D_+}{\mu_+ + \mu_-}\frac{1}{E_x} \triangleq \frac{D_a}{\mu_a E_x} \tag{9}$$

$$D_a \triangleq \frac{\mu_+ D_- + \mu_- D_+}{\mu_+ + \mu_-} \tag{10}$$

$$\mu_a \triangleq \frac{\mu_+ D_- + \mu_- D_+}{D_- - D_+} \tag{11}$$

$$\frac{e}{kT_{eq}} = \frac{\mu_a}{D_a} \tag{12}$$

$$\boxed{n = n_1 e^{\frac{eV(x)}{kT_{eq}}} + n_2} \tag{13}$$

$$\vec{J} = e(\vec{\Gamma}_+ - \vec{\Gamma}_-) = e n_2 \vec{E}(\mu_+ + \mu_-) \tag{14}$$

$$\nabla \cdot \vec{\Gamma}_+ = \nabla \cdot \vec{\Gamma}_- = -L_a^2 D_a n_1 e^{-\frac{x}{L_a}} \tag{15}$$

SOLUTION:

CASE (2), $E_x = 0$

$$\boxed{n = n_0 + \frac{n_d - n_0}{d} x} \tag{16}$$

$$J = e\frac{n_d - n_0}{d}(D_- - D_+) \tag{17}$$

$$\nabla \cdot \vec{\Gamma}_+ = \nabla \cdot \vec{\Gamma}_- = 0 \tag{18}$$

Fig. 3. Charge transport in a neutral plasma.

$$\vec{\Gamma}_+ = \mu_+ \vec{E} n_+ - D_+ \nabla n_+ \qquad (1)$$

$$\vec{\Gamma}_- = -\mu_- \vec{E} n_- - D_- \nabla n_- \qquad (2)$$

$$n_+ - n_- = n \qquad (3)$$

$$\nabla \cdot \vec{\Gamma}_+ = \nabla \cdot \vec{\Gamma}_- = z n_- \qquad (4)$$

$$\nabla \cdot \vec{E} = \frac{e}{\epsilon_o} n \qquad (5)$$

$$\nabla^2 n_- + \frac{z}{D_a} n_- = 0 \qquad (6)$$

$$\vec{E} \cdot \nabla n + \frac{e}{\epsilon_o} n^2 - \frac{D_+}{\mu_+} \nabla^2 n = 0 \qquad (7)$$

$$n \frac{e}{\epsilon_o} \left[n \frac{d^2 n}{dx^2} - 3 \left(\frac{dn}{dx} \right)^2 \right] - \frac{D_+}{\mu_+} \left[\left(\frac{d^2 n}{dx^2} \right)^2 - \frac{d^3 n}{dx^3} \frac{dn}{dx} \right] = 0 \qquad (8)$$

$$x = \gamma L \qquad (9)$$

$$L = \sqrt{\frac{\epsilon_o k T_-}{e^2 N}} \qquad (10)$$

$$\beta = \frac{n}{N} \qquad (11)$$

$$T_- / T_+ = \alpha \qquad (12)$$

$$\alpha \beta \left[\beta \frac{d^2 \beta}{d\gamma^2} - 3 \left(\frac{d\beta}{d\gamma} \right)^2 \right] - \left[\left(\frac{d^2 \beta}{d\gamma^2} \right)^2 - \left(\frac{d^3 \beta}{d\gamma^3} \right) \frac{d\beta}{d\gamma} \right] = 0 \qquad (13)$$

KINETIC THEORY STUDIES OF FUNDAMENTAL PLASMA PROBLEMS

C. S. Wu, Jet Propulsion Laboratory

Several plasma problems have been studied recently based on kinetic theory. These problems are concerned with plasma transport phenomena and stability. The first problem is on temperature relaxation. We found that electron-ion collisions, which in previous analyses have been neglected by many authors, can be very important in the relaxation of anisotropic temperature distribution. Our analysis also takes account of the effect of particle-wave interaction in the collision integral.

The second problem is the calculation of high-frequency conductivity of a two-temperature plasma. It is found that the incoherent ion waves can give rise to significant enhancement of the resistivity.

The third problem is concerned with the electromagnetic instability of a plasma in the absence of applied magnetic field. It is found that anisotropic ion distribution may result in unstable transverse waves. The instability is of an aperiodic nature.

GPO 907-067